Cardiovascular Magnetic Resonance in Cardiac Amyloidosis

Dr Ana Martinez de Azcona Naharro

Doctor of Philosophy

University College London

National Amyloidosis Centre
Division of Medicine
UCL Royal Free Campus
Rowland Hill Street
London NW3 2PF

2020

I, Dr Ana Martinez de Azcona Naharro, confirm that the work presented in this thesis is my own. Where information has been derived from other sources, I can confirm that this has been indicated in the thesis.

ABSTRACT

Background:

Systemic amyloidoses are an underdiagnosed, but increasingly recognized group of progressive disorders characterised by the extracellular deposition of misfolded proteins in one or more organs. Cardiac amyloid deposition leads to an infiltrative or restrictive cardiomyopathy and is the major driver of prognosis.

Aims:

In this thesis, by using cardiovascular magnetic resonance (CMR), I have aimed to assess the cardiac response to chemotherapy in AL amyloidosis; to assess morphological phenotypes and tissue characterization findings in ATTR cardiac amyloidosis, and compare these findings with AL amyloidosis; to evaluate the prognostic potential of native myocardial T1 in ATTR cardiac amyloidosis and compare native T1 with extracellular volume (ECV) in terms of diagnostic accuracy and prognosis; to study the prevalence of thrombus in the left atrial appendage in the cardiac amyloidosis population; and to explore the role of hypoperfusion at rest in cardiac amyloidosis.

Results and Conclusions:

I confirmed that CMR with T1 mapping and ECV measurements demonstrates that cardiac AL amyloid deposits frequently regress following chemotherapy that substantially suppresses clonal light chain production. I characterised the cardiac morphology in ATTR cardiac amyloidosis. I demonstrated that native T1 mapping and ECV are good diagnostic techniques in cardiac ATTR amyloidosis that associate

with prognosis. Both parameters also correlate with mortality, but only ECV remains independently predictive of prognosis. I confirmed that the prevalence of intracardiac thrombi in cardiac amyloidosis and atrial fibrillation is high despite anticoagulation, with significant thrombus prevalence even in sinus rhythm. I demonstrated that myocardial hypoperfusion is common and substantial in cardiac amyloidosis. CMR indicates a complex pathophysiology in which systolic dysfunction, diastolic dysfunction, and amyloid deposition are independently associated with reduced myocardial perfusion.

Patients with amyloidosis continue to have unmet needs, many of which stem from heart involvement, but outcomes are gradually improving.

IMPACT STATEMENT

The work in my thesis focuses on diagnosis, monitoring, and outcomes of patients with systemic amyloidosis. This is a rare and fatal disorder in which diagnosis is often delayed for years, associated with advanced cardiac failure in many cases. Despite advances in treatment, cardiac amyloidosis remains the commonest cause of death and management and treatment of patients remains a major challenge.

The work described here has led to a number of publications and national and international presentations that have improved awareness of amyloidosis, along with improved diagnostic and monitoring techniques, which have resulted in improved clinical outcomes.

Management and prognosis of patients with systemic amyloidosis is strongly influenced by cardiac involvement using the Mayo staging system for AL amyloidosis and the NAC staging system for ATTR amyloidosis. The work presented in this thesis has demonstrated that CMR can assess cardiac response to treatment in AL amyloidosis measuring the myocardial extracellular volume (where the amyloid fibrils deposit). 67% of the patients who achieved a good haematological response to chemotherapy (complete response or very good partial response) had a decrease in amyloid burden measured by ECV.

This thesis also describes novel findings regarding the morphological phenotype of patients with ATTR amyloidosis that differs from AL and the one traditionally described, with asymmetric LVH present in 79% of patients with ATTR amyloidosis versus 14% in AL amyloidosis. Reverse septal contour, classically associated with hypertrophic cardiomyopathy, is present in one-quarter of patients with ATTR. This

finding is particularly important to suspect the diagnosis of cardiac amyloidosis with asymmetric LVH. CMR has lately emerged as a robust technique that can provide information about tissue composition. CMR can visualize, with late gadolinium enhancement, and measure, with T1 mapping, the continuum of amyloid deposition in the heart. In this thesis, I have confirmed that native T1 mapping and ECV are good diagnostic techniques in cardiac ATTR amyloidosis and associate with prognosis. Both parameters also correlate with mortality, but only ECV remains independently predictive of prognosis, suggesting that it is a more robust marker in cardiac ATTR amyloidosis.

Cardiac amyloidosis reduces cardiac output, alters the atrial walls, and may induce hypercoagulability. In this thesis, I confirmed that intracardiac thrombi are prevalent in both AL and ATTR amyloidosis in atrial fibrillation despite anticoagulation, and there is a significant prevalence in patients even in sinus rhythm. CMR with early gadolinium imaging in the left atrial appendage should be considered when cardiac amyloidosis is suspected and a low threshold for anticoagulation could be appropriate.

Lastly, amyloid deposition in the extracellular space causes biventricular wall thickening, systolic and diastolic dysfunction, and low cardiac output, which coupled with capillary disruption and vessel lumen narrowing are factors that may reduce myocardial perfusion. Using a novel CMR technique, myocardial blood flow mapping, I confirmed in this work that myocardial hypoperfusion is common and substantial in cardiac amyloidosis. CMR indicates a complex pathophysiology in which systolic dysfunction, diastolic dysfunction, and amyloid deposition are independently associated with reduced myocardial perfusion.

ETHICAL APPROVAL

All individuals whose data has been used in the clinical research studies described in this thesis gave explicit informed consent by signing a consent form while visiting the centre. The consent form was approved by the Royal Free Hospital Ethics Committee (REC Ref 06/Q0501/42, 09/H0715/58). The dosage and administration of radioactive isotopes were approved by the Administration of Radioactive Substances Advisory Committee of the Department of Health.

FUNDING

My clinical research fellowship supporting the work of this thesis was funded by the National Amyloidosis Centre. I have no conflict of interest regarding the work of this thesis.

ACKNOWLEDGEMENTS

This thesis would not have been possible without the incredible support and supervision of Professor Marianna Fontana. She has been both a mentor and a role model for my academic career as well as a good friend. I am indebted to Professor Philip Hawkins and Professor Julian Gillmore for their guidance and mentoring as well as their enabling many aspects of my work at the National Amyloidosis Centre. I am additionally very grateful to Professor Helen Lachmann, Professor Ashutosh Wechalekar, Doctor Carol Whelan, and all the staff of the National Amyloidosis Centre for their support in caring for patients at our centre. I would like to thank the many patients and referring physicians for making this research possible.

I owe much gratitude to colleagues within the CMR unit, in particular Sarah Anderson, Doctor Dan Knight, and Doctor Tushar Kotecha, who have contributed greatly, not only in support of my academic productivity, but moreover in my experience and enjoyment of this period.

I would like to thank my husband John for his unending support, encouragement and love.

Lastly, I would like to dedicate this thesis to my parents, León and Ana María, for their vision in my early career as a physician and their unreserved faith and love throughout my life.

CONTENTS

LIST OF FIGURES

LIST OF TABLES

ABBREVIATIONS

6MWT	6 Minute Walk Test
AF	Atrial Fibrillation
AL	Light-chain amyloidosis
AL-CM	AL cardiomyopathy
ASCT	Autologous Stem Cell Transplant
ATTR	Transthyretin amyloidosis
ATTR-CM	Transthyretin cardiomyopathy
ATTRm	Mutant or hereditary transthyretin amyloidosis
ATTRwt	Wild-type transthyretin amyloidosis
BNP	Brain Natriuretic Peptide
CMR	Cardiovascular Magnetic Resonance
CPHPC	R-1-[6-[R-2-carboxy-pyrrolidin-1-yl]-6-oxo-hexanoyl] pyrrolidine-2-carboxylic acid
CR	Complete response
CT	Computed Tomography
CTD	Cyclophosphamide, Thalidomide (and) Dexamethasone
dFLC	difference between involved and uninvolved free light chains
DT	Deceleration time
ECG	Electrocardiogram
ECV	Extracellular Volume
eGFR	Estimated glomerular filtration rate

EQ-CMR	Equilibrium (contrast) Cardiovascular Magnetic Resonance
FAP	Familial Amyloid Polyneuropathy
FISP	Fast Imaging with Steady State Precession
FLASH (IR)	Fast Low Angle Shot (Inversion Recovery)
GLS	Global Longitudinal Strain
HCM	Hypertrophic Cardiomyopathy
ICD	Implantable Cardioverter Defibrillator
IVS	Interventricular Septum
LA	Left Atrium
LAA	Left Atrial Appendage
LBBB	Left Bundle Branch Block
LGE	Late Gadolinium Enhancement
LV	Left Ventricle
LVEDV	Left Ventricular End Diastolic Volume
LVEDVi	Left Ventricular End Diastolic Volume indexed
LVEF	Left Ventricular Ejection Fraction
LVESV	Left Ventricular End Systolic Volume
LVESVi	Left Ventricular End Systolic Volume indexed
LVH	Left Ventricular Hypertrophy
MAPSE	Mitral Annular Plane Systolic Excursion
MA Sa	Mitral annulus systolic velocity
MI	Myocardial Infarction

MOLLI	Modified Look Locker Inversion (recovery)
MRI	Magnetic Resonance Imaging
msec	Milliseconds
NR	No response
NT-proBNP	N-Terminal pro B-type Natriuretic Peptide
NYHA	New York Heart Association
PR	Partial Response
PSIR	Phase sensitive inversion recovery
RF	Radiofrequency
RNA	Ribonucleic acid
ROI	Region of interest
RV	Right Ventricle
SAP	Component to Serum Amyloid P
SD	Standard Deviation
ShMOLLI	Shortened Modified Look Locker Inversion (recovery)
SPECT	Single-photon emission computed tomography
SSA	Senile Systemic Amyloidosis
SSFP	Steady State Free Precession
SV	Stroke Volume
TAPSE	Tricuspid Annular Plane Systolic Excursion
TA Sa	Tricuspid Annulus Systolic Velocity
TD	Trigger delay

TDI	Tissue Doppler Imaging
TE	Echo Time
TI	Inversion Time
TNF	Tumour Necrosis Factor
TTR	Transthyretin
^{99m}Tc-DPD	^{99m}Tc-3,3-diphosphono-1,2-propanodicarboxylic acid
VGPR	Very good partial response

CHAPTER 1: INTRODUCTION

This thesis is built on the work of others. Key methods were developed at The Heart Hospital by my colleagues: (a) Dr Andrew Flett (UCL MD (Res), 2012) who designed and validated the use of Equilibrium contrast Cardiovascular Magnetic Resonance (EQ-CMR) to measure myocardial fibrosis in aortic stenosis and hypertrophic cardiomyopathy; (b) the work of Dr Daniel Sado (UCL MD (Res), 2013) who explored the role of extracellular volume (ECV) measurement, again for fibrosis, across a variety of cardiac diseases; (c) the work of Dr Sanjay Banypersad (UCL MD (Res), 2014) who explored the role of ECV, here as a measure of amyloid burden, for the investigation of the extracellular volume of the heart, liver and spleen in systemic light chain amyloid (AL) amyloidosis; and the work of Dr Marianna Fontana (UCL MD (Res), 2015) who explored the other main type of amyloidosis, transthyretin (ATTR) amyloidosis.

This introduction is based on the publications below:

- Martinez-Naharro A, Hawkins PN, Fontana M. Cardiac amyloidosis. *Clinical Medicine*. 2018 Apr 1;18(Suppl 2):s30-s35
- Martinez-Naharro A, Baksi AJ, Hawkins PN, Fontana M. Diagnostic imaging of cardiac amyloidosis. *Nat Rev Cardiol*. 2020 Feb 10. doi: 10.1038/s41569-020-0334-7. [Epub ahead of print]

I was primarily responsible for the content of both of the above manuscripts.

What is amyloidosis

Systemic amyloidosis comprises a family of diseases caused by deposition of misfolded fibrillar proteins in the extracellular space (1). More than 30 different precursor proteins can undergo the substantial molecular transformation to form amyloid fibrils in vivo (2), the resultant diseases being classified and having a clinical phenotype relating to the protein in question. Previously thought to be very rare, all forms of cardiac amyloidosis are now understood to be underdiagnosed (3). Timely diagnosis of cardiac amyloidosis is critical, given the recent availability of an array of new and effective treatments.

Many types of amyloidosis can involve the heart, but two types predominate (4): immunoglobulin light-chain (AL) amyloidosis and transthyretin (ATTR) amyloidosis. Cardiac involvement is the leading cause of morbidity and mortality in systemic amyloidosis, regardless of the underlying pathogenesis of amyloid production (5). Cardiac amyloidosis is a myocardial disease characterised by extracellular amyloid infiltration throughout the heart. The infiltrative process results in biventricular wall thickening with concentric ventricular remodelling and low cardiac output. The subsequent elevation of pressure in the atria is associated with atrial dilatation. Intramyocardial vessels are frequently infiltrated by amyloid, causing reduced myocardial perfusion (6). The conduction system is also frequently disrupted, with atrial arrhythmias (fibrillation, flutter or atrial tachycardia) and atrioventricular conduction delays being common. Ventricular arrhythmias may also occur although sustained ventricular tachycardia is identified infrequently.

Cardiac AL Amyloidosis

Light chain (AL) amyloidosis is consequent on a clonal plasma cell proliferative disorder in which misfolded immunoglobulin light chains are deposited as amyloid fibrils in multiple organs, including the heart in about half of cases. Cardiac dysfunction in AL amyloidosis results from extracellular infiltration of the myocardium but there is often also evidence for a cardio-toxic effect exerted by pre-fibrillar light chain aggregates. The severity of cardiac dysfunction is the major determinant of morbidity and mortality (5).

AL amyloidosis was previously thought to be the most common type of systemic amyloidosis, with an estimated incidence of 8-12 per million person-years (7). AL amyloidosis most frequently affects the kidneys and can lead to nephrotic syndrome (8), whereas cardiac involvement is the second most common presenting manifestation, occurring in 50-75% of all patients (9,10). Other organs that might be also involved include the peripheral and autonomic nervous system, vasculature, liver, gastrointestinal tract, and soft tissues (10).

Clinical presentation reflects the varying multisystem deposition of amyloid. Examination findings may reflect soft tissue and small vessel amyloid infiltration and include macroglossia, periorbital purpura, submandibular gland enlargement and nail dystrophy. Fatigue and weight loss are common. Hepatic or splenic infiltration may cause palpable organomegaly. Renal dysfunction is common, usually presenting as nephrotic range proteinuria.

Early cardiac amyloidosis is a major diagnostic challenge. The classical features of ‘right-sided’ congestive heart failure may not be evident until cardiac disease is very

advanced. Elevated jugular venous pressure, a third heart sound, hepatomegaly, and peripheral oedema may be very subtle or absent in patients who have already started diuretics.

Peripheral neuropathy is relatively common, presenting with paraesthesia or dysaesthesia typically in a ‘glove and stocking’ distribution. Autonomic neuropathy is an important diagnostic clue, manifesting as orthostatic hypotension, alternating diarrhoea and constipation, and erectile dysfunction.

Monoclonal immunoglobulin or free light chains can be identified in the serum and/or urine of at least 95% of patients using sensitive assays, but are often missed in routine serum electrophoresis. The absence of a detectable clone is problematic for diagnosis and monitoring response to treatment.

Cardiac Transthyretin Amyloidosis

Transthyretin is a liver derived plasma protein that in its wild-type form is the amyloid fibril precursor protein in the non-hereditary, late onset, predominantly male syndrome of cardiac ATTRwt amyloidosis. Genetic variants of transthyretin are associated with the dominantly inherited syndromes of familial amyloid polyneuropathy and familial amyloid cardiomyopathy, which can present from young adulthood onwards. The prognosis of cardiac ATTR amyloidosis is better than cardiac AL amyloidosis with median survival typically 4 to 5 years from diagnosis (11,12). Advances in non-invasive diagnosis, coupled with the development of effective therapies (13-16), have shifted ATTR cardiomyopathy from a rare and untreatable disease to a condition that clinicians should consider as a potential diagnosis on a daily basis.

Wild-type Transthyretin Amyloidosis

Nonhereditary transthyretin-related amyloidosis is commonly referred to as senile systemic amyloidosis (SSA) due to its late age of onset (usually after the seventh decade of life). ATTRwt has a strong male predominance, with between 25 and 50:1 male:female expression (17). The true prevalence of ATTRwt amyloidosis is unknown but it is likely to be underdiagnosed in many cases. Autopsy studies have revealed that amyloid deposits derived from plasma transthyretin are present in the heart of up to 25% of elderly individuals (18,19). Prevalence is increasing with the increasingly aging population and emerging diagnostic tools including cardiovascular MRI and DPD scintigraphy (20,21).

Despite being a systemic disease, the heart is generally the only organ involved clinically, with the exception of carpal tunnel syndrome and some other musculoskeletal disorders including lumbar canal stenosis, which may precede cardiac symptoms by 10-15 years.

An incidental clonal plasma cell dyscrasia is present in up to a quarter of ATTRwt amyloidosis patients reflecting their advanced years and raising the possibility of AL amyloidosis (22). A cardiac biopsy is often needed in such patients to obtain a definitive diagnosis (21).

Hereditary Transthyretin Amyloidosis

The TTR gene is located on chromosome 18 and contains four exons and 5 introns. There are more than 120 mutations in the TTR gene, most of which encode pathogenic variants of TTR with increased amyloidogenic potential. However only a few of these variants are responsible for the majority of cases of hereditary

transthyretin amyloidosis worldwide, notably including Val30Met, Thr60Ala, Ser77Tyr and Val122Ile (23,24).

The specific site of an amino acid substitution determines the phenotype of the disease. Inheritance is autosomal dominant with variable penetrance. Correlation between genotype and phenotype is strong for certain mutations, whereas with others the clinical features can vary substantially, even within a given family. The onset occurs from the third decade, most commonly after the age of 40. In some forms, peripheral neuropathy or autonomic dysfunction may predominate, with cardiac amyloidosis being either absent or limited to the conduction system. The most prevalent mutation in the white population in the UK and the US (25), Thr60Ala (substitution of alanine for threonine at position 60), can present with predominant cardiomyopathy characterised by heart failure and conduction system disturbances, autonomic dysfunction or peripheral neuropathy, or any combination of these features.

The TTR V30M variant is the commonest cause of familial amyloid polyneuropathy in the world, with large foci in Portugal, Japan, and Sweden. The disease usually presents with peripheral and autonomic neuropathy without cardiac involvement, especially in patients younger than 50 years of age, although cardiac amyloidosis does occur in older cases (26).

Worldwide, a polymorphism comprising substitution of isoleucine for valine at position 122 (Val122Ile) is particularly notable. Approximately 4% of African Americans and probably a similar proportion of Afro-Caribbeans are heterozygous for this variant, which appears to be associated with a greatly increased risk of

developing late-onset cardiac ATTR amyloidosis that is morphologically indistinguishable in cardiac imaging from the wild-type form (27). This mutation is also the most common ATTR mutation in the UK. There is a high prevalence of hypertensive heart disease in this population, which may lead to a possible diagnosis of amyloid being overlooked. The presence of right ventricular thickening, the absence of left ventricular hypertrophy on the ECG, and the clinical finding of right heart failure (particularly if there is history of carpal tunnel syndrome) should suggest the diagnosis.

Genetic testing to identify mutations in the *TTR gene* should be performed in all patients with ATTR cardiomyopathy, given the important implications for family members and the potential for genetic counselling.

Diagnosis of Systemic Amyloidosis

The diagnosis of amyloidosis relies on a high index of clinical suspicion. Unfortunately, the disease is frequently asymptomatic until a late stage and, even then, the symptoms can be very nonspecific.

Histology

Diagnosis of systemic amyloidosis usually requires histological confirmation of amyloid deposition through Congo red staining that produces the pathognomonic green birefringence when viewed under cross-polarized light (Figure 1). Amyloid deposits can usually be identified in biopsies of malfunctioning organs, but relatively noninvasive 'screening' biopsies provide an alternative, notably including abdominal fat aspirates that can identify amyloid deposits in 60–80% of patients with systemic AL amyloidosis, though fewer with ATTR type (28). Cardiac biopsy provides the

most definitive diagnostic evidence in amyloid cardiomyopathy and, if the diagnosis is not confirmed by biopsy of another tissue, endomyocardial biopsy is a safe and relatively simple procedure in skilled hands.

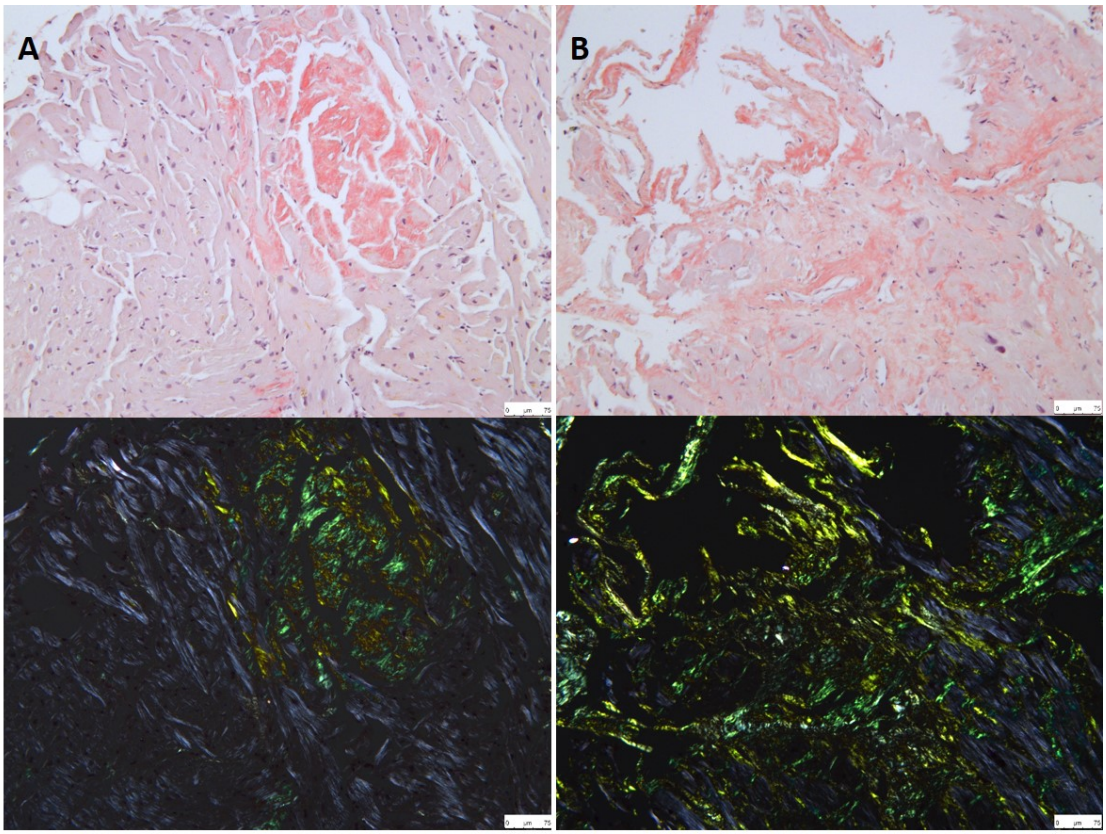

Figure 1. Congo red staining of myocardial tissue from two patients with amyloid cardiomyopathy. A, ATTR amyloidosis; B, AL amyloidosis. Top panel, light microscopy; bottom panel, polarized light microscopy.

Serum biomarkers

Cardiac biomarkers might be helpful for raising clinical suspicion of cardiac amyloidosis in a patient with a known plasma cell dyscrasia or suspected ATTR cardiomyopathy and should prompt further investigations with ECG and echocardiography. The combination of serum N-terminal pro-B-type natriuretic peptide (NT-proBNP), troponin, and renal function is useful for risk stratification (12,29) and can help guide treatment strategies (30).

Electrocardiography

Electrocardiography (ECG) has an important role in raising diagnostic suspicion of cardiac amyloidosis. Electrocardiographic assessment of voltage in patients with cardiac amyloidosis in not influenced by the same factors as in the general population. Classic predictors of voltage, such as age, sex, ethnicity, blood pressure levels, body surface area and smoking status, are not associated with voltage that is measured using limb and precordial (Sokolow) voltage criteria (31). In addition, the established linear relationship between left ventricular (LV) mass and voltage on the ECG does not hold true in cardiac amyloidosis, given that the ECG is abnormal in almost all patients with this disease (32,33). The classic hallmark of the disease has been described as the combination of low QRS voltage on the ECG and increased LV wall thickness on echocardiography (34,35). Because the thickening of the ventricular wall in amyloidosis is caused by myocardial infiltration rather than cardiomyocyte hypertrophy, the ECG limb lead voltages tend to decrease as the ventricle thickens and are often associated with extreme left-axis or right-axis deviation (Figure 2). However, only ~50% of patients with AL cardiomyopathy and about 25-40% of patients with ATTR cardiomyopathy meet true low-voltage criteria (QRS amplitude <5 mm in the limb leads or <10 mm in the precordial leads) (11,31,36). Therefore, the absence of low-voltage criteria does not exclude a diagnosis of cardiac amyloidosis. Although voltage criteria for LV hypertrophy are extremely uncommon in patients with AL amyloidosis, they can be present in up to 25% of patients with ATTR amyloidosis. A possible explanation for the discrepancy in QRS voltages between the two subtypes of cardiac amyloidosis is the ATTR amyloidosis is associated with a greater relative increase in cardiomyocyte hypertrophy and, therefore, higher QRS voltages than AL.

Another main feature of the ECG associated with cardiac amyloidosis is the presence of pseudoinfarct pattern with Q waves in the precordial limb leads that mimic a previous anteroseptal, inferior or lateral myocardial infarction (36,37). This finding is seen in ~50% of patients. Furthermore, atrioventricular heart block, particularly second-degree and third-degree atrioventricular block, are also common and often necessitate pacemaker implantation in patients with cardiac amyloidosis.

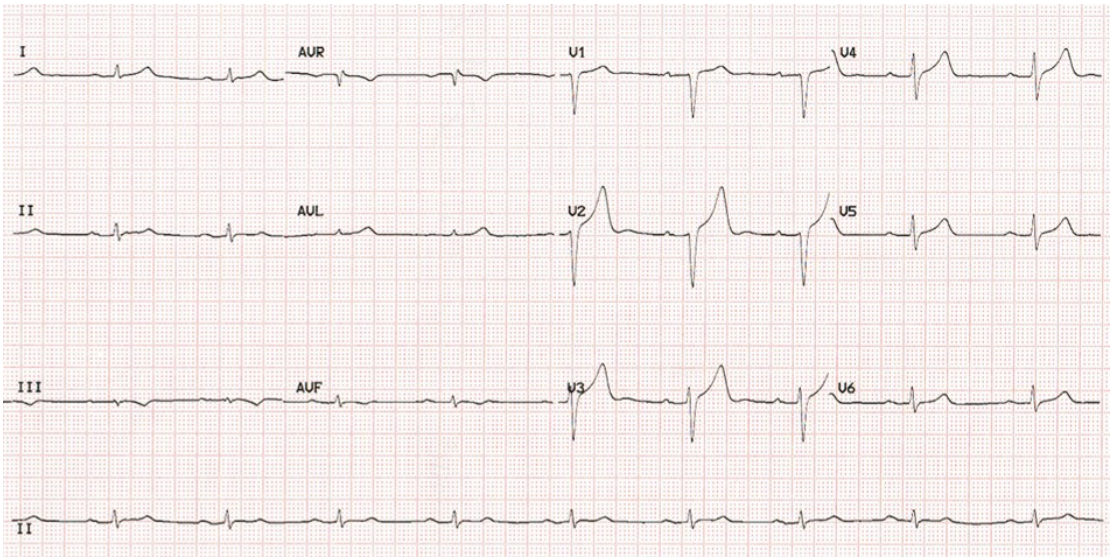

Figure 2. ECG of a patient with cardiac ATTR amyloidosis showing sinus bradycardia with first degree AV block and small QRS voltages (defined as ≤5 mm height), predominantly in the limb leads.

First-degree atrioventricular block has been reported in 56% of patients with ATTR cardiac amyloidosis associated with the Val122Ile variant (38).

Other common features present in the ECGs of patients with cardiac amyloidosis include left anterior hemiblock, ischaemic or non-specific T-wave abnormalities and rhythm disturbances, particularly atrial fibrillation, which has been reported in up to 70% of patients with ATTRwt amyloidosis (39). Ventricular arrhythmias are also common, although the first clinically apparent evidence of an abnormal ventricular rhythm might be ventricular tachycardia or fibrillation in the setting of non-resuscitable cardiac arrest.

Echocardiography

Amyloid deposits can accumulate in cardiac chambers, vessels, and valves, but the infiltrative process is most marked in the ventricular walls, which results in thickened, non-dilated ventricles. The subsequent elevation of pressure in the atria is associated with mild atrial dilatation, because the thickening of the atrial walls by amyloid deposition prevents severe dilatation.

Echocardiography is a useful and widely accessible tool for investigating heart failure. Although echocardiography often provides the first clues to the presence of cardiac amyloidosis, this imaging modality is neither sensitive nor specific for the disorder (6). Typical echocardiographic findings include thickening of ventricular walls, small LV chamber volume, valve thickening, atrial enlargement and signs of elevated filling pressures, such as pericardial and pleural effusions and a dilated vena cava owing to restrictive diastolic filling. A 'granular sparkling' appearance of the myocardium has traditionally been described as a typical sign, but over time has been proved to be a non-specific finding (40). Furthermore, an interventricular septal thickness of > 12 mm in the absence of aortic valve disease or substantial systemic hypertension remains and important echocardiographic feature that is indicative of cardiac involvement in patients with systemic AL amyloidosis (40).

Ejection fraction is typically preserved early in the disease process (41,42), but LV performance deteriorates with disease progression (43). Cardiac amyloidosis characteristically presents as a continuum of diastolic dysfunction that progresses from impaired relaxation to a pseudonormal pattern to a restrictive pattern involving increased deposition of amyloid in the myocardium (44). Stroke volume index and myocardial contraction fraction (ratio of stroke volume to myocardial mass) have

been shown to be better diagnostic markers of cardiac amyloidosis than ejection fraction (42). Myocardial contraction fraction is a volumetric measure of myocardial shortening that is independent of chamber size and geometry, can distinguish physiological from pathological hypertrophy (45) and is highly correlated with global longitudinal strain. In addition, a reduction in peak systolic wall motion velocities, which disproportionately affects the longitudinal rather than the radial axes, presents early in the course of the disease (42). Reduced ejection fraction at diagnosis is more common in patients with ATTR cardiomyopathy with the Val122Ile variant than those with ATTRwt (35), which is likely to reflect a more advanced stage of disease at diagnosis and perhaps accounts for the reduced survival reported in these patients (12).

The majority of conventional echocardiographic parameters have low accuracy for diagnosing cardiac amyloidosis, mostly owing to low sensitivity (46). However, several echocardiographic indices have high specificity, especially the E/E' ratio (>9.6 represents a sensitivity of 50% and specificity of 100%), left atrial volume index (≥47 ml/m^2 represents a sensitivity of 44% and a specificity of 93%) and myocardial contraction fraction (≤0.234 represents a sensitivity of 56% and a specificity of 96%) (47) and therefore might be useful in individuals who potentially have amyloidosis (48). Among the conventional echocardiographic parameters, myocardial contraction fraction has the best diagnostic accuracy, with an area under the curve (AUC) of 0.80 (47).

Longitudinal strain measured using tissue Doppler and echocardiographic speckle tracking have emerged as useful clinical markers of cardiac amyloidosis, which can help distinguish the disease from other causes of wall thickening, such as

hypertension and hypertrophic cardiomyopathy. A longitudinal strain gradient showing relative preservation of function at the apex and substantial impairment of the mid-segments and basal segments is a very consistent and characteristic finding in patients with cardiac amyloidosis (49,50). This phenomenon gives rise to a distinctive "bulls-eye" pattern when the segmental strain is plotted, which is rare in other cardiomyopathies (Figure 3).

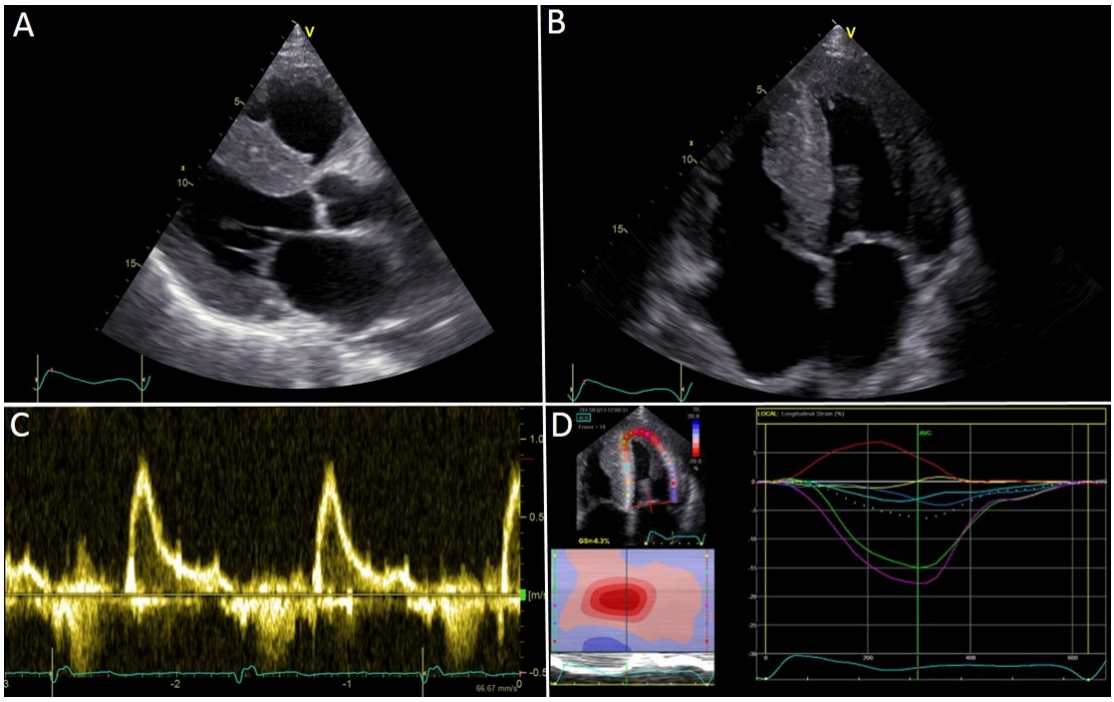

Figure 3. Echocardiography findings in a patient with cardiac ATTR amyloidosis. Parasternal long axis view (A) and four chamber view (B), showing concentric left ventricular hypertrophy; Pulse-wave Doppler showing restrictive flow pattern of left ventricular inflow (C); and strain pattern characteristic of an infiltrative process (D).

Despite the extensive literature on the apical sparing of longitudinal strain in amyloidosis (34,49,51), the pathophysiological mechanism underlying this phenomenon remains unclear. Several mechanisms have been proposed, including the presence of less amyloid deposition in the apex than the base, the diversity in myocardial fibre orientation at the apex and a greater tendency towards apoptosis and

remodelling in the basal segments related to higher parietal stress and turbulent flow (51). Furthermore, deformation-based parameters, such as longitudinal strain, have higher sensitivities and specificities for the detection of ATTR cardiomyopathy. Global longitudinal strain of -15.1 or greater has a sensitivity of 87% and a specificity of 72% for the diagnosis of ATTR amyloidosis, with an AUC of 0.85 (47).

Given the high degree of overlap between the echocardiographic features of cardiac amyloidosis and other cardiomyopathies, echocardiography alone cannot be used to differentiate the many different pathologies associated with increased wall thickness, but should prompt a low threshold for further multimodality assessment.

Cardiovascular magnetic resonance

In the past decade, cardiovascular magnetic resonance (CMR) has emerged as a robust imaging technique that not only provides structural and functional data but, most importantly, also conveys valuable information regarding tissue composition. An exponential increase has been observed in the use of CMR to assess the heart of patients with systemic amyloidosis, with approximately 85% of all publications on this subject arising in the past 10 years alone (52). This increase has largely been driven by the emergence of new CMR sequences and their subsequent technical development, which have led to an increased awareness and recognition of cardiac amyloidosis.

CMR can be used to produce high-resolution, 3D images of the heart and has many advantages over other traditional imaging techniques in that it does not depend on geometry, consistently providing excellent delineation of the endocardium and epicardium (53).

Importantly, CMR can accurately characterise myocardial tissue on the basis of the intrinsic magnetic properties of different tissues (T1, T2 and T2*), without the use of gadolinium-based contrast agents. However, these intrinsic properties can be accentuated by administration of gadolinium-based contrast agents as in the late gadolinium enhancement (LGE) technique and contrast-enhanced T1-weighted imaging for the calculation of extracellular volume (ECV) (54). Gadolinium-based contrast agents accelerate the relaxation of the water molecules present in tissues to give rise to an enhanced signal on T1-weighted images and, together with appropriate sequence parameters, provides improved image contrast (55,56) (Figure 4). Gadolinium chelates are extracellular contrast agents that cannot cross the intact cardiomyocyte cell membrane (57). In the normal myocardium, cardiomyocytes are densely packed, and cardiomyocyte intracellular space forms the greater part (~85%) of the myocardial volume (58). In cardiac amyloidosis, the extracellular space expands owing to increased amyloid deposition, which leads to elevated gadolinium concentrations in the myocardium and, therefore, hyper-enhancement (59).

LGE imaging provides pathognomonic findings with high diagnostic accuracy for cardiac amyloidosis (60,61). Amyloid cardiomyopathy initially presents as a typical pattern of diffuse subendocardial LGE that can become transmural in the later stages of the disease (62). This pattern is coupled with abnormal gadolinium kinetics in the myocardium, nulling before the blood pool (61,63). However, caution should be taken when using protein-bound contrast agents for myocardial enhancement in non-ischaemic cardiomyopathies, because diagnostic performance might not be the same as for non-protein-bound variants (64). Protein-bound contrast agents are partially

'intravascular', and concerns have been raised about their use in the quantification of ECV (65).

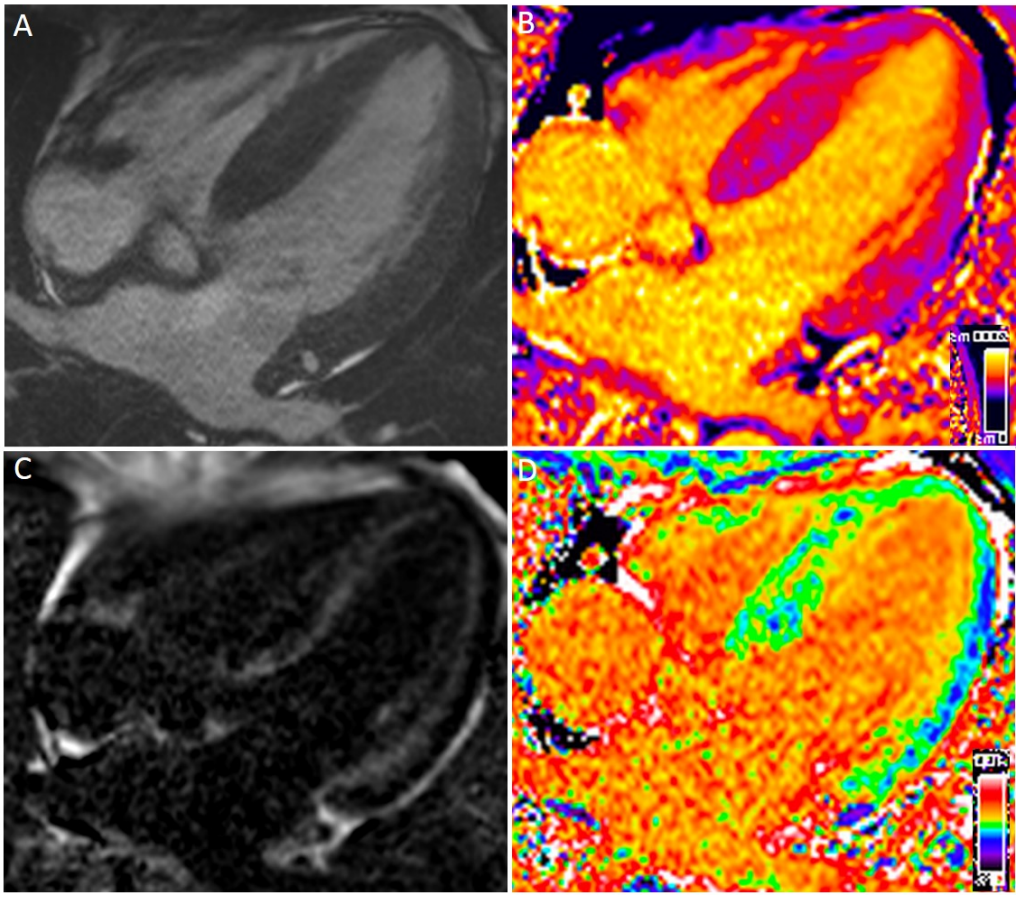

Figure 4. CMR findings in a patient with cardiac AL amyloidosis. Four-chamber SSFP cine (A); corresponding native T1 map (B); corresponding PSIR LGE image showing subendocardial LGE (C); and corresponding ECV map.

Traditional LGE imaging is a thresholding or comparison technique, whereby the operator chooses the null inversion time according to what is considered normal myocardium. By convention, areas with the most contrast should have a bright display, and normal myocardium should be displayed as black on LGE imaging. The accuracy of a chosen null inversion time in a clinical setting depends on operator expertise, clearance rate of the contrast agent, and patient tolerance to additional breath-hold acquisitions (66), which can all vary widely in clinical practice. Nulling the normal myocardium in cardiac amyloidosis can be very challenging because

infiltration is frequently diffuse throughout the myocardium, and areas of normal myocardium might not be available for comparison. For example, the operator might erroneously choose to null the abnormal myocardium and miss the global infiltration (67). Newer techniques, particularly phase-sensitive inversion recovery (PSIR), an LGE image reconstruction technique that is less sensitive to operator choice of null point and can render truly T1-weighted signal intensity, might be more accurate in determining the extent of cardiac involvement (66). Furthermore, PSIR LGE is also easier for the operator than traditional LGE imaging (given that less precision in setting the inversion time is needed) and is available from all manufacturers of CMR systems.

Three LGE patterns are widely recognized in patients with cardiac amyloidosis: no LGE, subendocardial LGE and transmural LGE (67). All of these patterns show good correlation with the degree of myocardial infiltration (68). However, LGE imaging has several limitations, particularly in patients with cardiac amyloidosis, many of whom have severe renal impairment and cannot have gadolinium-based contrast agents (69,70).

T1 mapping, before administration of a contrast agent (71,72), can be used to measure the intrinsic signal from the myocardium (known as native myocardial T1). Coupled with acquisitions performed after administration of the gadolinium-based contrast agent, T1 mapping can be used to calculate myocardial ECV – that is, how much of the extracellular space is occupied by amyloid deposits. Native T1 and ECV are elevated in cardiac amyloidosis (73). In a single-centre study, native myocardial T1 elevation was associated with high diagnostic accuracy for cardiac amyloidosis when the pre-test probability was high (74). A clinical algorithm using native myocardial

T1 has been developed to enable the diagnosis of cardiac amyloidosis without the need for gadolinium-based contrast agent in a large proportion of patients with suspected cardiac amyloidosis (74). Most importantly, native T1 can also be used in patients with severe renal disease, a common comorbidity in those with cardiac amyloidosis (74).

Contrast agent administration and ECV measurement enable isolation of the signal from the extracellular space, but native T1 provides a composite signal from the intracellular and extracellular spaces that is potentially influenced by other pathophysiological mechanisms beyond simple amyloid load. ECV is elevated during early cardiac infiltration before LGE is present, and conventional clinical testing has detected cardiac involvement in patients with high pre-test probability, suggesting that ECV is a better marker of early disease (75). Both native T1 and ECV are predictors of prognosis in patients with AL cardiac amyloidosis (76), but this hasn't been demonstrated in ATTR yet.

Another intrinsic property of the myocardium that can be measured with CMR is T2. High signal on T2 imaging of the heart is indicative of myocardial oedema, typically seen in acute myocarditis, acute infarction or inflammatory cardiomyopathies, such as cardiac sarcoidosis. T2 has been shown to be elevated in patients with AL and ATTR cardiomyopathy, with the greatest elevation of T2 in patients with AL cardiac amyloidosis before starting chemotherapy (77). T2 is also a predictor of mortality in patients with AL cardiomyopathy, lending support to an independent effect of myocardial oedema on outcomes in these patients.

CMR offers extensive structural and functional data, which, when coupled with LGE imaging and mapping (native T1, T2, and ECV), informs our understanding of the different processes underlying the progression of cardiac amyloidosis. These processes include pure amyloid infiltration (assessed by amyloid burden and ECV), myocardial oedema (with T2 being the most specific marker), cardiomyocyte response (calculated using LV mass and ECV) (5) and disease severity (graded with LGE and ECV).

Finally, myocardial perfusion can also be measured by CMR with fully automated myocardial blood mapping (78). Intramyocardial vessels are frequently infiltrated by amyloid, resulting in impaired vasodilatation, which can cause global myocardial

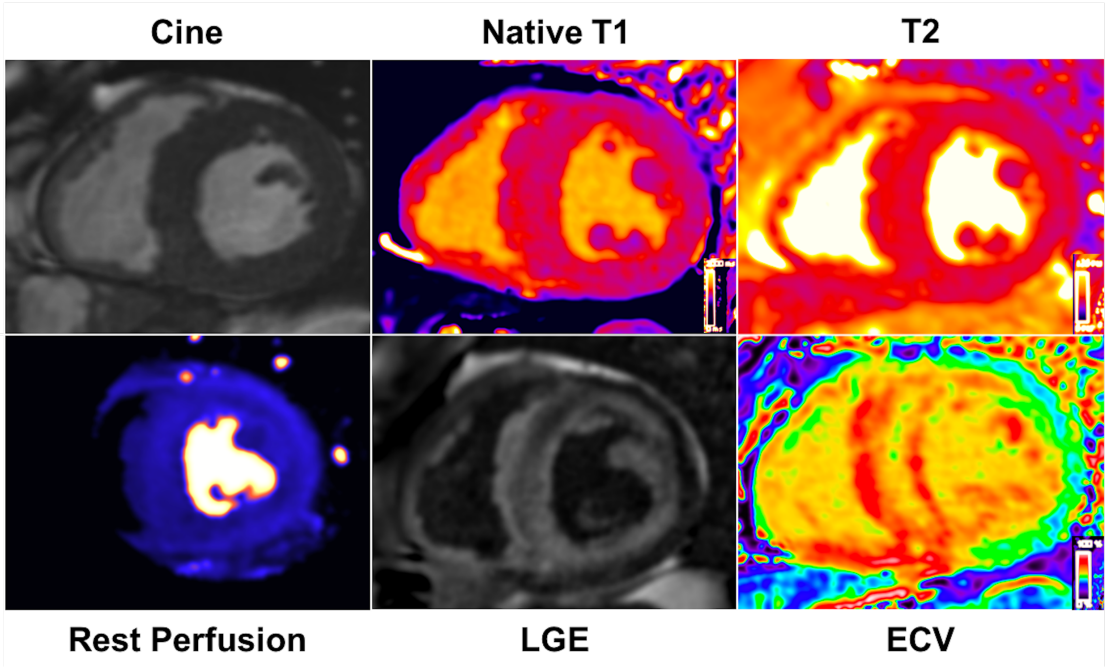

Figure 5. CMR shows different pathophysiological mechanisms in cardiac amyloidosis. Elevation of T1 and T2 seen in oedema. Typical LGE and elevated ECV are markers of amyloid burden. Perfusion at rest demonstrates low myocardial blood flow.

ischaemia (79). Cardiac biomarkers, such as troponin T and NT-proBNP, are known to be constantly elevated in patients with cardiac amyloidosis (80). Myocardial

perfusion at rest could be reduced in patients with cardiac amyloidosis, which might contribute to increased levels of cardiac biomarkers and could have an important role in measuring the response to new amyloid therapies that directly target amyloid deposits in the myocardium (Figure 5).

Radionuclide Bone Scintigraphy

The first nuclear imaging studies using bone-seeking agents in cardiac amyloidosis were performed as early as the 1980s (81), but it was not until 20 years later that Puille and colleagues described the potential use of bone scintigraphy to identify amyloid deposits in patients with ATTR cardiomyopathy (82). The intensity of retention of bone-avid radiotracers in the heart can be interpreted by semi-quantitative visual analysis, by grading myocardial uptake in relation to rib uptake on planar or single-photon emission computed tomography (SPECT) images and by quantifying radiotracer uptake using heart-to-contralateral lung (H/CL) ratio (83). The current diagnostic criteria for patients with ATTR cardiac amyloidosis include visual myocardial uptake equal to or greater than in bone (specifically in the ribs) or an H/CL ratio of ≥1.5 (84). An H/CL ratio of ≥1.6 is associated with poor survival (85).

Perugini and colleagues classified cardiac amyloid uptake on the basis of a simple visual scoring system of the delayed (3h) planar image, in which a grade of 0 means no cardiac uptake, a grade of 1 means mild cardiac uptake (less than in the bone), a grade 2 means cardiac uptake greater than in the bone (but uptake in the bone remains clearly visible) and a grade 3 means substantial cardiac uptake (with a weak or no signal evident in the bone) (86) (Figure 6). Although the basis for localisation of these agents to cardiac amyloid remains unknown, the techniques has been validated and seems to be very sufficiently sensitive to detect early cardiac ATTR amyloid deposits

in asymptomatic individuals in whom echocardiography and gadolinium-enhanced CMR images are normal (87).

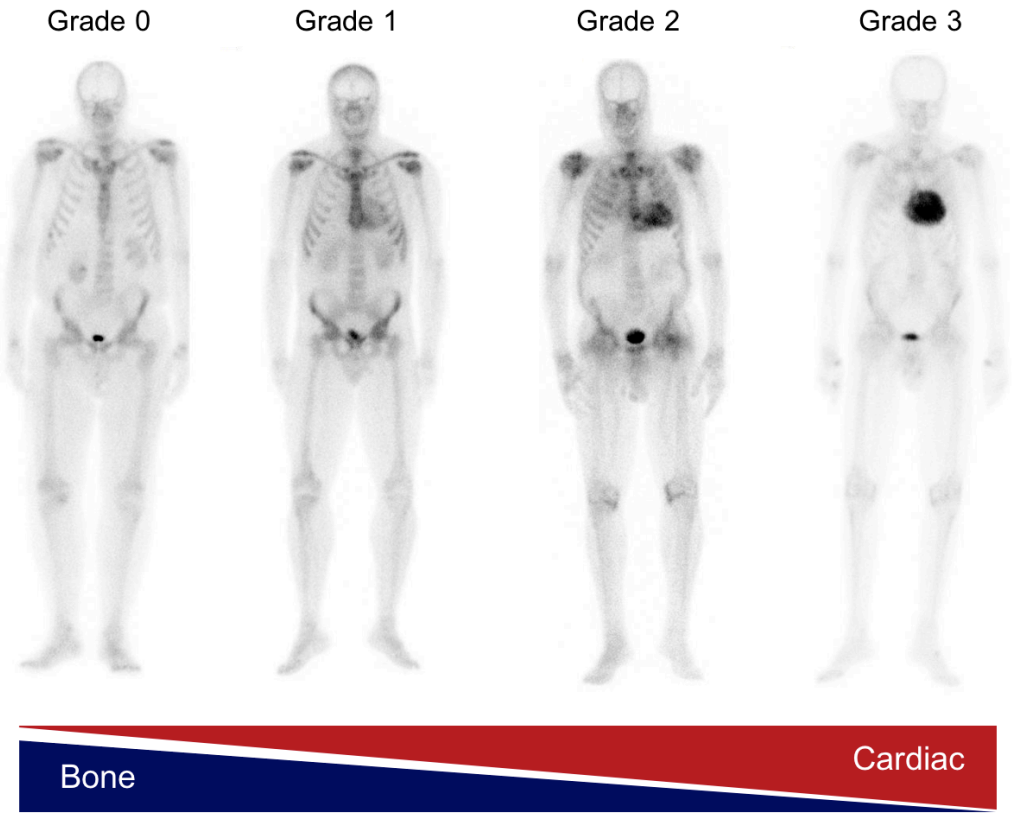

Figure 6. Whole-body Perugini visual scoring of cardiac uptake on 99mTc DPD scintigraphy.

Over the past few decades, different bone tracers, including ^{99m}Tc-pyrophosphate (^{99m}Tc-PYP) (85,88,89), ^{99m}Tc-hydroxymethylene diphosphate (^{99m}Tc-HMDP) (89,90) and ^{99m}Tc-DPD (82,86,87), have been used to detect cardiac amyloidosis with similar diagnostic performance (91). Importantly, however, not all bone tracers are suitable for diagnosing this condition. For example, the widely available bone tracer ^{99m}Tc-methylene diphosphate is considered inappropriate for the evaluation of patients with suspected ATTR cardiac amyloidosis, given its low sensitivity (91). The mechanism underlying the myocardial retention of the different radiotracers remains unknown but

it has been previously attributed to the presence of microcalcification in cardiac tissue that is more common in patients with ATTR amyloidosis than in those with AL amyloidosis (92,93).

Bone scintigraphy with a Perugini grade of 2 or 3 describing myocardial uptake showed a high sensitivity of >99% for ATTR cardiomyopathy but a lower specificity of 82-86%, given that a grade 1 or 2 can be observed in patients with AL cardiomyopathy (94). However, if urine and serum tests are negative for AL amyloidosis, the specificity of the test increases to 100%. Mild uptake of amyloid (grade 1) can also be noted in patients with other subtypes of cardiac amyloidosis, such as serum amyloid A and apolipoprotein A1 (21,95) These findings from studies in the past 5 years have changed the diagnostic pathway of patients with cardiac amyloidosis, such that only a minority of patients with ATTR cardiac amyloidosis require endomyocardial biopsy. In the absence of histological data, ATTR cardiac amyloidosis can be diagnosed with confidence when a patient presents with a clinical phenotype that is associated with echocardiographic or CMR findings consistent with amyloidosis, grade 2 or 3 tracer uptake in the heart on radionuclide bone scintigraphy (Figure 7), and absence of a detectable monoclonal immunoglobulin in the blood and urine using sensitive assays. Histological confirmation and typing of amyloid should be pursued in patients who do not meet all these criteria, most notably those in whom a monoclonal immunoglobulin is detected, which raises suspicion of AL amyloidosis (21). Thereafter, transthyretin genotyping is pertinent to distinguish between ATTRwt and ATTRm.

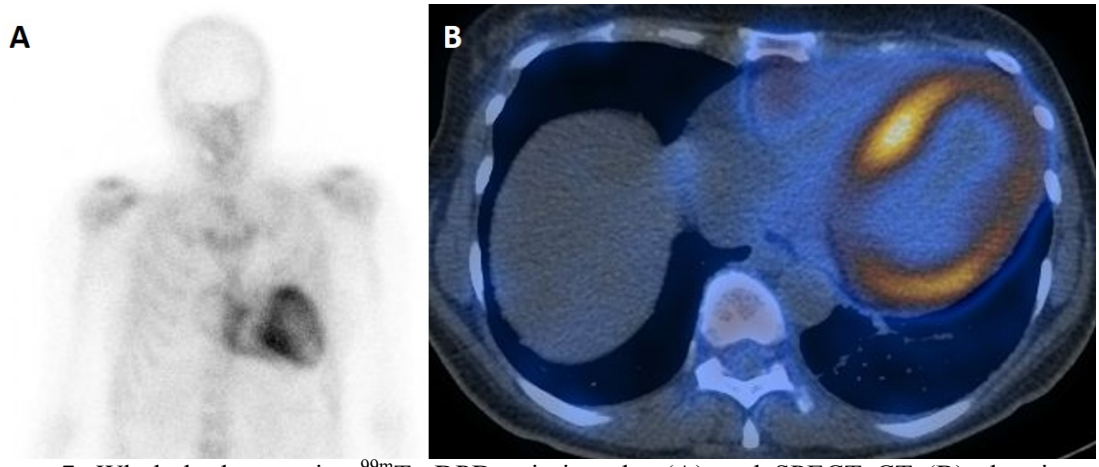

Figure 7. Whole-body anterior ^{99m}Tc-DPD scintigraphy (A) and SPECT CT (B) showing Perugini grade 2 abnormal uptake on a patient with cardiac ATTR amyloidosis.

In addition to its high sensitivity and specificity, quantitative assessment of bone tracer uptake also provides prognostic information. Increased myocardial retention of the different bone tracers is associated with major adverse cardiac events, acute heart failure and increased mortality (84,87,89). However, the comparative performance of the different tracers remains unclear as ^{99m}Tc-PYP is most commonly used in the USA, ^{99m}Tc-HMDP in France and ^{99m}Tc-DPD in other countries including Italy and the UK (85). The importance of low-grade cardiac uptake (in particular grade 1) is also unclear. With widespread availability of expensive new therapies, these questions will become important in considering the cost-benefit of each treatment.

Integration of diagnostic techniques

All the cardiac imaging techniques described need to be interpreted alongside the clinical findings, which can vary from patient to patient. These imaging techniques are not just useful for the diagnosis of cardiac amyloidosis, but can help identify the amyloid type, estimate disease severity, track disease progression, and monitor treatment response. An approach that integrates all imaging modalities with biomarker testing and tissue biopsy is key for the non-invasive diagnosis of suspected cardiac amyloidosis (21).

Table 1 summarises the benefits of the techniques most commonly used at each stage of the diagnostic process for cardiac amyloidosis.

AL cardiac amyloidosis				
	Subclinical	**Early**	**Established**	**Advanced**
Echo	**-**	+	++	++
CMR	+	++	+++	+++
Bone scintigraphy	+	++	+++	+++
ATTR cardiac amyloidosis				
	Subclinical	**Early**	**Established**	**Advanced**
Echo	**-**	+	++	++
CMR	+	++	+++	+++
Bone scintigraphy	+	+	+	+

Table 1: Benefits of imaging techniques at different stages of disease.

Diagnosis in specific populations

Certain populations benefit from exclusion or confirmation of cardiac amyloidosis as a differential diagnosis. Echocardiography is invariably the initial imaging modality used to assess all patients with cardiac symptoms and suspected cardiac amyloidosis, but although echocardiographic data can change the pre-test probability, in many cases, this remains equivocal with non-specific findings.

Elderly patients with unexplained heart failure with preserved ejection fraction.

Heart failure with preserved ejection fraction (HFpEF) currently accounts for up to half of all cases of heart failure (96,97). Importantly, ATTRwt has been proposed as an underdiagnosed disease that accounts for up to 13% of all cases of HFpEF (98). Although overlap between the clinical presentations of ATTRwt and HFpEF is high, several characteristics such as higher biomarker levels in the blood, increased LV mass, the presence of pericardial effusion and a lower voltage-to-mass ratio on the

ECG are clues that should increase the suspicion of ATTRwt in patients with HFpEF. If cardiac amyloidosis (presumably ATTRwt) is suspected in an elderly patient with HFpEF, bone scintigraphy should be performed. The presence of grade 2 or 3 cardiac uptake might indicate a diagnosis of ATTRwt. The presence of plasma cell dyscrasia in the blood or urine should be excluded (to exclude AL cardiac amyloidosis) and gene sequencing should also be performed because the diagnosis of ATTRm has familial implications.

Aortic stenosis.

ATTR cardiac amyloidosis associated with ATTRwt and calcific aortic stenosis is more often seen in elderly individuals. ATTR cardiac amyloidosis has a prevalence of 6-12% in patients with severe aortic stenosis undergoing valve replacement (99,100). The coexistence of these two conditions has several important clinical implications on diagnosis, management, and prognosis (101). Among 151 consecutive patients aged >65 years referred for transcatheter aortic valve implantation (TAVI), ^{99m}Tc-PYP imaging showed that 16% had cardiac uptake consistent with ATTR cardiac amyloidosis, and 62% met criteria for low-flow, low-gradient severe aortic stenosis (102). ATTR cardiac amyloidosis should also be considered when assessing the prognosis in patients who have undergone TAVI and with low-flow, low-gradient aortic stenosis, in whom bone scintigraphy could be routinely used as a screening tool.

LV hypertrophy.

If echocardiographic results raise the suspicion of cardiac amyloidosis, CMR should be considered if both AL and ATTR cardiac amyloidosis or another underlying cause of myocardial hypertrophy (such as hypertrophic cardiomyopathy, hypertensive heart

disease or Anderson-Fabry disease) are within the differential diagnosis (Figure 8). CMR has good sensitivity for both types of cardiac amyloidosis (67,68) and can also identify other common causes of LV hypertrophy (103). If the CMR findings are indicative of cardiac amyloidosis, serum-free light chains, serum and urine immunofixation and bone scintigraphy should be considered to differentiate between AL and ATTR amyloidosis. Grade 2 or 3 uptake on bone scintigraphy coupled with no evidence of a plasma cell dyscrasia in either blood or urine is highly specific for ATTR (21).

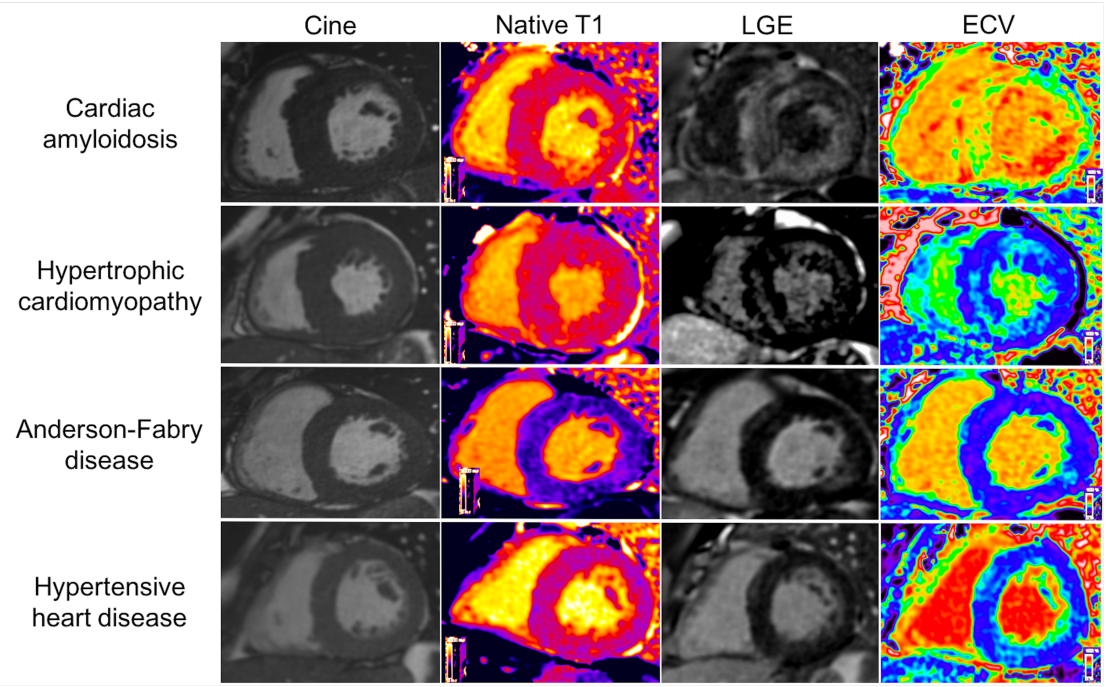

Figure 8. CMR findings in left ventricular hypertrophy. Short axis cine, native T1, late gadolinium enhancement (LGE) and extracellular volume in four different pathologies that cause left ventricular hypertrophy. Native T1 values are elevated in cardiac amyloidosis, hypertrophic cardiomyopathy and hypertensive heart disease, but reduced in Anderson-Fabry disease. This pattern of LGE is characteristic of cardiac amyloidosis (diffuse subendocardial, transmural at the basal septum), whereas patchy LGE in the septum is indicative of hypertrophic cardiomyopathy, and mid-wall LGE in the basal inferolateral wall is suggestive of Anderson-Fabry disease. ECV values are characteristically and diffusely high in cardiac amyloidosis but in the other pathologies are elevated only in the areas with LGE.

African American individuals aged >60 years with unexplained heart failure and LVH.

The clinical presentation of African American individuals with heart failure often includes salt-sensitive hypertension, diabetes mellitus, and LV hypertrophy (104). Cardiac amyloidosis, in particular ATTRm associated with the Val122Ile variant, might go undiagnosed when the clinician attributes ventricular hypertrophy or heart failure to other prevalent pathologies, such as hypertension, diabetes and obesity. Considering the heterogeneous presentation and relentless progression of this disease, diagnosis is often delayed until late stages. Bone scintigraphy and CMR should be considered to confirm the diagnosis of cardiac amyloidosis, whereby CMR can also identify other common or rare phenocopies of cardiac amyloidosis. To make the diagnosis of ATTR cardiomyopathy, plasma cell dyscrasia in the blood or urine has to be ruled out because AL cardiomyopathy is a possible, but unlikely diagnosis. Genetic sequencing of *TTR* should be performed to confirm the Val122Ile mutation.

Cardiac involvement in systemic AL amyloidosis.

If AL cardiac amyloidosis is suspected (evidence of plasma cell dyscrasia with suggestive findings on echocardiography or evidence of AL amyloidosis on extra-cardiac biopsy sample), CMR is the modality of choice to confirm cardiac involvement with high specificity and sensitivity (61,105,106). CMR can also detect early cardiac infiltration in AL amyloidosis that occurs before hypertrophy and can sometimes identify atypical manifestations, such as ventricular dilatation.

Cardiac involvement in individuals with known or suspected hereditary amyloidosis.

Bone scintigraphy and CMR should be considered in asymptomatic patients with ATTRm or patients with ATTRm and associated polyneuropathy. However, the data for these patient groups are limited, and further studies are required to confirm the sensitivity and specificity of the tests for this subgroup of patients.

Patients with previous carpal tunnel syndrome.

Patients with ATTR cardiac amyloidosis present with symptoms of carpal tunnel syndrome approximately 5-15 years before the onset of cardiac symptoms. Carpal tunnel syndrome has a reported prevalence of 39-46% in patients with ATTR cardiomyopathy (29,107). In a small study in 98 patients undergoing carpal tunnel release surgery, amyloid deposits were found in the tenosynovial tissue in ten patients, two of whom were found to have cardiac involvement (108). A 2019 study found that carpal tunnel syndrome is associated with a 12-fold increased risk of amyloidosis but that the absolute incidence of diagnosed amyloidosis is low (109). Therefore, carpal tunnel syndrome might not warrant direct referral for further evaluation of amyloidosis but could instead be considered as a red flag and an opportunity for early disease detection (109).

Treatment

Supportive

Patient education and multidisciplinary care are essential. Maintenance of euvolemia is central to management. Salt and fluid restriction, daily weights, and titrating combinations of different types of diuretic are key to managing heart failure symptoms.

There are no guideline-based recommendations for angiotensin-converting enzyme, angiotensin receptor blockers, or angiotensin receptor-neprilysin inhibitor therapies in cardiac amyloidosis, and such medications may not be well tolerated because they commonly reduce cardiac output and worsen symptoms.

Orthostatic hypotension can be treated with midodrine and compression stockings, whereas fludrocortisone merely tends to exacerbate fluid retention.

Disease-modifying treatment for AL amyloidosis

The mainstay of treatment in AL amyloidosis is chemotherapy directed towards the underlying clonal plasma cell population. The past decade has seen many new drugs developed for multiple myeloma being adopted for treatment of AL amyloidosis, although few randomised controlled trials have been performed in the latter. Frequent monitoring of serum free light chains enables the haematological response to be ascertained, and ineffective treatment to be modified rapidly. Whilst median survival has nearly doubled over the past decade, nearly 25% of patients die within months of diagnosis.

Bortezomib, a proteasome inhibitor used alone or usually in combination with other agents, has emerged as the most widely used first line treatment in AL amyloidosis, and is associated with haematological response rates of up to 90%, with 60% achieving complete response or very good partial response (110). No particular regimen has yet been shown to be superior in very high-risk (stage IIIb) patients (111,112).

Other combination regimens may be more appropriate in patients with significant peripheral or autonomic neuropathy, given the potential neurotoxicity of bortezomib, and in patients with underlying lymphoplasmacyctic lymphoma.

High-dose melphalan with autologous stem cell transplantation is associated with the most durable remissions, but strict selection of patients is paramount due to the risk of treatment-related mortality among older and sicker patients, including those with advanced cardiac or autonomic nerve involvement (113).

Disease-modifying treatment for ATTR amyloidosis

Treatment of patients with hereditary ATTR amyloidosis remains unsatisfactory.

Liver transplantation to remove the source of variant TTR was the treatment of choice in younger patients with early neuropathy associated with the Val30Met variant. It can be beneficial in some patients with other TTR mutations, but cardiac amyloidosis present at the time of liver transplantation continues to progress relentlessly in most cases. Liver transplantation to treat ATTRm has dramatically decreased with the advent of TTR stabilizers and is not indicated for ATTRwt.

Cardiac disease is the dominant feature of ATTRwt and V122I-related ATTR amyloidosis, and rare younger patients can do very well after cardiac transplantation. Most patients however are too old for this to be feasible.

There are numerous pharmacological strategies under development for ATTR amyloidosis:

Diflunisal: is a nonsteroidal anti-inflammatory drug that has been repurposed as a TTR stabilizer. It binds within the 2 thyroxine binding sites. In a phase III, randomized, placebo controlled trial of patients with ATTRm polyneuropathy, diflunisal (250 mg orally twice daily) improved symptoms of neuropathy versus placebo (15). The experience with diflunisal in ATTR cardiomyopathy has been limited to open-label, single-centre studies (114-116). Diflunisal (250 mg orally twice daily) was generally well tolerated, with side effects in a minority of subjects, including thrombocytopenia and renal dysfunction. Diflunisal is currently available for off-label use with limited data in ATTR cardiomyopathy.

Tafamidis binds the thyroxine-binding sites of TTR with high affinity and selectivity, slowing dissociation of TTR tetramers into monomers, which inhibits their aggregation. Tafamidis was shown to slow the progression of peripheral neuropathy in ATTR polyneuropathy (117), leading to its approval for the treatment of stage 1 and 2 ATTRm polyneuropathy in numerous countries. The ATTR-ACT (ATTR-CM Phase 3 Clinical Trial) study (118) compared tafamidis meglumine (20 or 80 mg) with placebo in 441 subjects with ATTR cardiomyopathy due to ATTRwt or ATTRm (16). Tafamidis treatment resulted in lower all-cause mortality than placebo, with a 13.4% absolute difference in mortality and a 32% relative risk reduction in cardiovascular hospitalisations. This translated into a number needed to treat of 7.5 to prevent 1 death after 2.5 years of treatment. Tafamidis treatment resulted in a lower rate of decline in the 6-min walk test ($p < 0.001$) and in the Kansas City Cardiomyopathy Questionnaire score ($p < 0.001$). Across 11 subgroups, the point estimates for the hazard ratios favoured tafamidis over placebo, except for the subjects in NYHA functional class III at baseline, for whom the rates of cardiovascular-related hospitalisations were higher among patients who received tafamidis. Tafamidis is

licensed for the treatment of ATTR cardiomyopathy but it is only funded in certain countries (USA and Japan). Tafamidis is presently under regulatory review by the National Institute for Clinical Excellence (NICE) for ATTR cardiomyopathy in the UK.

Patisiran: is a small-interfering RNA that specifically targets TTR mRNA, which leads to its degradation and lowering of TTR protein levels. Phase I and phase II studies of patisiran in healthy volunteers and in patients with ATTRm polyneuropathy showed a dose-dependent and robust mean reduction in serum TTR levels of up to 90% (119). In the APOLLO trial (A Phase 3 Multicenter, Multinational, Randomized, Double-blind, Placebo controlled Study to Evaluate the Efficacy and Safety of Patisiran [ALN-TTR02] in Transthyretin [TTR]-Mediated Polyneuropathy [Familial Amyloidotic Polyneuropathy-FAP]) 225 patients with ATTRm polyneuropathy underwent randomization 2:1 to receive patisiran (n = 148) or placebo (n = 77) at a dose of 0.3 mg/kg every 3 weeks for 18 months. Patisiran therapy was effective, with a highly significant difference in the change in the modified Neuropathy Impairment Score +7 after 18 months. Patisiran is currently approved and funded for the treatment of ATTRm polyneuropathy. In a cardiac subpopulation of the APOLLO trial, patisiran reduced mean LV wall thickness, increased end-diastolic volume, improved global longitudinal strain, and increased cardiac output at month 18 compared with placebo (120).

Inotersen: is a 20-O-methoxyethyl–modified antisense oligodeoxynucleotide that lowers hepatic production of TTR. NEURO-TTR (A Phase 2/3 Randomized, Double-Blind, Placebo-Controlled Study to Assess the Efficacy and Safety of ISIS 420915 in Patients with Familial Amyloid Polyneuropathy) was a phase III trial in adults with

stage 1 or 2 ATTRm polyneuropathy who received inotersen (300 mg subcutaneously weekly) or placebo in a 2:1 randomization. The primary endpoint included change in the modified Neuropathy Impairment Score +7. Primary efficacy assessment favoured inotersen. Inotersen is currently approved and funded for the treatment of ATTRm polyneuropathy. An open-label study of inotersen in 22 patients with ATTR cardiomyopathy, 15 of whom had completed 12 months of follow-up, demonstrated stabilization of disease as measured by LV wall thickness, LV mass, 6-min walk test, and global strain on echocardiography (121).

Immunotherapy

Therapeutic antibodies have potential to target amyloid deposits directly. Mu11-1F4 is a chimeric antibody that binds to many AL fibrils and has lately completed phase I clinical trial (122). A phase I/II study of another monoclonal antibody, NEOD001 (Onclave Therapeutics Limited, California) has also recently been completed in patients with AL amyloidosis, reporting good safety and tolerability and a suggestion of cardiac improvement. A global phase III randomized trial is currently in progress.

Serum amyloid P component binds to all amyloid fibrils in vitro and protects them from degradation. (R)-1-[6-[(R)-2-carboxy-pyrrolidin-1-yl]-6-oxo-hexanoyl] pyrrolidine-2-carboxylic acid (CPHPC) efficiently depletes SAP from the blood but leaves some SAP in the amyloid deposits. SAP in the amyloid deposits can then be specifically targeted by fully human monoclonal anti-SAP antibodies. Results of a phase 1 trial using the obligate combination of these agents yielded promising results showing marked and rapid reduction in amyloid deposits in the liver and elsewhere (123). No serious adverse events were observed. A phase II study to investigate patients with cardiac amyloidosis is in progress.

Given these emerging therapies, it is crucial that we have methods to accurately assess disease response.

CHAPTER 2: MATERIAL AND METHODS

Declaration

I have designed the studies, and carried out the data collection and analysis of the data. I collected the data and performed the statistical analysis in my role as a clinical research fellow at the National Amyloidosis Centre, University College Medical School (Royal Free Campus). Several diagnostic methods were carried out by other individuals in the department. They were as follows:

- Histological and immunohistochemical analyses were performed by Janet Gilbertson.
- Gene sequencing was performed by Dorota Rowczenio and Hadija Trojer.
- Echocardiography was performed by Babita Pawarova, Sevda Ward, Cecil Tabardero, and Brooke Douglas.
- ^{123}I-SAP scintigraphy and ^{99m}Tc-DPD scintigraphy were performed by David Hutt.
- Measurement for biochemical and haematological data was performed by the Royal Free Hospital laboratory services. Blood tests were performed on the same visit to the National Amyloidosis Centre, typically the same day or the before than the CMR study. N-Terminal pro-B-type natriuretic peptide was measured with an electrochemiluminescence sandwich immunoassay on the Elecsys system 2010 (Roche Diagnostics). High-sensitivity troponin T assay was performed with a second-generation assay after 16 December 2015, and prior to that, with a first-generation TnT assay.

Patients

Most patients included in this thesis were seen at the UK National Amyloidosis Centre. An Access database has been kept up to date with details of patients who have been referred to the NAC with suspected amyloidosis. All the patients included within the database have given explicit informed consent. Appropriate processes have been put in place to maintain patient confidentiality and conform with good clinical practice. All data will be stored and backed up on secure servers maintained by UCL Information Services Division (Research Data Services) and will be handled in compliance with UCL data policies, systems and procedures (ISO/IEC 27001 compliant).

Forty-four patients who fulfilled diagnostic criteria of hypertrophic cardiomyopathy (defined by the presence of increased ventricular wall thickness or mass in the absence of loading conditions such as hypertension or valvular disease sufficient to cause the observed abnormality) were included for chapter 5 (124).

Twenty-four patients with ATTR cardiac amyloidosis were recruited at Puerta de Hierro University Hospital in Madrid, Spain, between March and June 2018 for chapter 6.

Twenty-three healthy volunteers (control subjects) with no symptoms and no past history of cardiovascular disease, hypertension or diabetes were also recruited and underwent CMR only for chapter 7. Healthy volunteers were recruited by advertising in the Royal Free Hospital, without constraints.

Cardiac Assessment

Assessment of cardiac amyloidosis is performed using a combination of clinical parameters, serum biomarkers, and imaging modalities.

All patients referred to the centre with suspected cardiac amyloidosis underwent blood tests to assess cardiac biomarkers, as well as electrocardiography, echocardiography, CMR, and ^{99m}Tc-DPD scintigraphy.

Functional Assessment

Functional evaluation of patients was performed using a combination of subjective and objective parameters. New York Heart Association Classification (NYHA) was used to assess for symptoms of heart failure (Table 2: NYHA Classification). A history entailing baseline exercise tolerance is taken during the clinical consultation and for all patients able to perform it, a 6 minute walk test (6MWT) is completed with both a total number of metres walked and the percentage predicted for age calculated. 6MWT is performed according to standardised criteria (125) and has been shown to be a valuable measure of functional change in patients with systemic amyloidosis (126).

Table 2: NYHA Classification

NYHA Class	**Description**
Class 1	No symptoms and no limitation is ordinary physical activity, e.g. shortness of breath when walking, climbing stairs etc.
Class 2	Mild symptoms (mild shortness of breath and/or angina) and slight limitation during ordinary activity.

Class 3	Marked limitation in activity due to symptoms, even during less than ordinary activity, e.g walking short distances (20-100m). Comfortable only at rest.
Class 4	Severe limitations. Symptoms even while at rest. Mostly bedbound patients.

Echocardiography

Echocardiography was performed in all patients with two-dimensional, M-mode, Doppler settings using a GE Vivid 7 system. Parasternal long axis and apical long axis views were most commonly used. Evaluation of left ventricular wall thickness, left ventricular diastolic function, left ventricular systolic function, and atrial dimensions were measured using defined criteria from the British Society of Echocardiography (http://www.bsecho.org). Left atrial area was measured using criteria defined by the American Society of Echocardiography (http://www.asecho.org).

Cardiovascular Magnetic Resonance Protocol

All patients underwent CMR at 1.5T (Magnetom Aera, Siemens Healthcare, Erlangen, Germany). Scans were performed in accordance with local protocols.

Pilot images

All studies started with single shot pilot images with the following settings: repeat time (TR): 3.39ms, echo time (TE): 1.7ms, slice thickness, 5mm, field of view (FOV) 360 x 360mm, read matrix 256 and flip angle 60^{o}.

Cine imaging

After acquisition of pilot images, steady state free precession (SSFP) cine imaging was then undertaken, firstly in the long axis planes with a short axis cut through the aortic valve. A standard LV short axis stack was acquired using a slice thickness of 7mm with a gap between slices of 3mm. Retrospective ECG gating was used with 25 phases. Typical fast imaging with steady state precession (FISP) imaging parameters were TE: 1.6ms, TR: 3.2 ms, in plane pixel size 2.3 x 1.4mm, slice thickness 7mm, flip angle 60^{o}. These settings were optimized accordingly if the subject was unable to breath-hold or had an arrhythmia.

Native T1 mapping

T1 is the longitudinal, or spin-lattice, relaxation time of a tissue. T1 relaxation times can be estimated by acquiring multiple T1-weighted images and fitting the resulting signals to an appropriate exponential recovery curve. Each tissue type has a specific range of normal T1 values, deviation from which may indicate disease or a change in physiology. Myocardial T1 values are influenced by technical factors, such as magnetic field strength and the pulse sequence design, and physiological factors, including heart rate, temperature, age, gender, and disease (65). Advances in CMR imaging techniques over the last few years have made it feasible to quantify T1 in the myocardium and to generate colour-encoded T1 maps, in which the pixel values represent the T1 in each voxel. Native (pre-contrast) T1 measures of the myocardium permit non-invasive detection of biologically important processes, and in doing so, promise to improve diagnosis, and measures of disease severity and potentially those of prognosis (65).

A variety of techniques have been used to quantify myocardial T1 relaxation times. The most widely used clinical technique for T1 mapping to date is the Modified Look-Locker inversion recovery (MOLLI) sequence. In MOLLI, single-shot images are acquired intermittently in diastole during 3 to 5 heartbeats after the inversion pulse, resulting in images spaced by the RR-interval along the T1 recovery curve. A limitation of the standard MOLLI pulse sequence is the need to acquire data over 17 heartbeats, which may be too long of a breath-hold duration for some patients. The MOLLI variation 5(3)3 was used in some of the studies in this thesis. These numbers represent the number of images acquired after each inversion, and the number in parentheses represent the number of heartbeats for rest period between inversion recovery pulses. This acquisition only requires 11 heartbeats (127).

A further shortening of the acquisition time is achieved with the Shortened Modified Look-Locker (ShMOLLI) technique. ShMOLLI has a 5(1)1(1)1 acquisition strategy (3 Look-Locker cycles over 9 heartbeats) (128).

Pre-contrast (native) T1 maps of the 4-chamber long-axis view were acquired using the ShMOLLI and the modified look-locker inversion recovery sequence (MOLLI) after regional shimming (129). Because both MOLLI and to lesser extent ShMOLLI are sensitive to heart rate, in patients with arrhythmias the trigger delay was adjusted manually.

T2 mapping

T2, or the transverse (spin-spin) relaxation time, is the time constant governing the exponential decay of transverse magnetization. Similar to T1 values, T2 values represent a global signal from both intracellular and extracellular components. Each

tissue type has a normal range of T2 values, and increased T2 values typically indicate an increase in water content.

T2 maps of the 4-chamber long-axis matching the T1 maps were acquired using an investigational prototype (WIP 448B, Siemens Healthcare, Erlangen, Germany). This sequence uses 3 single-shot T2 prepared steady state free precession (SSFP) readouts each separated with 3 heartbeats for T1 recovery (54). The echo times (TE) for the individual T2 preparations were 0, 25, and 45ms. A monoexponential fit to a 2-parameter model, S=PDexp (-TE/T2), was used at each pixel to estimate proton density (PD) and T2.

Rest Perfusion imaging

Basal, mid-ventricular, and apical short-axis perfusion images were acquired at rest. The sequence used utilised a dual sequence approach with separate pulse sequences for AIF and myocardial tissue. Image acquisition was performed over 60 heart beats with a bolus of 0.1mmol/kg gadoterate meglumine (Dotarem, Guerbet SA, Paris, France) administered at 4 ml/sec followed by a 20 ml saline flush during acquisition of the perfusion sequence. The arterial input function (AIF) was calculated using the left ventricular (LV) blood pool signal which was automatically segmented from optimised low-resolution images acquired in parallel with higher spatial resolution images used for measuring myocardial perfusion. In order to achieve an accurate estimation of the gadolinium concentration from the AIF signal a number of steps were taken in the design of the sequence protocol and image reconstruction (78). In brief, the sequence uses a low flip angle FLASH low resolution protocol for AIF imaging with 2 echoes such that the echo times were short to minimize T2* losses at high concentration, and so that remaining T2* losses could be estimated and

corrected. The non-linearity of saturation recovery was minimized by using a short saturation delay achieved using a small matrix and parallel imaging to reduce the number of phase encoding lines. The remaining non-linear response was corrected by converting to gadolinium concentration units by means of a look-up table calculated by a Bloch simulation of the specific imaging protocol, which was recalculated for each scan as part of the image reconstruction. Myocardial perfusion was then calculated using a blood tissue exchange model (130) and pixel-wise perfusion maps were automatically generated in-line.

Rest perfusion maps were analysed using offline using Osirix MD 9.0 (Bernex, Switzerland). A region of interest was draw in the basal septum to assess the myocardial blood flow (MBF) in ml/g/min.

Early gadolinium enhancement (EGE) imaging

Following acquisition of rest perfusion images, EGE assessment was undertaken using a free breathing motion corrected phase sensitive inversion recovery (PSIR) sequence. Typical parameters were: Slice thickness 8 mm, TR: 9.8 ms, TE: 4.6ms, α: 21o, FOV 340 x 220 mm (transverse plane), sampled matrix size 256 x 115-135, 21 k–space lines acquired every other RR interval (21 segments with linear reordered phase encoding), spatial resolution 1.3 x 2.1 x 8 mm. These parameters were optimised according to individual patient characteristics. Early gadolinium images of the 4, 2, and 3-chamber long-axis views were acquired to confirm the presence or absence of intraventricular thrombus.

Late gadolinium enhancement (LGE) imaging

LGE was acquired with magnitude reconstruction and with phase sensitive inversion recovery (PSIR) reconstruction. Typical parameters were: slice thickness 8 mm, TR: 9.8 ms, TE: 4.6ms, α: 21o, FOV 340 x 220 mm (transverse plane), sampled matrix size 256 x 115-135, 21 k–space lines acquired every other RR interval (21 segments with linear reordered phase encoding), spatial resolution 1.3 x 2.1 x 8 mm. These parameters were also optimised according to individual patient characteristics. The inversion time (TI) was manually set to achieve nulling of the myocardium between 300 and 440 ms. When LGE was observed, images were acquired in phase swap and crosscut to ensure artefact elimination.

Extracellular volume (ECV) mapping

The myocardial ECV (the interstitial and intravascular compartments) can be measured using T1 mapping, an extracellular gadolinium based contrast agent, and the haematocrit. For blood, the ECV can be determined by a blood test:

$$ECV_{blood} = 100 - \text{haematocrit } [\%]$$

When T1 is measured in the myocardium and blood, both pre- and post-administration of an extracellular gadolinium based contrast agent, myocardial ECV is related to blood ECV according to the following formula (54):

$$ECV = \frac{\left(\frac{1}{T1_{myo\ postGD}} - \frac{1}{T1_{myo\ native}}\right)}{\left(\frac{1}{T1_{blood\ postGD}} - \frac{1}{T1_{blood\ native}}\right)} * (100 - \text{haematocrit})$$

After administration of contrast (0.1mmol/kg gadoterate meglumine [Dotarem, Guerbet SA, Paris, France]), and acquisition of EGE and LGE imaging, the T1 measurement was repeated with the ShMOLLI or MOLLI sequence, using exactly the same parameters than in the pre-contrast acquisition.

Cardiovascular Magnetic Resonance Image Analysis

All CMR images and maps were analysed offline. T1 and T2 measurements were performed by drawing a region of interest in the basal to mid septum of the appropriate 4-chamber map. For the ECV measurement, a single region of interest was drawn in each of the 4 required areas: myocardial T1 estimates (basal to mid septum in the 4-chamber map) and blood T1 estimates (LV cavity blood pool in the 4-chamber map, avoiding the papillary muscles) before and after contrast administration. Haematocrit was measured in all subjects immediately before each CMR study. ECV was calculated as: myocardial ECV = (1-haematocrit) x (Δ R1myocardium/ ΔR1blood), where R1=1/T1.

Before our adoption of phase-sensitive inversion recovery (PSIR) reconstruction for all amyloidosis patients, because myocardial nulling can be difficult in the presence of amyloid, any confusion with magnitude reconstruction images was resolved by selecting the images that most matched the post-contrast T1 maps, with bright LGE expected to correlate with areas of the lowest post-contrast T1 (i.e., the highest gadolinium concentration, the highest interstitial expansion).

The LGE pattern was classified into 3 groups according to the degree of transmurality: group 1, no LGE; group 2, subendocardial LGE (when there was global subendocardial but no transmural LGE); and group 3, transmural LGE (when the LGE

extended transmurally). A study was classified by the most extensive LGE identified. Thus, a patient with basal transmural LGE but apical subendocardial LGE would be classified as transmural (67).

Total amyloid volume was measured with the formula: total amyloid volume = ECV x LV myocardial volume (where LV myocardial volume was calculated as LV mass / 1.05).

^{99m}Tc-DPD scintigraphy

Subjects were scanned with hybrid single-photon emission computed tomography (SPECT) computed tomography (CT) gamma cameras after administration of 700 MBq of intravenously injected ^{99m}Tc-DPD. Whole-body planar images were acquired after 3 hours, followed by SPECT of the heart coupled with a low-dose, non-contrast CT scan (95). Gated and non-gated cardiac SPECT reconstruction and SPECT-CT image fusion were performed on the Xeleris workstation (GE Healthcare, Wauwatosa, Wisconsin). Cardiac retention of ^{99m}Tc-DPD was scored visually according to the grading devised by Perugini et al (86) using the following grading system: grade 0, absent cardiac uptake; grade 1, mild cardiac uptake less than bone; grade 2, moderate cardiac uptake equal or greater than bone; and grade 3, intense cardiac uptake associated with substantial reduction or loss of bone signal.

SAP scintigraphy

SAP scintigraphy was performed in patients with AL amyloidosis at baseline and during their follow up after receiving chemotherapy. Each subject undergoing SAP scintigraphy received approximately 200μg of SAP with 190MBq of ^{123}I, the equivalent of 3.8mSV of radiation. Thyroid uptake was blocked by the administration

of 60mg of potassium iodine immediately prior to the study and 5 further doses were given over the following three days. Anterior and posterior imaging was performed at either 6 or 24 hours after injection using an IGE-Starcam gamma-camera (IGE Medical Systems, Slough, UK). Female patients were asked to confirm that they were not pregnant prior to undergoing SAP scintigraphy.

Amyloid load was classified according to 4 criteria: normal, small, moderate, and large. 'Normal' was defined as no evidence of abnormal tracer location. 'Small' was defined as uptake in one or more organs whilst still maintaining normal intensity in the blood pool and 'moderate' when uptake was seen in one or more organs and the blood pool was diminished. 'Large' was defined as uptake in one or more organs with no evidence of tracer in the blood pool despite adjustment of the grey scale to encompass the visceral organs involved.

Progression of amyloid by SAP scintigraphy was defined as an increment within the 4 category staging system and regression of amyloid by SAP scintigraphy was defined as a decrement within the categorical staging of amyloid load.

Gene sequencing

Genotyping was performed in patients with suspected ATTR cardiac amyloidosis. Whole blood taken in an EDTA tube was frozen and stored for gene sequencing as required. Genomic DNA was isolated by a rapid method. The blood was added to NH_4CL and spun; the sample was then re-suspended in 0.9% NaCl and re-spun. It was then suspended again in 0.05M NaOH, incubated, cooled, and neutralised with 1M Tris pH8. Polymerase chain reaction (PCR) using 'Ready-To-Go' tubes (GE

Heathcare) were used to amplify the coding regions for tranthyretin genes (exons 2, 3, and 4).

Statistical analysis

Statistical analysis was performed using IBM SPSS Version 24 (IBM, Somers, New York) and MedCalc 13.2.1.0 (Ostend, Belgium). All continuous variables were tested for normal distribution (Shapiro-Wilk test). Normally distributed metrics are summarized by the mean ± standard deviation (SD) and non-normally distributed metrics as median (interquartile range). Statistical tests performed for each study are outlined in each results chapter.

CHAPTER 3: CMR-VERIFIED REGRESSION OF CARDIAC AL AMYLOID AFTER CHEMOTHERAPY

This chapter is based on the publication below:

Martinez-Naharro A, Abdel-Gadir A, Treibel TA, Zumbo G, Knight DS, Rosmini S, Lane T, Mahmood S, Sachchithanantham S, Whelan CJ, Lachmann HJ, Wechalekar AD, Kellman P, Gillmore JD, Moon JC, Hawkins PN, Fontana M. CMR-Verified Regression of Cardiac AL Amyloid After Chemotherapy. *JACC Cardiovasc Imaging*. 2018 Jan;11(1):152-154. doi: 10.1016/j.jcmg.2017.02.012.

My contribution to this work was analysing all the data as first operator, doing the statistical analysis, and writing the paper.

Introduction

Systemic light-chain (AL) amyloidosis is a complication of clonal B-cell disorders, which is characterised by deposition in the interstitial space of aggregated misfolded monoclonal immunoglobulin light chains (LC) in the form of amyloid fibrils. The presence and severity of cardiac involvement in AL amyloidosis is the main driver of prognosis (131). Patients with cardiac AL amyloidosis and symptomatic heart failure frequently die in less than 6 months (131), but median survival has nearly doubled over the past decade, mainly due to the remarkable progress in chemotherapy. The direct effect of chemotherapy, i.e. the hematologic response, is predominantly evaluated by serial measurements of serum free light chains (132).

Plasma concentration of B-type natriuretic peptides and echocardiographic parameters are currently the reference standard for assessing cardiac responses (133), but neither directly quantifies the amyloid burden (134). Both B-type natriuretic peptide and myocardial strain are markers of prognosis in cardiac AL amyloidosis (133), but represent processes downstream of amyloid deposition, with B-type natriuretic

peptide confounded by renal impairment (135) and strain not well standardized and affected by changes in preload and afterload.

Cardiovascular magnetic resonance (CMR) with tissue characterization is a sensitive tool for characterizing myocardial amyloid deposits: late gadolinium enhancement (LGE) shows a continuum of cardiac infiltration, from subendocardial LGE to increasing transmurality as the disease progresses (67). T1 mapping can distinguish and measure the myocyte and extracellular amyloid compartments separately (5,20,72,76). Native myocardial T1 and extracellular volume (ECV) measurements have been shown to track clinical disease in cardiac amyloidosis, and improve diagnostic accuracy and patient stratification (72,134,136-139). SAP scintigraphy can specifically quantify amyloid in non-cardiac organs. Several studies have shown turnover and regression of amyloid deposits from the liver, kidneys and elsewhere with corresponding clinical benefit in terms of organ function and survival as well as the relation of this process to production of the amyloid fibril precursor protein (140-145).

However the usual lack of significant structural and functional changes on conventional echocardiography after successful chemotherapy has led to the common belief that regression of myocardial amyloid takes place either extremely slowly or not at all (146).

The aim of this study was to evaluate cardiac AL amyloid serially using state of the art cardiovascular MR (CMR) including measurements of the myocardial extracellular volume (ECV), which is the site of the amyloid deposits.

Methods

Setting and study design

A retrospective study of patients with biopsy proven AL amyloidosis undergoing chemotherapy. The study group comprised all consecutive patients diagnosed with cardiac AL amyloidosis who underwent serial CMR evaluation with T1 mapping (at least 2 CMR scans) as well as comprehensive clinical assessment (ECG, echocardiogram, CMR, SAP scintigraphy, and NT-proBNP measurements) at the National Amyloidosis Centre, Royal Free Hospital, London, UK from 2011 to 2015. The clonal hematologic response was evaluated using repeated serum and urine electrophoresis and immunofixation and serum free light chain (FLC) measurements, according to international consensus criteria. Normal FLC levels with normal kappa/lambda ratio and negative serum and urine immunofixation was considered a complete response (CR), a reduction in the dFLC (the difference in concentration between the aberrant versus uninvolved class of light chain) to <40 mg/L a very good partial response (VGPR), >50% reduction in dFLC was a partial response (PR), and no response (NR) was less than PR (i.e. a <50% reduction in dFLC) (30,40).

Echocardiography acquisition and analysis

Echocardiographic assessments were performed using a Vivid E9 ultrasound machine (GE, Healthcare, Milwaukee, Wisconsin, USA). Image quality was optimised by adjusting probe frequency (range 1.7-2.0MHz), utilising high frame rates (60-120 s-1), and acquisition during quiet respiration. LV structure, systolic, and diastolic assessment were performed according to published recommendations (147-149). Pulse wave Tissue Doppler velocity was measured in the septal and lateral mitral annulus region in the 4-chamber view to obtain peak systolic (S'), peak early diastolic (e') and peak late diastolic (a') tissue velocities; septal and lateral velocities were

averaged to obtain a mean value. Myocardial strain assessment was performed with appropriate image optimisation. 2-3 cardiac cycles of all views were digitally stored for offline analysis using standard software (EchoPac PC dimension software version 112, GE Healthcare).

All the echocardiogram analysis was performed blinded to CMR results. Myocardial deformation was assessed using speckle tracking. The LV was divided into 6 segments in each of the long axis (LAX) views. The endocardium was manually traced in each segment and a region of interest (ROI) automatically generated to cover the myocardium. The ROIs were adjusted to optimise the tracking quality if needed.

SAP scintigraphy acquisition and analysis

All patients underwent whole body anterior and posterior scintigraphic imaging 24 h after administration of ^{123}I-labeled serum amyloid P component (SAP) using a GE Infinia Hawkeye gamma camera (GE Healthcare, Iowa, MN) as previously described (140-145,150). The amyloid load was categorized according to the intensity of ^{123}I-SAP uptake in the organs and the residual blood-pool signal at 24 hours after tracer injection.

CMR Image Acquisition and Analysis

All subjects underwent CMR on a 1.5-T clinical scanner (Avanto or Aera, Siemens Healthcare, Erlangen, Germany). Within a conventional clinical scan (pilots, transverse white and black-blood images, SSFP-cines images to assess volumes and mass), LGE imaging was acquired with both magnitude inversion recovery (MAG-IR) and phase-sensitive inversion recovery (PSIR) sequence reconstructions with either FLASH or SSFP read-outs. T1 measurement was performed with the use of the Modified Look-Locker inversion (MOLLI) recovery sequence or the Shortened Modified Look-Locker inversion (ShMOLLI) recovery sequence. A single region of

interest covering the basal and mid inferoseptum in the 4-chamber view was drawn. After a bolus of gadoterate meglumine (0.1 mmol/kg, gadolinium-DOTA, Dotarem, Guerbet S.A. France) and LGE imaging, ECV was measured as previously described (54). Total amyloid volume was measured with the formula total amyloid volume = ECV x LV myocardial volume (where LV myocardial volume was calculated as LV mass x 1.05). The LGE pattern was classified by 2 different observers (A.M.N. and M.F.) blinded to the other data into 3 groups according to PSIR LGE transmurality: group 1, no LGE; group 2, subendocardial LGE only; and group 3, transmural LGE (Figure 9).

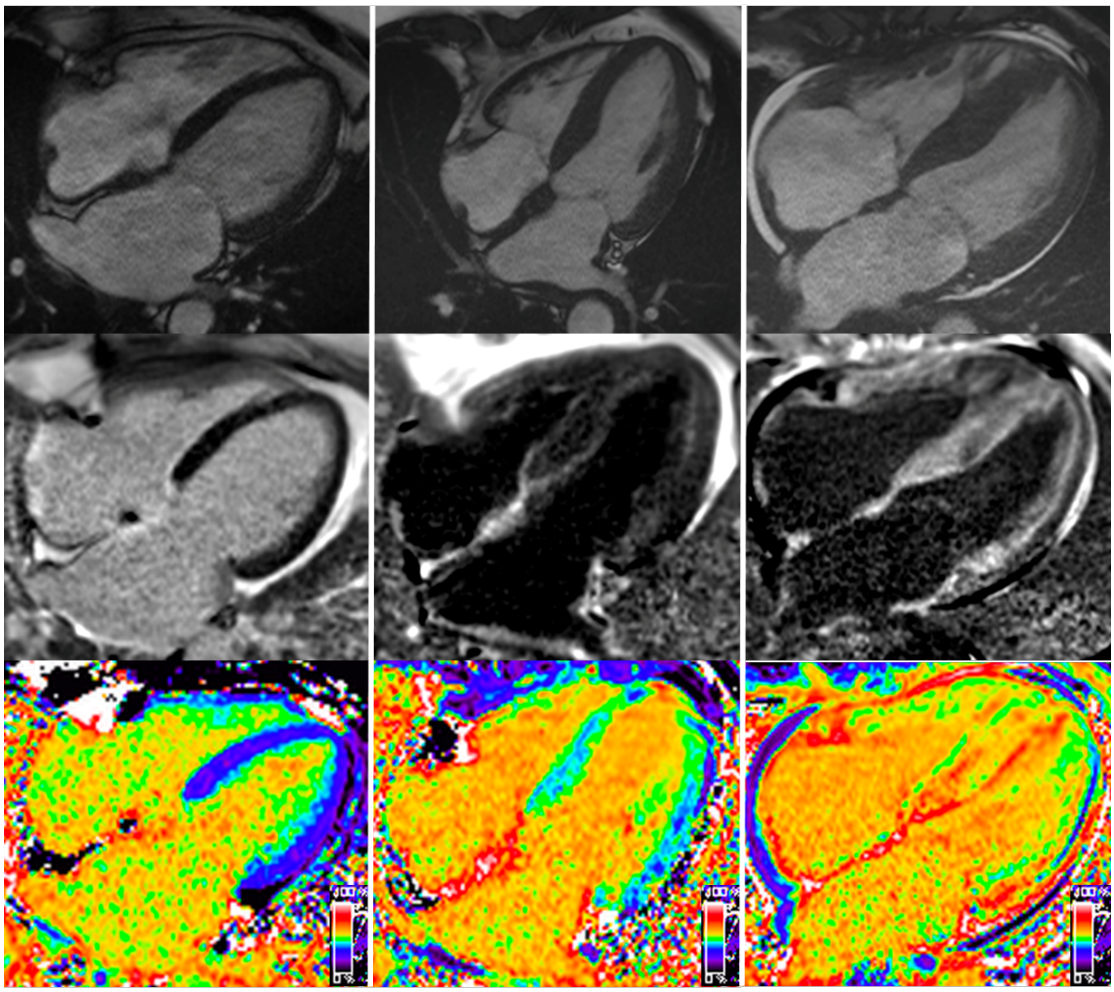

Figure 9. Four-chamber SSFP cine image in diastole of three patients (top); corresponding late gadolinium enhancement image (middle) showing no LGE (middle left), subendocardial LGE (centre) and transmural LGE (middle right); and corresponding ECV maps (bottom).

Regression in the cardiac amyloid burden was considered when there was a significant decrease in ECV, defined here as a fall of 2SD from the mean ECV for this cohort of amyloid patients (0.05). This is greater than the reported reproducibility for ECV (129). Changes in the visceral amyloid burden were assessed using SAP scintigraphy.

Statistical Analysis

Statistical analysis was performed using IBM SPSS Statistics Version 22 (IBM, Somers, New York). All continuous variables were normally distributed (Shapiro-Wilk), other than NT-proBNP, which was ln transformed for bivariate testing. These are presented as mean ± standard deviation (SD) with non-transformed NT-proBNP presented as median and interquartile range. Comparisons between groups were performed by unpaired T test; the χ^2 test or Fisher exact test was used to compare discrete data, as appropriate. Statistical significance was defined as $p < 0.05$. To assess the agreement of the assignment of the LGE pattern by 2 different observers, the intraclass correlation coefficient was calculated. Statistical significance was defined as $p<0.05$.

Results

Study Population and baseline characteristics

Demographic and clinical features of the patient cohort are summarized in

Table 3.

Thirty-one patients with biopsy proven systemic AL amyloid were included (21 male, 68%; age 61±9 years). The mean interval between the serial assessments was 20±11months.

At baseline, the overall prevalence of LGE was 27 of 31 (87%) patients with an average ECV of 54±11%. Three patterns of LGE are observed: no LGE; subendocardial LGE and transmural LGE, (figure 1). The pattern of LGE was transmural in 9 subjects (29%) and subendocardial in 18 (58%); four patients (13%) had no LGE. There was good agreement in the assignment of these patterns between two observers (ICC 0.92, 95% CI 0.87-0.95).

Table 3: Baseline characteristics, biomarkers, echocardiographic and CMR parameters in patients with AL amyloidosis

Characteristics	**TOTAL (N=31)**
Sex	
Men	21
Women	10
Age (y)	61± 9
eGFR (mL/min/1.73m^2)	76 ± 17
Biomarkers	
NT-proBNP (pmol/L)	182 (86-302)
Echocardiographic parameters	
E wave (m/s)	0.91 ± 0.21
A wave (m/s)	0.55 ± 0.26
Average E' (m/s)	0.07 ± 0.03
E/E'	16 ± 8
DT (msec)	176 ± 46
MA Sa (cm/s)	0.07 ± 0.02
TA Sa (cm/s)	0.12 ± 0.03
2D GLS	-13 ± -4
CMR parameters	
LVEDV (mL)	125 ± 26
LVESV (mL)	46 ± 16

Maximal IVS (mm)	14 ± 4
LV mass (g)	187 ± 64
SV (mL/m^2)	79 ± 20
LVEF (%)	64 ± 10
LA area (cm^2)	27 ± 5
MAPSE (mm)	9 ± 3
TAPSE (mm)	15 ± 5
ECV	0.54 ± 0.11
Total amyloid volume (ml)	104 ± 48

AL, light-chain amyloidosis; eGFR, estimated glomerular filtration rate; NT-proBNP, N-terminal pro-B-type natriuretic peptide; DT, deceleration time; MA Sa, mitral annulus systolic velocity; TA Sa, tricuspid annulus systolic velocity; GLS, global longitudinal strain; LVEDV, left ventricular end-diastolic volume; LVESV, left ventricular end-systolic volume; IVS, interventricular septum; LV, left ventricle; SV, stroke volume; LVEF, left ventricular ejection fraction; LA, left atrium; MAPSE; mitral annulus plane systolic excursion; TAPSE, tricuspid annulus plane systolic excursion; ECV, extracellular volume.
All continuous variables are presented as mean and standard deviation with non-transformed NT-proBNP presented as median and interquartile range.

Chemotherapy treatment and haematological response

Twenty-nine patients maintained a stable clonal response throughout the period between the first and second scan having received combination chemotherapy that included one or more of the following drugs; thalidomide, bortezomib, lenalidomide, melphalan and dexamethasone. Ten achieved a CR, 8 a VGPR and 7 achieved a PR (133). Four of 26 patients did not achieve a clonal response despite receiving ongoing chemotherapy (five cycles of cyclophosphamide, bortezomib and dexamethasone in one patient, three cycles of cyclophosphamide, thalidomide and dexamethasone in another, and lenalidomide and dexamethasone in the third case). Two patients had a variable response to treatment during the period between the two scans; one was in a VGPR for 24/30 months of the interval between scans before losing a degree of response (to PR) and the other was in a PR for 20/37 months of the interval between scans but achieved a VGPR with bortezomib and lenalidomide chemotherapy, 17 months before the follow up scan. These two patients were classified as having achieved a VGPR and PR respectively.

The overall haematologic response rate was 61% (19 patients), and the categorization of haematologic response in the whole cohort was therefore CR in 36% (10 patients), VGPR in 29% (9 patients), and PR or NR in 39% (12 patients).

CMR findings: amyloid regression

Thirteen patients had a measurable regression by CMR (classified by reduction in ECV): 6 of the 10 (60%) attaining a CR, 6 of the 9 (67%) in VGPR and 1 of the 8 (13%) in PR. There was no regression in patients on the NR category. The prevalence of regression was significantly higher in patients in CR/VGPR versus patients in PR/NR ($p < 0.01$). Patients with no haematological response did not show evidence of amyloid regression (Figure 10).

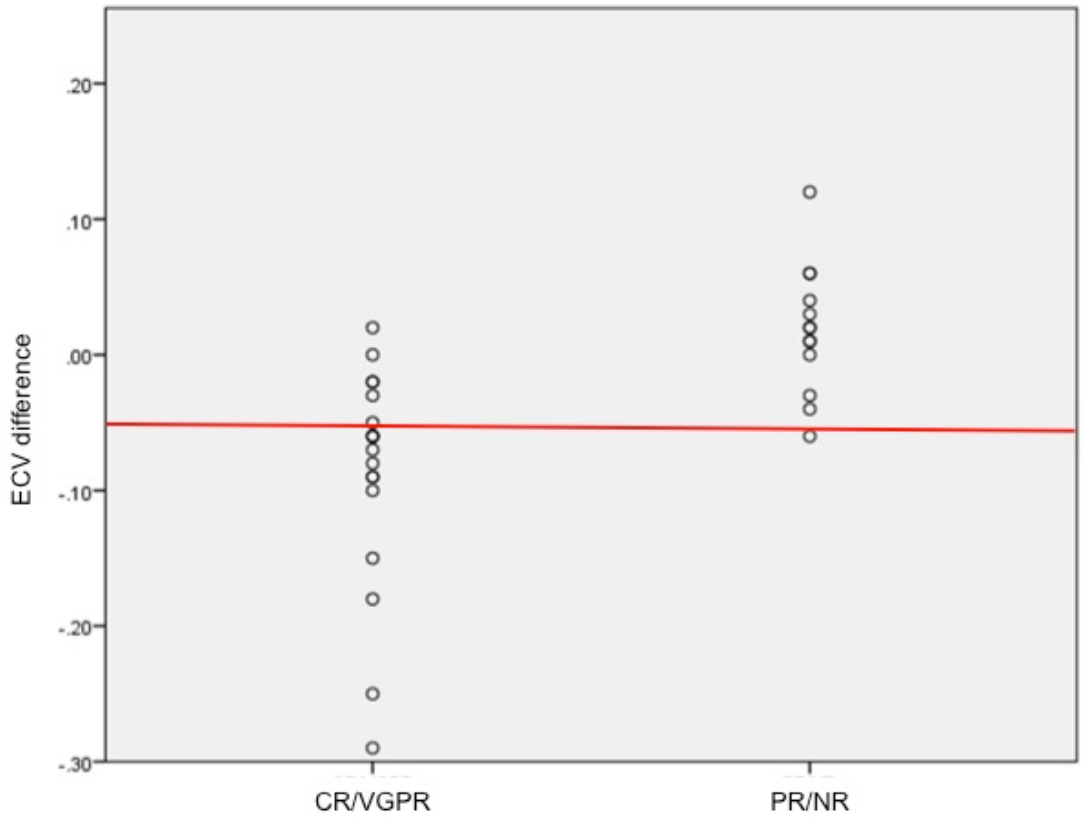

Figure 10. Dotplot showing the difference of ECV before and after chemotherapy and type of clonal response in the 31 AL amyloidosis patients. The red line indicates a significant reduction in ECV (difference of -5%).

Changes in the ECV consistent with regression of amyloid were concordant with the changes with reduction in amyloid volume. The mass changed concordantly in 7 of the 13 patients (54%) whose amyloid regressed and the LGE pattern changed in 5 (38%). In one patient the LGE pattern went from transmural to subendocardial and in 4 from subendocardial to no LGE (Figure 11). More than 30% reduction in NT-proBNP levels was present in 9 (69%) of the patients with amyloid regression.

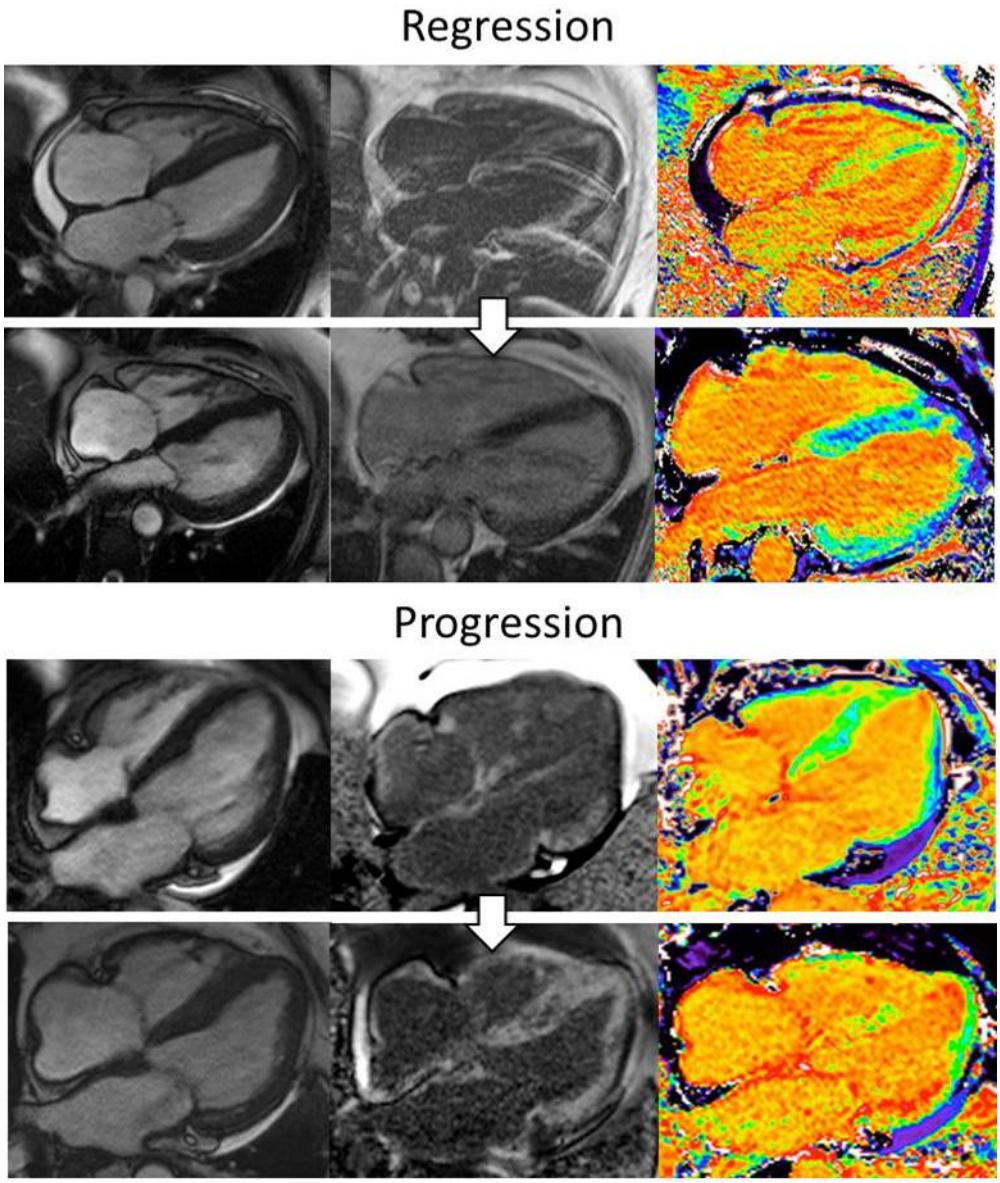

Figure 11. Four-chamber image (left); corresponding LGE image (middle) and ECV mapping (right) before and after chemotherapy in two patients, one regressor by CMR (top) and one that progressed by CMR (bottom).

Overall regression of amyloid was associated with improvements in NT-proBNP, LV mass, left atrial area and diastolic function parameters (Table 4). Regression of cardiac amyloid by CMR correlated with regression of visceral (non-cardiac) amyloid measured by SAP scintigraphy (Figure 12). By contrast, among patients whose ECV did not diminish ("non-regressors"), there were deteriorations in parameters of LV and RV systolic function and maximal wall thickness.

Table 4: Biomarkers, echocardiographic and CMR findings in patients with AL according to amyloid burden regression by CMR.

	Regressors N = 13			**Non-regressors N = 18**		
	First scan	Second scan	p	First scan	Second scan	p
Clonal response	CR = 6 (46%) VGPR = 6 (46%) PR = 1 (8%) NR = 0 (0%)			CR = 4 (22%) VGPR = 3 (17%) PR = 7 (39%) NR = 4 (22%)		
Biomarkers						
NT-proBNP (pmol/L)	251 (96-416)	52 (18-212)	**0.021**	182 (97-272)	255 (91-402)	0.239
Echocardiographic parameters						
E wave (cm/s)	9.0 ± 2.4	7.7 ± 2.6	**0.010**	9.2 ± 1.9	8.3 ± 2.1	**0.046**
A wave (cm/s)	6.0 ± 1.7	6.7± 1.3	0.183	5.2 ± 3.2	5.3 ± 2.8	0.898
E/A	1.60 ± 0.69	1.18 ± 0.40	0.105	2.90 ± 2.98	2.02 ± 1.33	0.128
Average e' (cm/s)	6 ± 3	7 ± 3	0.323	7 ± 3	7 ± 2	0.229
E/e'	17 ± 9	12 ± 5	**0.006**	14 ± 6	15 ± 6	0.783
DT (ms)	195 ± 39	200 ± 63	0.752	163 ± 47	185 ± 54	0.098

MA Sa (cm/s)	7 ± 2	8 ± 2	0.151	7 ± 2	7 ± 3	0.790
TA Sa (cm/s)	13 ± 4	12 ± 4	0.792	12 ± 2	11 ± 4	**0.016**
2D GLS	-14 ± 4	-15 ± 4	0.086	-13 ± 4	-12 ± 5	0.368
CMR parameters						
LV mass (g)	178 ± 43	162 ± 38	**0.027**	193± 76	200 ± 84	0.391
Maximal IVS (mm)	14 ± 4	14 ± 4	0.487	14 ± 4	15 ± 5	**0.010**
LVEDV (mL)	121 ± 21	126 ± 25	0.269	128± 29	123 ± 33	0.351
LVESV (mL)	40 ± 10	41 ± 15	0.782	50 ± 19	54 ± 21	0.270
LVEF (%)	66 ± 7	67 ± 8	0.633	62 ± 11	57 ± 11	**0.0001**
LA area (cm^2)	27 ± 4	23 ± 4	**0.001**	27 ±5	26 ± 6	0.187
RA area (cm^2)	24 ± 4	23 ± 4	0.508	26 ± 6	26 ± 7	0.524
MAPSE (mm)	8 ± 2	10 ± 3	0.192	9 ± 3	8 ± 3	0.463
TAPSE (mm)	14 ± 4	15 ± 5	0.079	16 ± 5	14 ± 6	**0.029**

AL, light-chain amyloidosis; NT-proBNP, N-terminal pro-B-type natriuretic peptide; DT, deceleration time; MA Sa, mitral annulus systolic velocity using spectral pulse wave tissue Doppler imaging; TA Sa, tricuspid annulus systolic velocity using spectral pulse wave tissue Doppler imaging; GLS, global longitudinal strain; IVS, interventricular septum; LVEDV, left ventricular end diastolic volume; RVESV, right ventricular end systolic volume; LVEF, left ventricular ejection fraction; LA, left atrium; RA, right atrium; MAPSE, mitral annular plane systolic excursion; TAPSE, tricuspid annular plane systolic excursion; ECV, extracellular volume. All continuous variables are presented as mean and standard deviation with non-transformed NT-proBNP presented as median and interquartile range

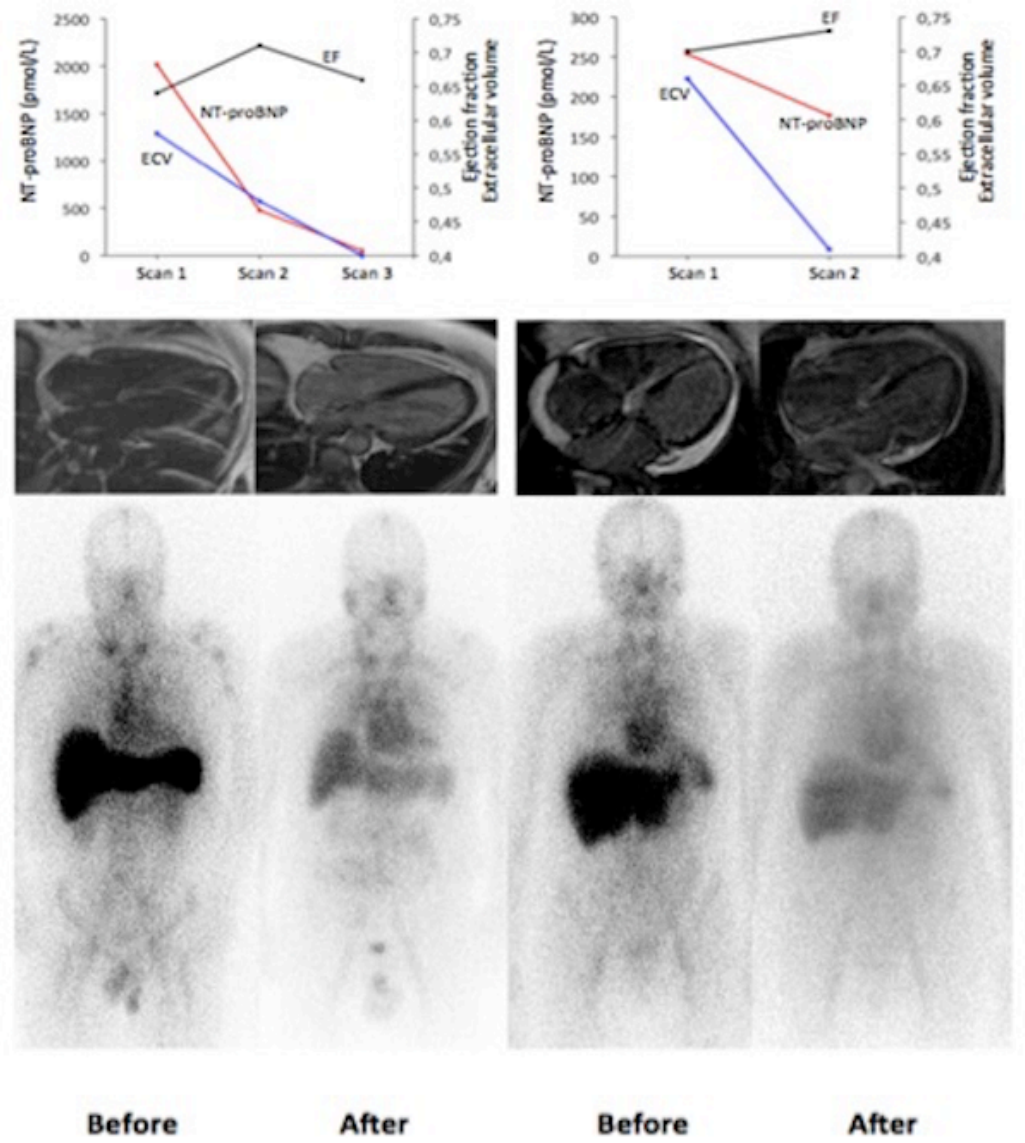

Figure 12. Response to chemotherapy in two patients whose amyloid regressed. Panels A and B show serum concentrations of NT-proBNP, ECV and ejection fraction by CMR. C and D show LGE images at baseline and follow-up scans. E and F show anterior SAP scintigraphy.

Discussion

The remarkable progress in drug therapies developed for multiple myeloma has translated into improved outcomes in AL amyloidosis (151). Median survival in patients with AL amyloidosis has nearly doubled over the past decade (4) but mortality in the first year after diagnosis remains unchanged at approximately 45%, reflecting the high incidence of advanced cardiac involvement. There are two interrelated measures of response to treatment in AL amyloidosis: the haematologic and organ responses, i.e. suppression of the underlying clonal B-cell disorder (and hence reduced production of amyloid-forming immunoglobulin light chain protein), and the consequent benefit of reduced amyloid formation in terms of amyloidotic organ function. The measurement of serum free light chains has proven to be a robust marker of clonal disease response and a very good partial response, currently defined as dFLC (the difference in concentration between the aberrant versus uninvolved class of light chain) less than 40 mg/L, or better is associated with much improved survival (152,153). Cardiac organ response has historically been sought using echocardiography, but improvements are seldom evident, even after prolonged periods. Cardiac organ response is mostly now sought by reduction in serum NT-proBNP concentration, which surprisingly often falls within just weeks to months after a substantial haematologic response has been achieved. The early rapid decrease in NT-proBNP is thought to more greatly reflect diminished cardiotoxicity resulting from reduced abundance of harmful pre-fibrillar light chain aggregates than a reduction in myocardial amyloid burden. Whatever the mechanism, falls in NT-proBNP concentration of 30% or 300 ng/L from baseline following a clonal response to chemotherapy are associated with favourable clinical outcomes (154,155). Whilst SAP scintigraphy is unable to image amyloid in the moving heart, this and other

clinical measurements have confirmed that extra-cardiac amyloid deposits, for example in the liver, spleen and kidneys, are often gradually cleared when the supply of the respective amyloid precursor protein is substantially reduced. The characteristic absence of echocardiographic improvements under these circumstances has engendered the belief that cardiac amyloid, in contrast, may only stabilize following successful chemotherapy (155).

The emergence of advanced myocardial tissue characterization by magnetic-resonance, specifically T1 mapping with native T1 and ECV measurements has made it possible to estimate cardiac amyloid load *in vivo* for the first time. The serial CMR studies we report here compellingly demonstrate that substantial regression of cardiac amyloid following an adequate response to chemotherapy is a relatively common phenomenon, happening in 42% of our patient's population. Our results confirm the importance of achieving a good haematological response, as the prevalence of amyloid regression was significantly higher in patients attaining a CR/VGPR compared to patients attaining only a PR or NR but also show the great potential of CMR to shed light on the cardiac response to treatment. We also demonstrated substantial reduction in cardiac amyloid burden combined with improvement in NT-proBNP, LV mass, left atrial area, and diastolic function parameters.

Whilst reduction in native T1 and ECV could in part be related to reduction in myocardial oedema, which has been postulated to contribute to remarkably high native T1 values during phases of rapid amyloid accumulation, the magnitude of reduction in native T1 and ECV, and reversal of LGE pattern provide compelling evidence of cardiac amyloid regression. Furthermore, the improvements indicated by CMR correlate with evidence of regression of visceral amyloid measured by SAP

scintigraphy, which has been validated in over 30,000 patient studies in our centre over the past 30 years.

These results could have immediate clinical implications for the management of patients with AL amyloidosis. Chemotherapy improves survival in patients with systemic AL amyloidosis, but chemotherapy is associated with substantial toxicity; mortality is highest during the first 3 months of treatment. Tracking changes in cardiac amyloid burden could redefine cardiac response to treatment, acknowledging that long term studies remain required to correlate changes in cardiac amyloid load with overall survival. It is possible that the ability to demonstrate evidence of cardiac amyloid regression in patients who have had a suboptimal clonal disease response, i.e. to identify individuals with greater capacity to clear amyloid, could identify patients with lower risk of progression and better prognosis and in whom the need to intensify chemotherapy may not be required.

The development of immunotherapies to promote regression of amyloid is well advanced (122,156). At least three antibody therapies are currently in clinical trial, one of which that targets the SAP present in all types of amyloid has already been confirmed to trigger rapid clearance of amyloid in the liver and kidney. The ability to measure changes in cardiac amyloid load over time could be of great value as an endpoint in early stage drug development and dose ranging.

This study has several limitations. First, this is a retrospective analysis of a small patient cohort with different time intervals between the first and follow-up scans, with the second scan always performed after completion of treatment. We therefore do not have information on how quickly it may be possible to identify regression of amyloid or on other changes that might occur in the myocardium during treatment, for example the possibility of reactive oedema. Patients underwent different

chemotherapy regimens, but there is no evidence to date that suggests different treatments of the underlying clonal disease have any direct influence on clearance of amyloid. There is a survival bias in that we quote only subjects with paired scans – it may be that the extent of differences are underestimated if, for example, PR or NR subjects who amyloid accumulate die before follow-up scanning. Finally, two different T1 mapping techniques were used during the period in which these patients were recruited.

The findings of this study shed new light on the pathophysiology and natural turnover of cardiac amyloid, demonstrating a dynamic process that encourages efforts to achieve early deep clonal responses and development of new treatments to accelerate the endogenous amyloid clearing process.

CHAPTER 4: MAGNETIC RESONANCE IN TRANSTHYRETIN CARDIAC AMYLOIDOSIS.

This chapter is based on the publication below:

Martinez-Naharro A, Treibel TA, Abdel-Gadir A, Bulluck H, Zumbo G, Knight DS, Kotecha T, Francis R, Hutt DF, Rezk T, Rosmini S, Quarta CC, Whelan CJ, Kellman P, Gillmore JD, Moon JC, Hawkins PN, Fontana M. Magnetic Resonance in Transthyretin Cardiac Amyloidosis. *J Am Coll Cardiol*. 2017 Jul 25;70(4):466-477. doi: 10.1016/j.jacc.2017.05.053

My contribution was analysing all the data as first operator, doing the statistical analysis, and writing the paper.

Introduction

Cardiac transthyretin amyloidosis (ATTR) is a progressive and fatal form of amyloidosis caused by extracellular deposition of amyloid fibrils from liver-derived transthyretin (TTR) (157). ATTR may be hereditary, in which genetic variants of TTR are implicated and are associated with the overlapping syndromes of familial amyloid cardiomyopathy and familial amyloid polyneuropathy, or it may be sporadic, associated with deposition of wild-type transthyretin as amyloid. The latter predominantly involves the hearts of older individuals and the disorder is also known as senile systemic amyloidosis. At autopsy, cardiac ATTR amyloid deposition can be remarkably common, present in up to 25% of individuals older than 80 years (18). Conversely, cardiac ATTR is rarely diagnosed during life, but greater awareness and better imaging methods have increased its recognition lately among elderly patients with left ventricular hypertrophy (LVH) and in specific at-risk ethnic populations (17).

Diagnosing cardiac ATTR amyloidosis is challenging. A suggestive constellation of electrocardiography, echocardiography, and biomarker findings are present in advanced disease, but interpretation may be confounded by common comorbidities such as hypertensive heart disease, diabetes, diastolic dysfunction, and renal disease (22,158,159). Bone tracer scintigraphy, using ^{99m}Tc-3,3-diphosphono-1,2-propanodicarboxylic acid (^{99m}Tc-DPD), ^{99m}Tc-pyrophosphate (^{99m}Tc-PYP), and ^{99m}Tc-hydroxymethylene diphosphonate (^{99m}Tc-HMDP), has recently emerged as a sensitive tool for the identification of cardiac ATTR (21,84,160). However, this nuclear medicine method is typically only performed to confirm ATTR when a clinical suspicion exists, as it does not provide information on any of the other differentials of LVH, cardiac morphology, or function, and is semi-quantitative only (161), a limitation given the development of therapies able to stop or remove cardiac amyloid deposits (4).

In the past decade, CMR has emerged as a robust imaging technique that provides detailed information about the presence, location, and distribution of hypertrophy, as well as visualization of cardiac amyloid infiltration with LGE imaging and measurement of cardiac amyloid burden with T1 mapping and ECV (20,72,134,136-139). One retrospective study in patients with cardiac amyloidosis (n = 51) suggested that a high proportion of patients have morphological phenotypes that differ from the classical description of concentric symmetric hypertrophy (46) but the amyloidosis type was not specified. No study has assessed the morphology in a large cohort of patients with ATTR.

The aim of this study was to examine the CMR morphological phenotypes and tissue characterization findings in ATTR, to correlate these with clinical outcomes, and compare these findings with AL amyloidosis.

Methods

Ethical approval was granted by the University College London/University College London Hospitals Joint Committees on the Ethics of Human Research Committee and all participants provided written informed consent.

A total of 342 subjects were prospectively recruited between 2011 and 2015. The study population underwent comprehensive clinical evaluation and follow-up at the National Amyloidosis Centre, London, and comprised the 3 groups described below. Patients were systematically followed-up until October 4, 2016, the date of censor.

Cardiac ATTR was defined as the combination of symptoms with an echocardiogram consistent with or suggestive of cardiac amyloidosis, a grade 2 or 3 cardiac uptake on ^{99m}Tc-DPD scintigraphy in the absence of a monoclonal gammopathy, or, in the presence of monoclonal gammopathy, a cardiac biopsy positive for TTR (21). Suspected cardiac ATTR was defined by grade 1 cardiac uptake on ^{99m}Tc-DPD scintigraphy in the absence of a monoclonal gammopathy. All subjects underwent sequencing of exons 2, 3, and 4 of the *TTR* gene.

We recruited 263 consecutive patients (227 male; age 74 ± 9 years) with cardiac ATTR and 17 with suspected cardiac ATTR.

TTR gene mutation carriers were defined as individuals with no evidence of clinical disease (no cardiac uptake on ^{99m}Tc-DPD scintigraphy and normal echocardiography,

CMR, N-terminal pro-B-type natriuretic peptide [NT-proBNP], and troponin T). Twelve *TTR* gene mutations carriers were recruited (4 male; age 47 ± 11 years).

Cardiac AL amyloidosis was determined on the basis of international consensus criteria, (162) and 50 consecutive patients with cardiac AL amyloidosis (37 male; age 63 ± 10 years) were recruited as a comparator group.

Subjects with contraindications to CMR included those with glomerular filtration rate <30 ml/min.

CMR protocol

All participants underwent standard CMR on a 1.5-T clinical scanner. A standard volume and LGE study was performed. The gadolinium-based contrast agent used was 0.1 mmol/kg of gadoterate meglumine. LGE imaging was acquired using magnitude reconstruction in all patients and phase-sensitive inversion recovery reconstruction (PSIR) in 82% of patients. For native T1 and post-contrast mapping, basal and mid-ventricular short-axis and 4-chamber long-axis images were acquired using the Modified Look-Locker inversion recovery (MOLLI) or shortened MOLLI sequence after regional shimming, as previously described (129). After the bolus of gadoterate meglumine and standard LGE imaging (standard fast low-angle shot inversion recovery or balanced steady state free precession sequence with magnitude reconstruction and PSIR reconstruction), the T1 measurement was repeated with the MOLLI or shortened MOLLI sequence (54). In 17 patients with ATTR, post-contrast T1 map acquisition was not performed; 5 patients requested to terminate the scan early and 12 had claustrophobia.

CMR image analysis

All CMR images and maps were analysed offline. The presence of LVH was defined as increased LV mass based on age- and sex-indexed reference values. Asymmetric septal hypertrophy was defined as the ratio between the septal and posterior wall >1.5 (46). Asymmetric septal hypertrophy comprised, in turn, 2 different patterns: 1) sigmoid septum, with the septum being concave to the LV cavity and a prominent basal septal bulge; and 2) reverse septal contour with an abnormal convexity of the septum toward the LV cavity (163,164). The ratio between the septal and posterior wall ≤1.5 and increased mass was considered symmetric concentric LVH.

T1 measurement was performed by drawing a region of interest in the basal to mid septum of the appropriate 4-chamber map. For ECV measurement, a single region of interest was drawn in each of the 4 required areas: myocardial T1 estimates (basal to mid septum in 4-chamber map) and blood T1 estimates (LV cavity blood pool in 4 chamber map, avoiding the papillary muscles) before and after contrast administration. Hematocrit was measured in all subjects immediately before each CMR study. ECV was calculated as myocardial ECV = (1-hematocrit) x ($\Delta R1_{myocardium}/\Delta R1_{blood}$), where R1 = 1/T1.

Before our adoption of PSIR for all amyloidosis patients, because myocardial nulling can be difficult in the presence of amyloid, any confusion with magnitude reconstruction images was resolved by selecting the images that most matched the post-contrast T1 maps, with “bright” LGE expected to correlate with areas of the lowest postcontrast T1 (i.e., the highest gadolinium concentration, the highest interstitial expansion).

The LGE pattern was classified into 3 groups according to the degree of transmurality: group 1, no LGE; group 2, subendocardial LGE (when there was global subendocardial but no transmural LGE); and group 3, transmural LGE (when the LGE was extending transmurally). Thus, a patient with basal transmural LGE but apical subendocardial LGE would be classified as transmural LGE (67).

^{99M}TC-DPD scintigraphy

Subjects were scanned using hybrid single-photon emission computed tomography (SPECT) computed tomography (CT) gamma cameras following administration of 700 MBq of intravenously-injected ^{99m}Tc-DPD. Whole-body planar images were acquired after 3 h, followed by SPECT of the heart coupled with a low-dose, noncontrast CT scan as previously described (95). Gated and nongated cardiac SPECT reconstruction and SPECT-CT image fusion was performed on the Xeleris workstation (GE Healthcare, Wauwatosa, Wisconsin). Cardiac retention of ^{99m}Tc-DPD was scored visually according to the grading devised by Perugini et al. (86) using the following grading system: grade 0, absent cardiac uptake; grade 1, mild cardiac uptake less than bone; grade 2, moderate cardiac uptake equal or greater than bone; and grade 3, intense cardiac uptake associated with substantial reduction or loss of bone signal.

Statistical analysis

Statistical analysis was performed using IBM SPSS Statistics version 22 (IBM, Armonk, New York). All continuous variables were normally distributed (Shapiro-Wilk test), other than NT-proBNP, which was natural log transformed for bivariate testing. These are presented as mean ± SD with non-natural log transformed NT-proBNP presented as median and interquartile range. Comparisons between groups

were performed by 1-way analysis of variance with post hoc Bonferroni correction. The chi-square test or Fisher exact test was used to compare categorical data as appropriate. Correlations between parameters were assessed using Pearson (r) or Spearman's rho. The Pearson correlation evaluates the linear relationship between two continuous variables. The Spearman correlation evaluates the monotonic relationship between two continuous or ordinal variables. Spearman correlation is often used to evaluate relationships involving ordinal variables. Statistical significance was defined as $p < 0.05$.

Survival was evaluated using Cox proportional hazards regression analysis, providing estimated hazard ratios (HR) with 95% confidence intervals (CI), and Kaplan-Meier curves. HRs were estimated for pre-defined increments or decrements in the variables based on clinically relevant changes (71, 76). All variables were selected a priori for clinical relevance: ECV as marker of amyloid infiltration; ejection fraction for systolic function; E/E' for diastolic function; LV mass for structural changes; and NT-proBNP as blood biomarker. A multivariable model was used to investigate factors associated with overall survival.

Results

The details of the 342 subjects are shown in Table 5. Of the 263 consecutive patients with ATTR, 168 had wild-type ATTR and 95 hereditary ATTR (ATTRm). Of the 17 patients with suspected cardiac ATTR, 9 had wild-type *TTR* gene sequence and 8 had amyloidogenic *TTR* gene mutations. The *TTR* mutations in cardiac amyloidosis were: V122I (n = 49); T60A (n = 26); V30M (n = 8); S77Y (n = 2); and E54G, E54L, E89K, D38Y, D39V, E89K, V20I, F44L, G89L and L12P in 1 case each. The mutations among the possible cardiac amyloidosis subjects were: S77Y (n = 3) and

V30M, I107F, E54G, G47V, and I84S in 1 case each. Finally, the mutations among the mutation carriers were: T60A (n = 6); V30M (n = 5); and S77Y (n = 1).

Table 5. Patient Characteristics

	All ATTR Subjects (n = 292)	Tc-DPD Grade 0 (n = 12)	Tc-DPD Grade 1 (n = 17)	Tc-DPD Grade 2 (n = 204)	Tc-DPD Grade 3 (n = 59)	AL (n = 50)
Age, years	72 ± 11	47 ± 11	70 ± 14	75 ± 8	72 ± 11*	63 ± 10†
Male, %	83	33	65	89	76*	74†
Ethnicity	White 78% Afro-Caribbean 19% Asian 1% Mixed (White/Afro-Caribbean) 1% Chinese 1%	White 100%	White 94% Asian 6%	White 83% Afro-Caribbean 16% Mixed (White/Afro-Caribbean) 1%	White 53% Afro-Caribbean 41% Asian 2% Mixed (White/ Afro-Caribbean) 2% Chinese 2%	White 96% Afro-Caribbean 4%
Body surface area, m^2	1.90 ± 0.26	1.92 ± 0.33	2.03 ± 0.56	1.93 ± 0.21	1.78 ± 0.19*	1.90 ± 0.25
Heart rate, bpm	73 ± 12	80 ± 13	71 ± 12	72 ± 13	77 ± 12*	85 ± 14†
Systolic blood pressure, mmHg	124 ± 17	124 ± 13	141 ± 19	124 ± 16	121 ± 18*	112 ± 17†
Diastolic blood pressure, mmHg	73 ± 10	72 ± 9	71 ± 12	73 ± 10	77 ± 12	69 ± 12†
Comorbidities						
Diabetes mellitus	7	0	0	8	7	0†
Hypertension	17	0	24	18	14	10†
Ischemic heart disease	10	0	18	13	2	10

Biomarkers						
NT-proBNP, ng/l	1,886 (576-1,217)	21 (10-31)	247 (47-288)	2,001 (690-2,168)	2,342 (741-3,683)*	1,886 (575-2,168)
Echocardiographic parameters						
IVS, cm	1.61 ± 0.29	0.95 ± 0.12	1.12 ± 0.28	1.65 ± 0.22	1.72 ± 0.24*	1.49 ± 0.18†
LPW, cm	1.31 ± 0.25	0.88 ± 0.11	1.11 ± 0.27	1.34 ± 0.23	1.38 ± 0.23*	1.24 ± 0.23†
LVEDD, cm	4.50 ± 1.77	4.73 ± 0.54	4.52 ± 0.58	4.40 ± 0.59	4.28 ± 0.70	4.20 ± 0.55
LA area, cm^2	28.82 ± 6.20	15.10 ± 5.35	21.09 ± 4.59	27.06 ± 5.74	25.2 ± 5.63*	22.78 ± 4.54†
E wave, m/s	0.84 ± 0.20	0.79 ± 0.12	0.75 ± 0.16	0.85 ± 0.19	0.84 ± 0.25*	0.85 ± 0.21
A wave, m/s	0.50 ± 0.24	0.67 ± 0.17	0.73 ± 0.16	0.47 ± 0.23	0.46 ± 0.24*	0.55 ± 0.28†
E/A	2.92 ± 7.79	1.23 ± 0.25	1.05 ± 0.25	2.88 ± 5.52	4.12 ± 13.58	1.84 ± 1.07
Average E', m/s	0.10 ± 0.68	0.10 ± 0.05	0.09 ± 0.03	0.14 ± 0.06	0.25 ± 1.52	0.06 ± 0.02
E/E'	16 ± 8	13 ± 18	10 ± 4	16 ± 6	19 ± 9*	17 ± 8
E wave deceleration time, ms	180 ± 56	181± 48	187 ± 45	183 ± 55	168 ± 62	184 ± 52
2-dimensional GLS (%)	-11.6 ± 4.6	-18.8 ± 3.4	-17.7 ± 5.0	-11.4 ± 4.2	-8.8 ± 2.8*	-11.3 ± 4.6
CMR parameters						
LV mass, g	244 ± 77	114 ± 37	162 ± 76	252 ± 64	264 ± 89*	197 ± 65†
LV $mass_i$, g/m^2	130 ± 41	59 ± 12	84 ± 44	132 ± 33	149 ± 46*	103 ± 30†
Maximal IVS, mm	18 ± 5	8 ± 1	13 ± 4	20 ± 4	21 ± 4*	17 ± 4†
LVEDV, ml	131 ± 36	124 ± 25	132 ± 28	133 ± 36	128 ± 39	115 ± 26†

$LVEDV_i$, ml/m^2	69 ± 18	66 ± 13	69 ± 13	70 ± 18	70 ± 22	61 ± 15†
LVESV, ml	60.65 ± 30.77	38.58 ± 12.24	43.47 ± 22.92	62.11 ± 30.41	65.75 ± 33.41*	44.66 ± 15.28†
$LVESV_i$, ml/m^2	32 ± 16	20 ± 6	23± 13	32 ± 15	36 ± 18*	24 ± 9†
LVSV, ml	71 ± 20	85 ± 16	89 ± 23	71 ± 19	63 ± 16*	70 ± 20
$LVSV_i$, ml/m^2	38 ± 10	45 ± 8	45 ± 11	37 ± 10	36 ± 8*	37 ± 12
LVEF, %	56 ± 14	69 ± 5	69± 11	55 ± 14	52 ± 14*	61 ± 11†
RV mass, g	77 ± 24	38 ± 12	48 ± 20	82 ± 21	80 ± 22*	63 ± 16†
RV $mass_i$, g/m^2	41 ± 13	20 ± 6	26 ± 11	43 ± 11	44 ± 12*	33 ± 8†
RVEDV, ml	131 ± 36	124 ± 26	115 ± 22	135 ± 38	125 ± 34	114 ± 24†
$RVEDV_i$, ml/m^2	70 ± 19	68 ± 13	62 ± 10	71 ± 20	69 ± 19	60 ± 12†
RVESV, ml	64 ± 30	45 ± 10	41 ± 15	68 ± 32	65 ± 27*	54 ± 19†
$RVESV_i$, ml/m^2	34 ± 16	25 ± 5	22 ± 8	35 ± 17	36 ± 15*	28 ± 10†
RVSV, ml	67 ± 19	80 ± 18	74 ± 15	68 ± 19	58 ± 17*	61 ± 17†
$RVSV_i$, ml/m^2	36 ± 10	43 ± 9	40 ± 8	36 ± 10	32 ± 9*	32 ± 9†
RVEF, %	53 ± 13	64 ± 3	65 ± 10	52 ± 13	49 ± 12*	54 ± 12
LA area, cm^2	31 ± 8	22 ± 4	25 ± 6	33 ± 9	29 ± 5*	26 ± 5†
RA area, cm^2	28 ± 8	20 ± 2	23 ± 5	30 ± 8	27 ± 6*	25 ± 6†
MAPSE, mm	8 ± 3	14 ± 2	11 ± 3	7 ± 2	6 ± 2*	7 ± 4
TAPSE, mm	13 ± 5	23 ± 3	22 ± 5	12 ± 4	11 ± 4*	14 ± 6†
ECV, %	59 ± 13	29 ± 3	39 ± 12	59 ± 10	66 ± 10*	53 ± 8†

Values are mean ± SD, %, or median (interquartile range).*$p < 0.05$ for trend (1-way analysis of variance) in patients with transthyretin amyloidosis (ATTR) across different grades of uptake by Tc-DPD scintigraphy. †$p < 0.05$ AL versus ATTR (Tc-DPD grade 2 and 3).

Morphological phenotypes

Asymmetric septal hypertrophy, defined as the ratio between the septal and posterior wall >1.5 (46,165), was the most common form of ventricular remodeling in ATTR,

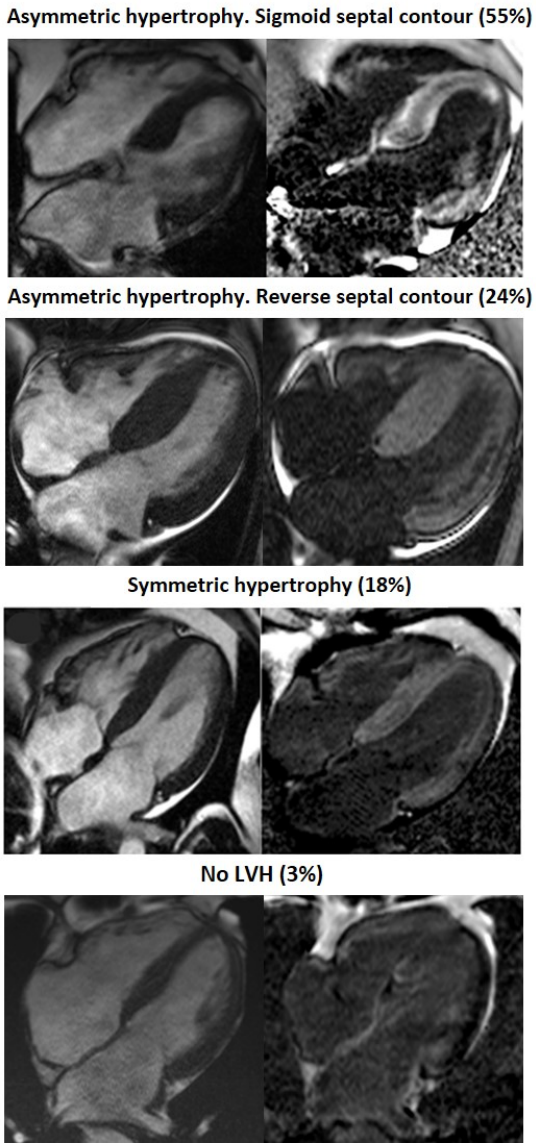

Figure 13. Morphology pattern in cardiac ATTR amyloidosis. 4-chamber image and corresponding LGE illustrate asymmetrical hypertrophy with sigmoid septal contour; asymmetrical hypertrophy with reverse septal contour; symmetrical hypertrophy and no hypertrophy

being present in 79% of patients with cardiac ATTR. The pattern of asymmetric septal hypertrophy was divided into the morphological subtypes of sigmoid septum

(55%) and reverse septal contour (24%). Symmetric concentric LVH, considered typical for amyloidosis, was present in only 18% of patients with ATTR (Figure 13).

There were no differences in the prevalence of the different morphological phenotypes in wild-type ATTR and ATTRm (sigmoid septal 53% vs. 60%, reverse septal curvature 25% vs. 20%, and symmetric concentric LVH 19% vs. 18%, respectively). Seven patients (3%) with cardiac ATTR amyloidosis (grade 2 or 3 cardiac uptake on ^{99m}Tc-DPD scintigraphy) had no LVH (2 with ATTRm and 5 with wild-type ATTR).

Prevalence of asymmetric septal hypertrophy was significantly higher in ATTR compared to patients with cardiac AL amyloidosis (79% vs. 14%; $p < 0.001$), where the most common form of ventricular remodeling was symmetric concentric LVH (34 patients [68%]), followed by asymmetric pattern with sigmoid septal contour in 7 patients (14%). The asymmetric pattern with reverse septal contour was not found in the AL amyloidosis cohort. Nine patients (18%) with cardiac AL amyloidosis had no LVH.

Tissue characterisation findings

In patients with cardiac amyloidosis, LGE was always present and the pattern of LGE was typical for amyloidosis, being diffuse subendocardial LGE in 29% of patients and transmural LGE in 71% (Figure 14). Right ventricular (RV) LGE was extremely frequent, being present in 96% of patients. There was no difference in LGE prevalence between wild-type ATTR and ATTRm (transmural LGE 71% vs. 72% and subendocardial LGE 29% vs. 28%; $p > 0.05$ for both). As previously reported, the prevalence of transmural LGE and RV LGE was significantly higher in ATTR

compared to AL (transmural LGE 71% vs. 50% and RV LGE 96% vs. 77%; $p < 0.01$ for both). In this population, transmural LGE was not associated with a worse prognosis than subendocardial LGE ($p = 0.327$).

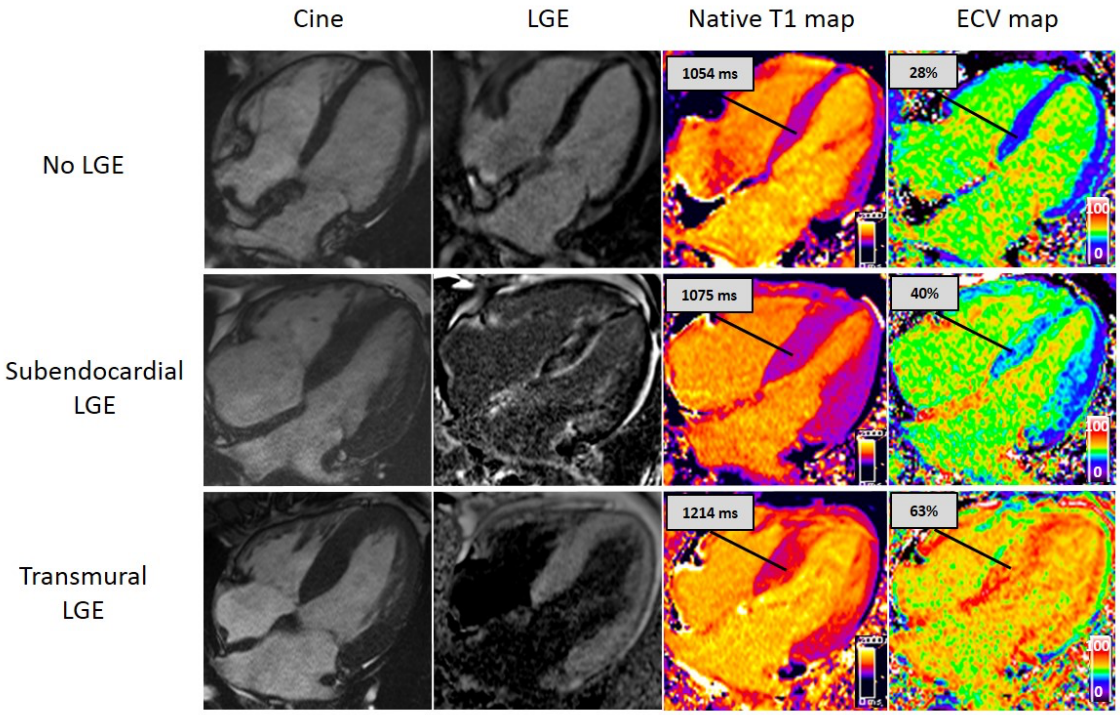

Figure 14. LGE patterns correlating with T1 and ECV measurements. 4-chamber cine, corresponding LGE images, native T1 maps and ECV maps in 3 patients with cardiac ATTR amyloidosis.

Patients with suspected cardiac amyloidosis (17 patients with grade 1 uptake on ^{99m}Tc-DPD) did not show characteristic LGE of amyloidosis with the notable exception of patients with the Se77Tyr variant (3 patients in our cohort with ^{99m}Tc-DPD grade 1). The rest of the patients showed no LGE (n = 10), subendocardial LGE with ischemic pattern (n = 2), and mid wall LGE in the basal infero-lateral wall (n = 2). The 3 patients with Se77Tyr and ^{99m}Tc-DPD grade 1 had typical LGE pattern (1 presented subendocardial LGE and 2 transmural LGE). The clinical, morphological, and functional features of these 3 patients were also in keeping with cardiac amyloidosis on echocardiogram, ECV measurements, and biomarkers (Figure 15), suggesting that they have less DPD uptake than they should, given the amyloid burden.

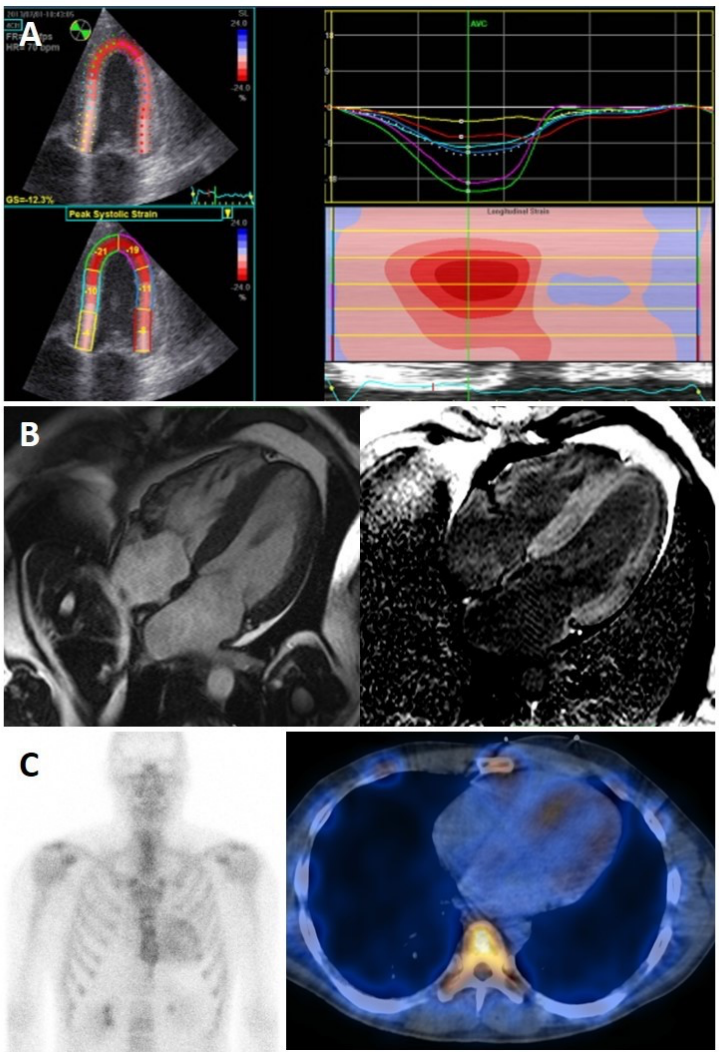

Figure 15. Patient with cardiac ATTR amyloidosis with Se77Tyr variant. Panel A shows strain pattern characteristic of amyloidosis. Panel B shows SSFP image and LGE with transmural LGE; and C shows Perugini grade 1 cardiac uptake on DPD scintigraphy

There was good correlation between ECV and cardiac uptake on ^{99m}Tc-DPD scintigraphy ($r = 0.533$; $p < 0.05$). Except for patients with the Se77Tyr variant and grade 1 on ^{99m}Tc-DPD scintigraphy, ECV discriminated patients with ATTR with cardiac amyloidosis from patients with no or possible cardiac involvement (Figure 16). ECV was not significantly different in ATTRm compared to wild-type ATTR. When ECV was compared across the different mutations in patients with cardiac ATTR, patients with V30M had a significantly lower ECV than patients with wild-

type ATTR, T60A, and V122I (42 ± 10% vs. 59 ± 11%, 54 ± 15, and 64 ± 13%, respectively; all $p < 0.05$) and patients with V122I had significantly higher ECV than patients with V30M and T60A (65 ± 13% vs. 42 ± 10%, and 54 ± 15%, respectively; all $p < 0.05$)

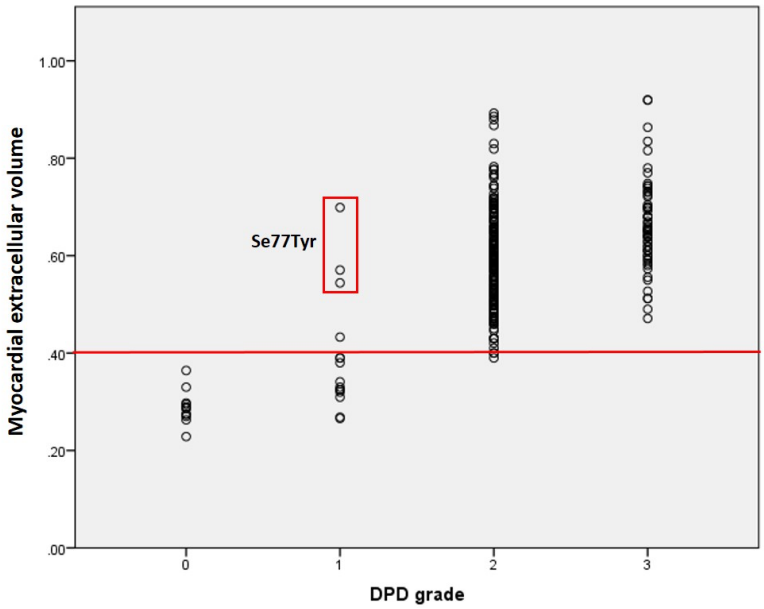

Figure 16. ECV and cardiac uptake on DPD scintigraphy. Only patients with Se77Tyr variant had high ECV measurements with grade 1 abnormal uptake.

Discussion

In a prospective study at a single center, we describe here the specific morphological and tissue characteristics of ATTR cardiac amyloidosis using state-of-the-art imaging with CMR and identify what distinguishes it from AL and specific ATTR prognostic determinants.

This study had 2 major findings (Figure 17). First, the morphological phenotype of patients with ATTR differed from AL and the one traditionally described, with

asymmetric LVH present in 79% of patients with ATTR amyloidosis versus 14% in AL amyloidosis. Reverse septal contour, classically associated with hypertrophic cardiomyopathy, was present in one-quarter of patients with ATTR. Additionally, LGE and ECV presented typical features in patients with ATTR, with very elevated ECV values and subendocardial or transmural LGE pattern. ECV correlated with cardiac uptake by ^{99m}Tc-DPD scintigraphy in all patients, except for those with the Se77Tyr mutation where the degree of cardiac uptake on ^{99m}Tc-DPD scintigraphy stood out as being disproportionately low compared to the severity of cardiac involvement assessed by ECV.

The LVH morphology in ATTR was surprising. The conventional view is that cardiac amyloidosis leads to symmetrically increased wall thickness. We suspect this happens due to several reasons. The literature is heavily weighted towards AL where the morphology is mainly concentric, as ATTR could until recently only be diagnosed definitively by endomyocardial biopsy. Furthermore, patients with ATTR are typically elderly, and increased aorto-septal angulation could confound ascertainment, particularly by echocardiography. In addition, a focus on nomenclature, as to whether

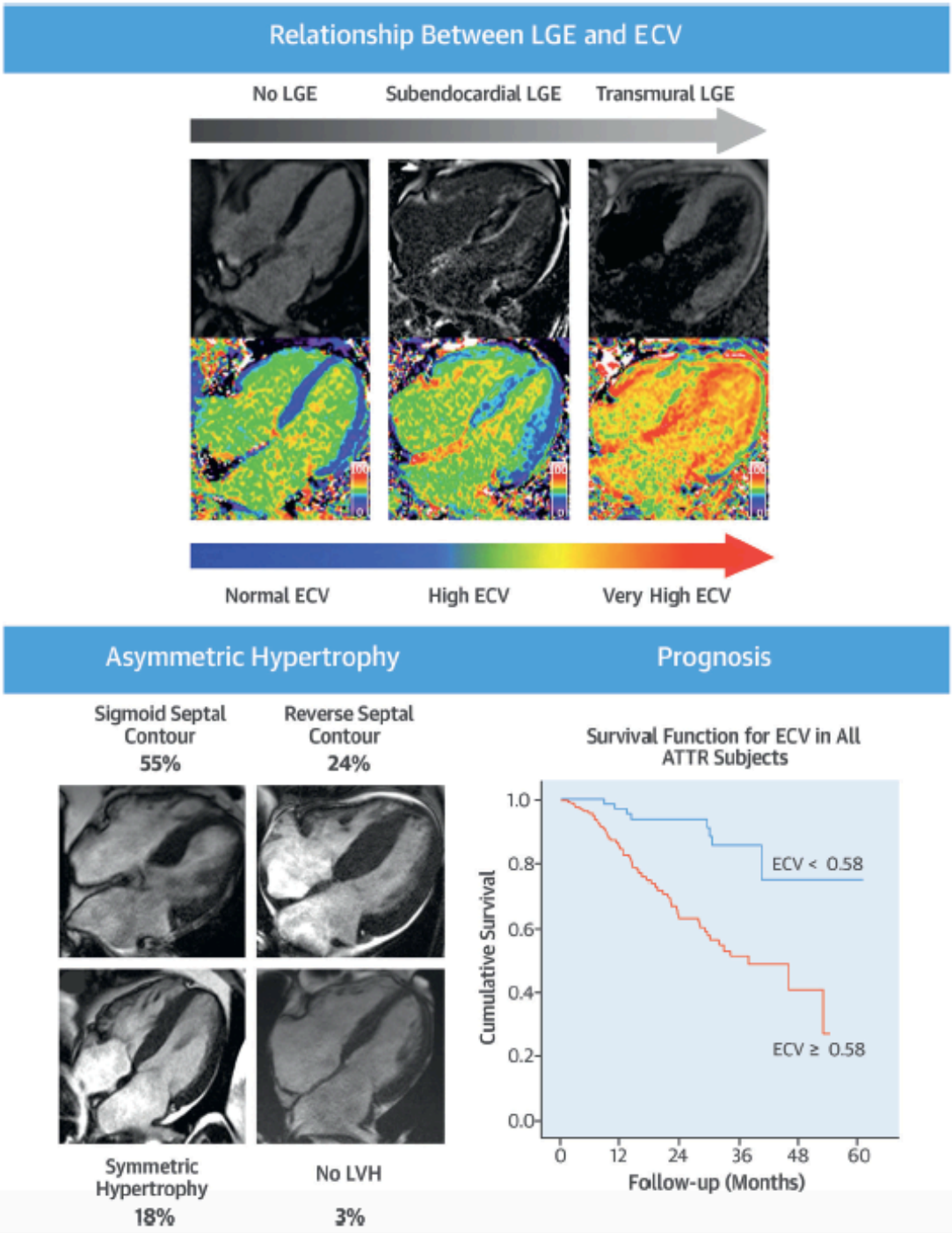

Figure 17. Summary of findings in ATTR cardiac amyloidosis. Relationship between LGE and ECV (top); morphological patterns in ATTR (bottom left); and survival analysis (bottom right).

the wall thickening should be called hypertrophy or not, might have prevented additional scrutiny. Looking further, we also note that the asymmetric pattern with

reverse septal contour was not found among the cardiac AL patients. This observation has important immediate diagnostic implications, as the association between amyloidosis and symmetric septal hypertrophy could play an important role in the misdiagnosis of ATTR. One possibility that could explain why this pattern occurs is related to differential rates of effective cell hypertrophy in AL versus ATTR. Our prior work highlighted that in ATTR, total cell mass increased, whereas it remained the same in AL (5). It is possible that while infiltration was global, a triggered myocyte response differentially induced septal hypertrophy. Another possibility is that AL patients died before their total infiltration achieved the levels found in ATTR, so they were unable to get to the reverse septal contour stage.

We found that in all patients with cardiac ATTR, the pattern of late gadolinium enhancement was always typical of cardiac amyloidosis, with a subendocardial or transmural LGE pattern (61,67). Subendocardial LGE was found in 29% and the remainder (71%) showed transmural LGE. RV LGE was present in 96% of patients. This confirmed previous reports on the high prevalence of transmural LGE and RV LGE in ATTR (166), but it also highlighted the important role that CMR could have in diagnosing this disease. The typical appearance of LGE in patients with cardiac ATTR with subendocardial or transmural LGE has the potential to revolutionize the diagnostic pathway of this disease, as CMR is currently the diagnostic reference standard for the differential diagnosis of cardiomyopathies with hypertrophic phenotype.

With the exception of patients with the Se77Tyr variant, none of the patients with suspected rather than proven cardiac ATTR (defined as grade 1 cardiac uptake on ^{99m}Tc-DPD scintigraphy) showed LVH, typical LGE, or very elevated ECV (although

a mild elevation in ECV was noted). In patients with the Se77Tyr variant and grade 1 cardiac uptake on ^{99m}Tc-DPD scintigraphy, CMR showed typical features of cardiac involvement with LVH, characteristic LGE, and increased ECV. As assessed by functional, structural, and clinical parameters, there was good agreement between the CMR characterisation of the degree of cardiac involvement and the echocardiographic and clinical features, while a discrepancy was observed with the degree of cardiac uptake on ^{99m}Tc-DPD scintigraphy that had been disproportionately low (Figure 15). The mechanism for this phenomenon remains unknown, but raises the possibility of the degree of cardiac uptake being variant dependent.

Extracellular volume is the first noninvasive method for quantifying the cardiac interstitium, and several papers have shown correlation with markers of disease severity in both types of cardiac amyloidosis (76,137,167). When ECV was compared across the different mutations in patients with cardiac ATTR, patients with V30M had a significantly lower ECV than patients with wild-type ATTR, T60A, and V122I. The disease associated with the TTR V30M variant usually causes a predominant sensorimotor peripheral neuropathy and autonomic neuropathy. Although cardiac amyloidosis might occur in older patients with this TTR variant, the vast majority of patients have minor degrees of cardiac involvement or, in younger affected individuals, none at all. Therefore, the lower ECV likely represents the different clinical phenotype of this variant compared with other variants that are characterised by predominantly cardiac features (even though the neurological phenotype can coexist). A spectrum of disease burden exists, ranging from small incidental deposits with no clinical consequence to very extensive deposits causing severe organ failure. LGE can confirm the diagnosis and divide patients with cardiac amyloidosis into groups that likely represent different stages of myocardial infiltration with the

transmural pattern being associated with a higher ECV compared to the subendocardial one. ECV can measure the continuum of amyloid infiltration, enabling the clinician to fully characterise phenotypes, their stages of evolution, and the prognostic implication of amyloid deposition. Some patients in the cohort had modest ECV increase without evidence of cardiac involvement by echocardiogram, LGE, or blood biomarkers; suggesting that, like in AL, ECV can detect early cardiac involvement (5). The presence of low grade disease was also confirmed by a low degree of cardiac uptake on the ^{99m}Tc-DPD scintigraphy that seemed to show a similar sensitivity.

This study has several limitations. We used the proposed noninvasive criteria for ATTR (21) meaning cardiac biopsy was performed only in a minority of patients. Two different T1 mapping techniques were used during the period in which these patients were recruited and a wide range of *TTR* mutations were included in the analysis.

These observations redefine classical expectations of morphology in cardiac amyloidosis and underpin the importance of considering amyloidosis in the presence of asymmetrical ventricular hypertrophy. Future characterisation of patients with ATTR amyloidosis by CMR could identify earlier features of the disease, an under-recognised (and potentially modifiable) cause of heart failure in the elderly.

CHAPTER 5: NATIVE T1 AND ECV IN ATTR AMYLOIDOSIS

This chapter is based on the publication below:

Martinez-Naharro A, Kotecha T, Norrington K, Boldrini M, Rezk T, Quarta CC, Treibel TA, Whelan CJ, Knight DS, Kellman P, Ruberg FL, Gillmore JD, Moon JC, Hawkins PN, Fontana. Native T1 and ECV in ATTR amyloidosis. *JACC Cardiovasc Imaging*. 2019 May;12(5):810-819. doi: 10.1016/j.jcmg.2018.02.006

My contribution was analysing all the data as first operator, doing the statistical analysis, and writing the paper.

Introduction

Systemic amyloidosis is caused by deposition of insoluble amyloid fibrils in the extracellular space of tissues and organs, leading to progressive organ failure and death. More than 30 different precursor proteins have the propensity to form amyloid fibrils (2), but only two types account for most cases of ventricular cardiac amyloidosis: immunoglobulin light-chain (AL) and transthyretin (ATTR). Transthyretin-related amyloidosis, in turn, may be either hereditary (ATTRm) arising from misfolding of mutated TTR or non-hereditary, caused by misfolding of wild-type transthyretin (ATTRwt, also known as senile systemic amyloidosis). Cardiac involvement is the principal driver of prognosis in systemic amyloidosis although outcome differs markedly between types (11).

Cardiac ATTR amyloidosis is a progressive and usually fatal cause of heart failure, typically occurring in older people, for which awareness and clinical recognition have greatly increased in recent times.

Formerly, diagnosis of cardiac ATTR amyloidosis required demonstration of amyloid deposits with an endomyocardial biopsy (168) but advances in diagnostic imaging, including cardiac magnetic resonance imaging (20,67) and re-purposed bone

scintigraphy (86,90,169,170) along with the and blood/urine exclusion of free light chains now enable non-invasive, non-histological diagnosis of cardiac ATTR amyloidosis, which has resulted in a greater than 30-fold increase in the diagnosis of this condition in our Centre during the past decade (171).

CMR has lately emerged as a robust technique that can provide unique information about tissue composition. CMR can visualise, with LGE imaging, and measure, with T1 mapping, the continuum of cardiac amyloid deposition. The T1 mapping technique, before the administration of contrast (20,72), can measure the intrinsic signal from the myocardium (native myocardial T1), whilst T1 maps pre- and post-administration of gadolinium-based contrast can be used to calculate the myocardial ECV. Both native myocardial T1 and ECV have been extensively validated in cardiac amyloidosis as surrogate markers of infiltration. They have been shown to correlate with disease burden, detect early disease, and have good diagnostic accuracy. Furthermore, in cardiac AL amyloidosis, higher T1 and ECV measurements have been shown to be associated with a shorter event free survival (76). However, in cardiac ATTR amyloidosis, although the prognostic significance of ECV has been presented (68), neither the prognostic potential of native T1, nor the relative diagnostic accuracy or ability for native T1 versus ECV to track disease severity have been studied.

From anecdotal observation and our previous work in AL amyloidosis, we hypothesized that native myocardial T1 predicts survival in cardiac ATTR amyloidosis (76) and that there may be significant differences between the ability native T1 and ECV to track disease progression.

Methods

Ethical approval was granted by the University College London/University College London Hospitals Joint Committees on the Ethics of Human Research Committee, and all participants provided written informed consent.

Study population

A total of 271 subjects were prospectively recruited between 2011 and 2015. The study population underwent comprehensive clinical evaluation and follow-up at the National Amyloidosis Centre, London, and comprised the three groups described below. Patients were systematically followed up until June 13, 2017, the date of censoring.

ATTR amyloidosis patients: Cardiac ATTR amyloidosis was defined as the combination of symptoms with an echocardiogram consistent with or suggestive of cardiac amyloidosis, a grade 2 or 3 cardiac uptake on the ^{99m}Tc-DPD scintigraphy in the absence of a monoclonal gammopathy or, in the presence of monoclonal gammopathy, a cardiac biopsy confirming ATTR (21). Possible cardiac ATTR amyloidosis was defined by grade 1 cardiac uptake on ^{99m}Tc-DPD scintigraphy in the absence of a monoclonal gammopathy (20,68). All subjects underwent sequencing of exons 2, 3, and 4 of the *TTR* gene.

271 subjects included in this study, 198 had definitive cardiac ATTR amyloidosis (171 male, 86%; age 74 ± 8 years), 17 had possible cardiac ATTR amyloidosis (11 male, 65%; age 70 ± 14 years), 12 were *TTR* gene mutation carriers, and 44 had hypertrophic cardiomyopathy.

TTR gene mutation carriers: Individuals with amyloidogenic *TTR* gene mutations were defined as carriers on the basis of being clinically asymptomatic, having no

cardiac uptake on ^{99m}Tc-DPD scintigraphy and having normal echocardiography, CMR, N-terminal proB-type natriuretic peptide (NT-proBNP) and Troponin T. Twelve *TTR* gene mutation carriers were recruited (4 male, 33%; age 47 ± 11 years).

HCM patients: There were 44 patients with HCM (32 male, 73%; 51 ± 13 years) fulfilling diagnostic criteria. Hypertrophic cardiomyopathy is defined by the presence of increased ventricular wall thickness or mass in the absence of loading conditions (hypertension, valve disease) or a systemic disease (e.g. amyloidosis or glycogen storage disease) sufficient to cause the observed abnormality (124). In addition to the *TTR* gene carrier group described above, HCM patients constituted the non-cardiac ATTR group.

Exclusion criteria

We excluded patients with contraindications to CMR including glomerular filtration rate <30 mL/min.

CMR protocol

All participants underwent standard CMR on a 1.5T clinical scanner. A standard volumetric and LGE study was performed. The gadolinium-based contrast agent used was 0.1 mmol/kg of gadoterate meglumine (Dotarem, Guerbet S.A., France). LGE imaging was acquired using magnitude reconstruction in all patients and phase-sensitive inversion recovery reconstruction (PSIR) in 82% of patients with either standard fast low-angle shot inversion recovery or balanced steady state free precession sequence. For native and post-contrast T1 mapping, 4-chamber long-axis images were acquired using the Shortened Modified Look-Locker inversion recovery (ShMOLLI) sequence after regional shimming, as previously described (129). After

the bolus of contrast and LGE, the T1 measurement was repeated with the ShMOLLI (54).

CMR image analysis

All CMR images and maps were analysed offline. T1 measurement was performed by drawing a region of interest in the basal to mid septum of the appropriate 4-chamber map. For ECV measurement, a single region of interest was drawn in each of the 4 required areas: myocardial T1 estimates (basal to mid septum in 4 chamber map) and blood T1 estimates (LV cavity blood pool in 4 chamber map, avoiding the papillary muscles) before and after contrast administration. Haematocrit was measured in all subjects immediately before each CMR study. ECV was calculated as: myocardial ECV = (1-hematocrit) x (ΔR1myocardium/ΔR1blood), where R1=1/T1.

Before our adoption of PSIR for all amyloidosis patients, because myocardial nulling can be difficult in the presence of amyloid, any confusion with magnitude reconstruction images was resolved by selecting the images that most matched the post-contrast T1 maps, with “bright” LGE expected to correlate with areas of the lowest postcontrast T1 (i.e., the highest gadolinium concentration, the highest interstitial expansion).

The LGE pattern was classified into 3 groups according to the degree of transmurality: group 1, no LGE; group 2, subendocardial LGE (when there was global subendocardial but no transmural LGE); and group 3, transmural LGE (when the LGE was extending transmurally). A scan was classified by the most extensive LGE identified. Thus, a patient with basal transmural LGE but apical subendocardial LGE would be classified as transmural (67).

^{99m}Tc-DPD Scintigraphy

Subjects were scanned using hybrid single-photon emission computed tomography (SPECT) computed tomography (CT) gamma cameras following administration of 700 MBq of intravenously-injected ^{99m}Tc-DPD. Whole-body planar images were acquired after 3 h, followed by SPECT of the heart coupled with a low-dose, noncontrast CT scan (95). Gated and nongated cardiac SPECT reconstruction and SPECT-CT image fusion was performed on the Xeleris workstation (GE Healthcare, Wauwatosa, Wisconsin). Cardiac retention of ^{99m}Tc-DPD was scored visually according to the grading devised by Perugini et al. (86) using the following grading system: grade 0, absent cardiac uptake; grade 1, mild cardiac uptake less than bone; grade 2, moderate cardiac uptake equal or greater than bone; and grade 3, intense cardiac uptake associated with substantial reduction or loss of bone signal. Uptake was verified by visual review of SPECT imaging.

Statistical analysis

Statistical analysis was performed using IBM SPSS Statistics version 22 (IBM, Armonk, New York). All continuous variables were normally distributed (Shapiro-Wilk test), other than NT-proBNP, which was natural log transformed for bivariate testing. These are presented as mean ± SD with untransformed NT-proBNP presented as median and interquartile range. Comparisons between multiple groups were performed by 1-way analysis of variance with post hoc Bonferroni correction. The chi-square test or Fisher exact test was used to compare categorical data as appropriate. Correlations between parameters were assessed using Pearson (r) or Spearman's rho. Receiver-operating characteristic (ROC) curve analysis was

performed to define the diagnostic accuracy of native T1 and ECV. The AUCs were compared statistically for correlated ROC curves with DeLong method.

Survival was evaluated using Cox proportional hazards regression analysis, providing estimated hazard ratios (HR) with 95% confidence intervals (CI) and Kaplan-Meier curves. All variables were first explored with univariate Cox regression. Separate multivariate models evaluated the independent predictive value of T1 and ECV above other clinically and statistically significant covariates. Statistical significance was defined as $p < 0.05$.

Results

The details of the 271 subjects are shown in Table 6. A total of 198 patients with definitive ATTR amyloidosis, 17 patients with possible ATTR amyloidosis and 12 mutation carriers were enrolled. These subjects were compared with 44 patients with HCM.

Table 6: Biomarkers, echocardiographic parameters and CMR findings in patients with ATTR amyloidosis and mutations carriers.

	All ATTR patients (n = 227)	**ATTRwt (n = 134)**	**ATTRm (n = 81)**	**ATTR Mutation Carriers (n = 12)**
Age, years	72 ± 11	76 ± 7	69 ± 10	47 ± 11
Biomarkers				
NT-proBNP, ng/L	286 (142 – 538)	322 (179 – 518)	258 (126 – 614)	6 (3 – 8)
6 min WT	318 ± 143	313 ± 134	290 ± 142	521 ± 49
Echocardiographic Parameters				
IVS, cm	1.59 ± 0.28	1.64 ± 0.24	1.61 ± 0.25	0.95 ± 0.12
LA area, cm^2	25.65 ± 6.57	26.66 ± 6.05	25.46 ± 6.31	15.10 ± 5.35

E-wave, m/s	0.83 ± 0.20	0.84 ± 0.19	0.82 ± 0.21	0.79 ± 0.12
A-wave, m/s	0.49 ± 0.24	0.48 ± 0.24	0.48 ± 0.23	0.67 ± 0.17
E/A	3.14 ± 8.71	3.16 ± 6.48	3.50 ± 12.12	1.23 ± 0.25
Average E', m/s	0.11 ± 0.78	0.06 ± 0.02	0.20 ± 1.30	0.1 ± 0.05
E/E'	16 ± 7	16 ± 6	17 ± 7	13 ± 18
E-wave deceleration time, ms	178 ± 54	179 ± 55	177 ± 54	181 ± 48
2D GLS, %	-11.7 ± 4.9	-11.4 ± 4.5	-11.3 ± 5.0	-18.8 ± 3.4
CMR parameters				
LV mass, g	241 ± 77	255 ± 72	238 ± 72	114 ± 37
LV $mass_i$, g/m^2	129 ± 41	134 ± 37	132 ± 40	59 ± 12
Maximal IVS, mm	19 ± 5	20 ± 4	19 ± 4	9 ± 2
LVEDV, mL	134 ± 36	137 ± 37	130 ± 35	124 ± 25
$LVEDV_i$, mL/m^2	71 ± 18	71 ± 19	71 ± 17	66 ± 13
LVESV, mL	62 ± 31	63 ± 32	64 ± 30	39 ±12
$LVESV_i$, mL/m^2	32 ± 16	32 ± 16	35 ± 16	20 ± 6
LVSV, mL	72 ± 20	74 ± 20	67 ± 21	85 ± 16
$LVSV_i$, mL/m^2	38 ± 10	38 ± 10	37 ± 10	45 ± 8
LVEF, %	56 ± 14	56 ± 14	53 ± 15	69 ± 5
RVEDV, mL	132 ± 38	134 ± 37	130 ± 42	125 ± 27
$RVEDV_i$, mL/m^2	70 ± 19	70 ± 19	71 ± 20	68 ± 14
RVESV, mL	63 ± 31	64 ± 31	65 ± 34	43 ± 11
$RVESV_i$, mL/m^2	34 ± 16	34 ± 16	35 ± 18	23 ± 6

RVSV, mL	68 ± 20	70 ± 19	63 ± 19	82 ± 17
$RVSV_i$, mL/m^2	36 ± 10	36 ± 10	34 ± 9	44 ± 9
RVEF, %	53 ± 13	54 ± 13	51 ± 14	66 ± 4
LA area, cm^2	31 ± 9	33 ± 11	30 ± 6	22 ± 4
RA area, cm^2	28 ± 8	30 ± 8	28 ± 8	19 ± 2
MAPSE, mm	8 ± 3	8 ± 3	7 ± 3	14 ± 2
TAPSE, mm	13 ± 5	13 ± 5	13 ± 5	23 ± 3
ECV, %	56 ± 16	60 ± 11	63 ± 13	29 ± 3
Native Myocardial T1, ms	1079± 64	1092 ± 51	1104 ± 49	968 ± 41

Values are mean ± SD, %, or median (interquartile range).

Of the patients with definitive ATTR, 125 had wild-type ATTR and 73 hereditary ATTR (ATTRm); the TTR mutations were V122I (n = 40); T60A (n = 20); V30M (n = 5); and S77Y, E54G, E54L, E89K, D38Y, F44L, G89L and L12P in one case each. Among 17 patients with suspected cardiac ATTR (DPD grade 1 DPD scintigraphy), 9 had wild-type TTR gene sequence and 8 had amyloidogenic TTR gene mutations comprising S77Y (n = 3) and V30M, I107F, E54G, G47V, and I84S in 1 case each. The variants present in the healthy mutation carriers were T60A (n = 6); V30M (n = 5); and S77Y (n = 1).

T1 and ECV diagnostic accuracy

As predicted, T1 and ECV were elevated in ATTR patients compared with HCM and mutation carriers (native T1: 1096 ± 51ms vs 1013 ± 64ms, $p<0.001$; ECV: 0.61 ± 0.12 vs 0.36 ± 0.13, $p<0.001$).

The receiver operator characteristics (ROC) curve analysis was performed for the discrimination of definitive cardiac ATTR amyloidosis or possible cardiac ATTR amyloidosis from the combined differential diagnoses of HCM or ATTR mutation carriers without evidence of cardiac amyloidosis.

The combined group of definitive ATTR and possible ATTR patients had an area under the ROC curve (AUC) of 0.87 (95% confidence interval [CI]: 0.82 – 0.91) for T1 and of 0.91 (95% confidence interval [CI]: 0.87 – 0.94) for ECV. The T1 cut-off value to diagnose definitive or possible cardiac ATTR was 1048ms with a specificity of 80.36% and sensitivity of 86.54% and for ECV was 0.469 with a specificity of 82.14% and sensitivity of 92.46%

When a subgroup analysis was performed according the ATTR aetiology (ATTRm, ATTRwt) diagnostic accuracy remained similarly good. The AUC for T1 diagnostic accuracy in ATTRm was 0.88 (95% confidence interval [CI]: 0.82 – 0.93) compared with an AUC for ECV of 0.92 (95% confidence interval [CI]: 0.87 – 0.96). T1 and ECV also had similar diagnostic accuracy in ATTRwt patients: T1 AUC was 0.86 (95% confidence interval [CI]: 0.80 – 0.90) and ECV AUC of 0.90 (95% confidence interval [CI]: 0.85 – 0.94) (Figure 18). The T1 cut-off value to diagnose definitive or possible cardiac ATTRm was 1051ms with a specificity of 82.14% and sensitivity of 86.08% and for ECV was 0.469 with a specificity of 82.14% and sensitivity of 91.89%. The T1 cut-off value to diagnose definitive or possible cardiac ATTRwt was

1048ms with a specificity of 80.36% and sensitivity of 86.05% and for ECV was 0.469 with a specificity of 82.14% and sensitivity of 92.80%.

There were no statistically significant differences in the AUC for native T1 and ECV in all subgroup comparisons.

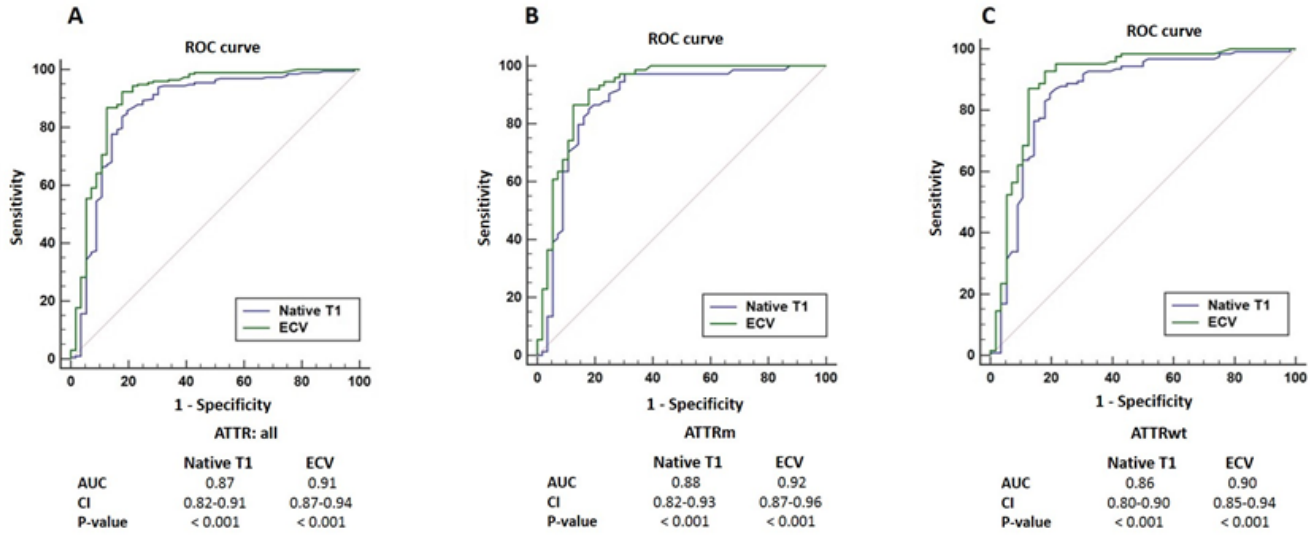

Figure 18. ROC curve for discrimination of possible or definite cardiac amyloidosis by native T1 and ECV from the combined HCM or ATTR mutation carriers.

T1, ECV, and DPD/LGE findings, cardiac function, biomarkers, and 6-min walk test

Both native T1 and ECV increased with increasing cardiac uptake as assessed by bone scintigraphy ($p < 0.001$ for trend). Native T1 and ECV were not elevated in mutation carriers (native T1: 968 ± 41ms; ECV 0.29 ± 0.03) but were elevated in the 17 patients with possible ATTR (isolated DPD grade 1) (native T1: 1023 ± 64 ms, ECV:

0.41 ± 0.13, $p < 0.05$ for both), all of which had no amyloid-like LGE by CMR, with the exception of patients with the Se77Tyr variant (Figure 19).

Correlations were broadly similar for T1 and ECV across ATTR types with (Table 7), but ECV correlated more strongly with parameters of cardiac function, biomarkers and 6 minute walking test than T1. Overall in all ATTR patients, T1 and ECV correlated with indexes of systolic and diastolic function, indexed LV mass, and known prognostic biomarkers as well as functional markers (6-minute walk test performance) in keeping with our previous findings (20,72,76). Furthermore, ECV correlated with indexed stroke volume but T1 did not. For subgroup analyses (ATTRm and ATTRwt), correlations were lower, reflecting the smaller sample sizes. In asymptomatic ATTR mutations carriers, there were no statistically significant correlations.

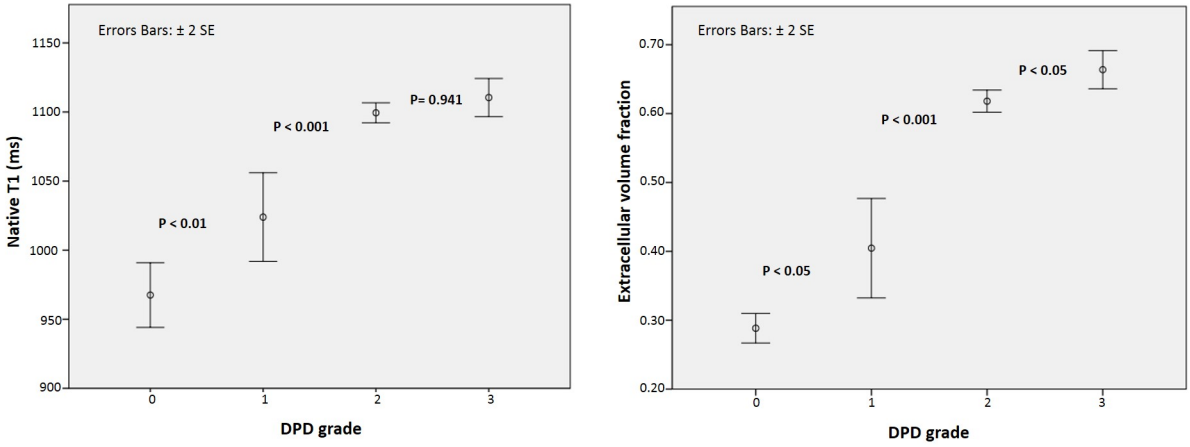

Figure 19. DPD grade versus native T1 (left) and ECV (right) in gene carriers and ATTR patients.

Table 7. Correlations between T1 and ECV and cardiac function, biomarkers and 6-minute walking test in ATTR patients.

	All ATTR (n=227)		**ATTRm (n=81)**		**ATTRwt (n=134)**		**Mutation carriers (n=12)**	
	T1	**ECV**	**T1**	**ECV**	**T1**	**ECV**	**T1**	**ECV**
CMR parameters								
LV $mass_i$, g/m^2	**0.537***	**0.619***	**0.356***	**0.504***	**0.483***	**0.535***	-0.188	-0.428
LA $area_i$, cm^2/m^2	**0.244***	**0.403***	-0.004	**0.267†**	**0.179†**	**0.319***	-0.159	0.222
LVEF, %	**-0.273***	**-0.567***	-0.015	**-0.625***	**-0.301***	**-0.466***	0.550	0.479
SV_i, ml/m^2	-0.115	**-0.402***	**0.247†**	**-0.460***	**-0.184†**	**-0.304***	-0.198	-0.076
Echocardiographic parameters								
E/E'	**0.277***	**0.306***	**0.238†**	**0.324***	**0.241***	**0.313***	0.540	**0.679†**
E-wave deceleration time, ms	-0.006	**-0.149†**	-0.077	**-0.260†**	0.072	-0.112	-0.402	-0.158
2-dimensional GLS, %	**-0.461***	**-0.671***	**-0.397***	**-0.699***	**-0.374***	**-0.574***	0.355	0.147
6 minute walk test								
6-minute walk test, m	**-0.246***	**-0.341***	-0.051	-0.051	-0.071	**-0.233†**	0.271	0.235
Biomarkers								
NT-proBNP, pmol/l	**0.482***	**0.731***	0.210	**0.648***	**0.338***	**0.597***	-0.184	-0.038
Troponin T, pmol/l	**0.462***	**0.618***	0.022	**0.340†**	0.200	**0.458***	0.326	-0.179

Values are Pearson's r correlation coefficient. *p< 0.01 †p<0.05

Association between T1, ECV, and outcome

At follow-up (mean 32 ± 17 months), 95 of 227 (42%) subjects had died (55 with wild-type ATTR and 40 with ATTRm). Native T1 and ECV predicted death in the ATTR population (T1: HR 1.225 each 59ms increase; 95% confidence interval, 1.010-1.486; p<0.05 and ECV: HR, 1.155 each 3% increase; 95% confidence interval, 1.097-1.216; p<0.001), and ECV also predicted death separately in the wild-type ATTR and ATTRm groups (p<0.01 for both). However, native T1 was not predictive of death when wild-type ATTR and ATTRm groups were analysed separately (Figure 20).

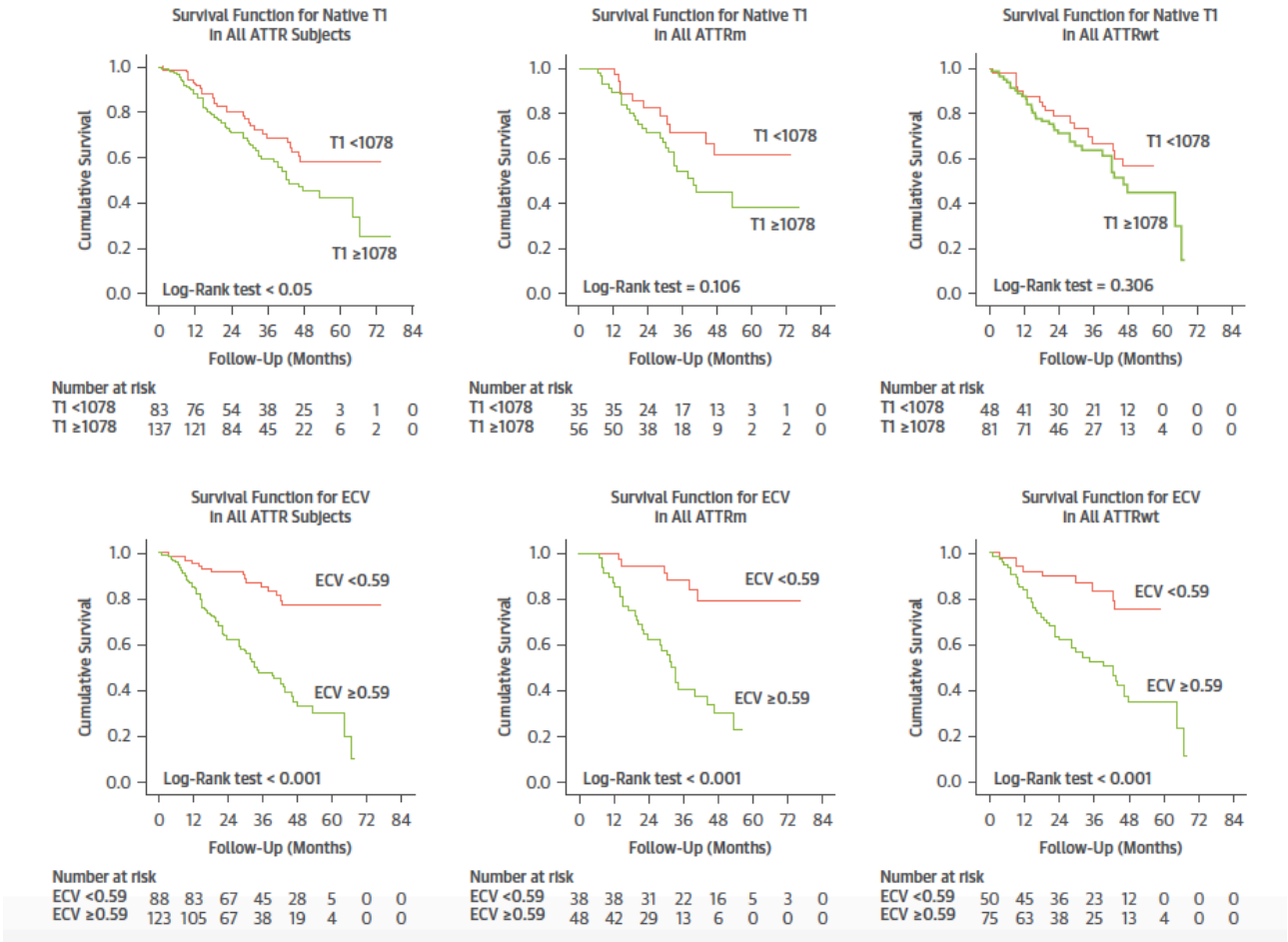

Figure 20. Kaplan-Meier curves for ECV and native T1. Native T1 correlated with mortality in all patients with ATTR, but it was not correlated when the analysis was performed in ATTRm and ATTRwt. ECV was correlated with mortality in all patients.

ECV remained significantly associated with mortality (HR: 1.101 each 3% increase; 95% CI: 1.022 to 1.187; $p < 0.05$) in multivariate Cox models that included age, NT-proBNP, LV ejection fraction, E/E', LV mass index, and DPD grade. Only age, ECV, and NT-proBNP remained significantly associated with mortality when LGE was added to the multivariate model (ECV, HR: 1.106 each 3% increase; 95% CI: 1.011 to 1.209; $p < 0.05$). In contrast, native T1 didn't remain significantly associated with mortality after adjustment for age, NT-proBNP, LV ejection fraction, E/E', LV mass index, and DPD grade ($p=0.971$). Native T1 remained not significant after the addition of LGE to the model. ($p = 0.729$).

Discussion

In this large ATTR amyloidosis population, we describe for the first time that native T1 mapping and ECV are good diagnostic techniques in cardiac ATTR amyloidosis, however in high levels of infiltration, native T1 and ECV can be discordant. Both parameters also correlate with mortality in cardiac ATTR amyloidosis. Nevertheless, only ECV remains independently predictive of prognosis, suggesting that it is a more robust marker in cardiac ATTR amyloidosis. In addition, we demonstrate that non-diagnostic DPD uptake (grade 1), previously held to be indeterminate but inconsistent with definitive ATTR amyloidosis, is associated with abnormal myocardial T1 and ECV, suggesting that CMR can detect a phenotype of early amyloid infiltration.

Native T1 and ECV have lately emerged as the first non-invasive quantitative markers of myocardial amyloid infiltration. Our earlier work in ATTR amyloidosis demonstrated that elevated native myocardial T1 in cardiac ATTR amyloidosis, was more sensitive than LGE imaging and had high diagnostic accuracy. Similarly, ECV was also elevated in patients with early stage disease when conventional clinical testing and LGE were normal, it tracked a range of markers of disease severity and

correlated with prognosis in ATTR amyloidosis (68). Whilst initial studies suggested the two biomarkers had similar clinical implications, important differences have recently emerged between the two main types of cardiac amyloidosis, with native T1 being relatively higher in AL amyloidosis compared to ATTR, and vice versa for ECV (5). The present study extends these intriguing observations, demonstrating that native T1 correlated with prognosis in ATTR amyloidosis and highlighting differences between the two biomarkers in ATTR amyloidosis, where both native T1 and ECV show a similar diagnostic accuracy, but ECV has significantly better correlation with all markers of amyloid burden and better prognostic power than native T1.

We believe that these differences represent different biological information provided by native T1 and ECV measurements. Cardiac amyloidosis is emerging as a spectrum characterised by variable degrees of amyloid infiltration, myocardial oedema, inflammation, and differential myocyte response with myocyte hypertrophy. The administration of contrast and ECV measurements enables us to isolate the signal from the extracellular space, but native myocardial T1 provides a composite signal from the intra and extracellular spaces, a signal potentially influenced by other pathophysiological mechanisms beyond simple amyloid load. Native myocardial T1 is highly influenced by water content in the tissue and will therefore be significantly raised by the presence of myocardial oedema (172). There are two types of myocardial oedema: intracellular and extracellular. ECV is elevated when there is extracellular oedema and T1 is elevated in both types (173). Myocardial oedema therefore influences both native T1 and ECV, however this influence is disproportionate when the oedema is mainly intracellular, with the degree of elevation

being higher in native T1 than in ECV. On the other hand, a relative increase in myocyte hypertrophy compared to amyloid burden will likely decrease the native T1.

In cardiac ATTR amyloidosis, progressive amyloid deposition is thought to be the main driver of disease progression, whilst in AL amyloidosis light chain toxicity and/or rate of amyloid deposition are believed to also play an important role, especially in contributing to early mortality. In this context, the better correlation of ECV not only with markers of disease severity but also prognosis in ATTR amyloidosis is not surprising, but in keeping with the hypothesis of ECV being a better marker of amyloid deposition. This hypothesis is also in line with the different significance of native T1 in AL amyloidosis as a powerful independent predictor of prognosis, since the ability to track both amyloid load and associated myocardial oedema is important in this particular amyloid subtype.

From this study, different roles emerge for measurements of native T1 and ECV in ATTR amyloidosis. The similar diagnostic performance supports the use of native T1 for diagnosis of ATTR amyloidosis, which also has the significant advantage of being a non-contrast technique. Lack of requirement for contrast means that native myocardial T1 mapping can be performed in patients with advanced renal failure, in whom administration of contrast is contraindicated. However, in this study we excluded patients with severe renal impairment leaving a knowledge gap on the clinical utility on non-contrast CMR in this setting. Lack of need to give contrast is also attractive in the general population given reduced cost and recent potential concerns about gadolinium accumulating in the brain, even though this has not been demonstrated for the cyclic gadolinium agents, such as that used in this study (174). On the other hand, ECV is a better marker in ATTR amyloidosis for risk stratification and probably for tracking disease progression. These differences are also supported

and at least in part explained by the relationship between native T1 and ECV. There is a good correlation between native T1 and ECV up to and ECV of 0.4, but when the extracellular volume expansion is higher the correlation between the two measurements becomes poor. The inability of native T1 to track increasing amyloid burden when the ECV is greater than 0.4 is likely to represent the main reason for the worse prognostic performance on native myocardial T1 compared to ECV. Both biomarkers do increase in subclinical disease, supporting their equivalent role as diagnostic markers, as confirmed by similar AUCs in the ROC curve analysis.

Study limitations. Cardiac biopsy was available in only a minority of patients, but this cohort of patients was fully characterised using the validated and now widely used non-invasive criteria for ATTR (21). Patients with pacemakers or defibrillators were also excluded. A wide range of TTR mutations were included in the analysis. In this study, T1 measurements were performed by drawing a ROI in the basal to mid septum of the appropriate 4-chamber map and the same approach was used for ECV measurements, therefore the total extent of cardiac amyloid infiltration was not assessed. T2 maps were not acquired in this study, limiting the possibility of exploring the hypothesis of myocardial oedema as a potential mechanism for the increase in T1. Finally, this was a single centre study where one T1 mapping technique was used. Care must be taken with interpretation of the different T1 cut-offs as T1 varies with magnetic field strength, different sequences and thus establishment of normal ranges for a given system, with use of standardisation tools, is recommended.

These observations confirm that native T1 and ECV have similar diagnostic accuracy identifying ATTR amyloidosis and both correlate with mortality. However, ECV is a

more robust predictor of prognosis. Future studies with T2 mapping could help to identify differences in amyloid biology between AL and ATTR amyloidosis.

CHAPTER 6: HIGH PREVALENCE OF INTRACARDIAC THROMBI IN CARDIAC AMYLOIDOSIS

This chapter is based on the publication below:

Martinez-Naharro A, Gonzalez-Lopez E, Corovic A, Mirelis J, Baksi AJ, Moon JC, Garcia-Pavia P, Gillmore JD, Hawkins PN, Fontana M. Native T1 and ECV in ATTR amyloidosis. High Prevalence of Intracardiac Thrombi in Cardiac Amyloidosis. *J Am Coll Cardiol*. 2019 Apr 9;73(13):1733-1734. doi: 10.1016/j.jacc.2019.01.035.

My contribution was analysing all the data as first operator, doing the statistical analysis, and writing the paper.

Introduction

Cardiac involvement is the major determinant of survival in systemic amyloidosis. Cardiac amyloidosis is characterised by extracellular amyloid infiltration (175). Two types commonly affect the heart leading to a restrictive cardiomyopathy: monoclonal immunoglobulin light-chain (AL or primary systemic) type and transthyretin (ATTR) type. Amyloid can infiltrate all cardiac chambers (176). The infiltrative process results in biventricular wall thickening with non-dilated ventricles, systolic and diastolic dysfunction, and low cardiac output, but it also involves the atria. The effects of systolic and diastolic ventricular dysfunction along with direct amyloid infiltration of atrial walls lead to mechanical dysfunction and atrial enlargement, which cause blood stasis and risk of thrombus formation (6,177).

A high prevalence of intracardiac thrombi has been identified in patients with cardiac amyloidosis at autopsy (178,179) and using transoesophageal echocardiography (TOE). However, the high frequency of intracardiac thrombi can be overestimated at

autopsy, and intracardiac thrombi identified during TOE may reflect referral bias since TOE studies have mostly been performed to discern a source of embolisation in patients with AF. It is not known whether such observations are applicable to the general cardiac amyloidosis population (180).

In the past decade, cardiovascular magnetic resonance (CMR) has emerged as a highly informative imaging technique in cardiac amyloidosis that provides complex diagnostic information as well as the ability to track changes over time (181). CMR is also a sensitive non-invasive method for detecting intracardiac thrombi; it is superior to echocardiography and TOE for identifying thrombus in the left ventricle (182,183) and offers a comparable and equally specific alternative to TOE for evaluation of thrombus in the left atrial appendage (LAA) (184).

The aim of this study was to assess the prevalence of intracardiac thrombi using CMR in an unselected cohort of patients with newly diagnosed cardiac amyloidosis.

Methods

Ethical approval was granted by the University College London/University College London Hospitals Joint Committees on the Ethics of Human Research Committee, and all participants provided written informed consent.

Study population

Three hundred consecutive subjects were prospectively recruited at the National Amyloidosis Centre, London, between June 2017 and December 2017, and 24 patients were recruited at Puerta de Hierro University Hospital in Madrid between March and June 2018. All patients underwent comprehensive clinical assessment including clinical evaluation, echocardiography, CMR, ECG, and serum biochemistry including NT-proBNP. Patients with suspected ATTR amyloidosis also underwent

technetium-labelled bone scintigraphy using 3,3-diphosphono-1,2-propanodicarboxylicacid (^{99m}Tc-DPD scintigraphy).

ATTR amyloidosis patients: Cardiac ATTR amyloidosis was defined as the combination of symptoms with an echocardiogram consistent with or suggestive of cardiac amyloidosis, a grade 2 or 3 cardiac uptake on ^{99m}Tc-DPD scintigraphy in the absence of a monoclonal gammopathy or, in the presence of monoclonal gammopathy, a cardiac biopsy positive for TTR (21). All subjects underwent sequencing of exons 2, 3, and 4 of the TTR gene. One-hundred-and-sixty-six consecutive patients (148 male, 89%; age 75 ± 9 years) with cardiac ATTR amyloidosis were recruited.

AL amyloidosis patients: Cardiac AL amyloidosis was determined on the basis of international consensus criteria (185) as well as the combination of typical features on CMR and biopsy proven systemic AL amyloidosis on cardiac or non-cardiac biopsy. One-hundred-and-fifty-five consecutive patients with cardiac AL amyloidosis (105 male, 68%; age 66±10 years) were recruited.

Apolipropotein A-I and A-IV amyloidosis patients: One patient with Apolipoprotein A-I amyloidosis (AApoAI) and two with Apoliprotein A-IV (AApoAIV) were recruited. The diagnosis was confirmed through histology, genetic sequencing, and proteomic amyloid fibril typing.

We excluded patients with contraindications to CMR including glomerular filtration rate <30 mL/min.

CMR protocol

All participants underwent CMR on 1.5T clinical scanners. A standard volumetric study with early gadolinium enhancement (EGE) and late gadolinium enhancement (LGE) was performed. The gadolinium-based contrast agent used was 0.1 mmol/kg of

gadoterate meglumine (Dotarem, Guerbet S.A., France). Early gadolinium images of the LAA where acquired using a 5mm contiguous stack through the LAA and a fixed long inversion time of 440ms to confirm the presence or absence of thrombus vs normal pectinate muscle and exclude slow flow-related enhancement seen on non-contrast images (Figure 21). For 300 patients, both EGE and LGE imaging used a free-breathing b-SSFP sequence with respiratory motion corrected (MOCO) averaging to improve SNR. By using the MOCO protocol with 8 averages, it was possible to acquire high resolution images with thin slices and with excellent SNR thereby enabling detection of small thrombi. EGE typically acquired 5 slices in 80 heartbeats. Early gadolinium images of the 4, 2, and 3-chamber long-axis views were also acquired. LGE imaging was acquired using magnitude and phase-sensitive inversion recovery reconstruction (PSIR) in all patients with balanced steady state free precession sequence. In 300 patients, T1 and T2 mapping were also acquired. For native and post-contrast T1 mapping, 4-chamber long-axis images were acquired using the Modified Look-Locker Inversion recovery (MOLLI) sequence after regional

shimming. After a bolus of contrast and standard LGE imaging, the T1 measurement was repeated with the MOLLI sequence.

CMR image analysis

All images and maps were analysed offline. T1 measurement was performed by drawing a region of interest (ROI) in the basal to mid septum of the appropriate 4-chamber map (68,186). For ECV measurement, a single ROI was drawn in each of the 4 required areas: myocardial T1 estimates (basal to mid septum in 4 chamber map) and blood T1 estimates (LV cavity blood pool in 4 chamber map, avoiding the papillary muscles) before and after contrast administration. Haematocrit was measured in all subjects immediately before each CMR study. ECV was calculated as: myocardial ECV = (1-haematocrit) x (ΔR1myocardium/ΔR1blood), where R1=1/T1.

T2 measurement was performed similarly with a region of interest (ROI) in the basal to mid septum of the 4-chamber map.

Early gadolinium images were reviewed blind by two specialist CMR cardiologists (AMN and MF) who determined the presence/absence of thrombus. Ventricular

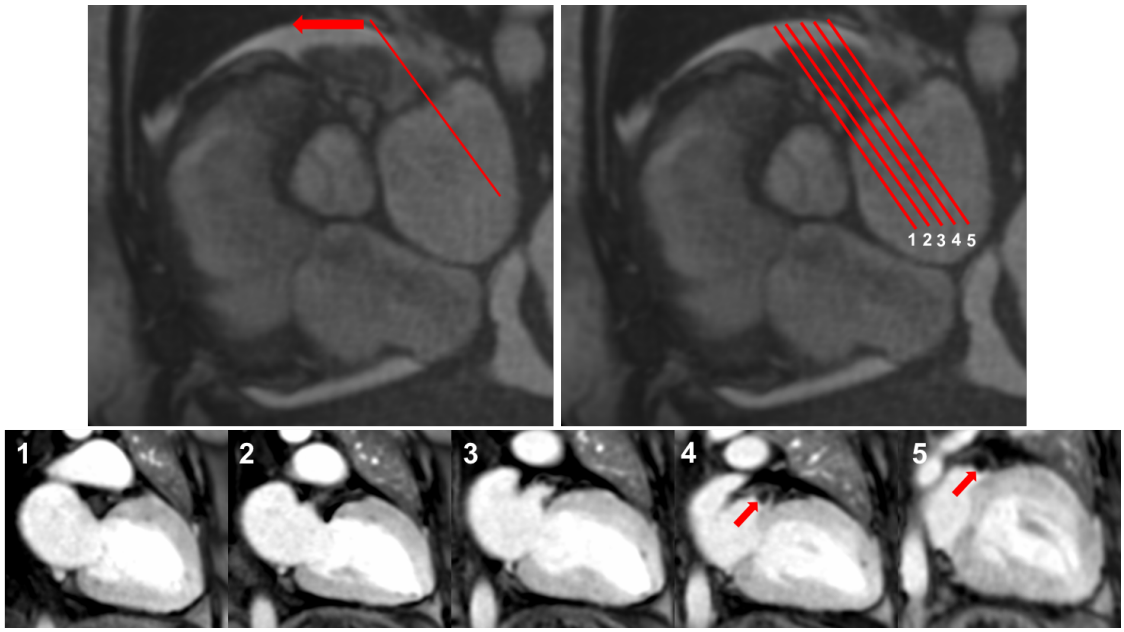

Figure 21. Acquisition of stack through the left atrial appendage on early gadolinium imaging.

myocardial LGE pattern was classified into 3 groups reflecting the degree of transmurality: group 1, no LGE; group 2, subendocardial LGE (when there was global subendocardial but no transmural LGE); and group 3, transmural LGE. The scans were classified according to the most extensive LGE identified, i.e. a patient with basal transmural LGE but apical subendocardial LGE was classified as transmural involvement (67).

Statistical Analysis

Statistical analysis was performed using IBM SPSS Statistics Version 22 (IBM, Somers, New York). All continuous variables were normally distributed (Shapiro-Wilk), other than N-terminal pro-brain natriuretic peptide (NT-proBNP) and troponin T, which were natural log (ln) transformed for bivariate testing. These are presented as mean ± standard deviation (SD) with non-ln transformed NT-proBNP and troponin T presented as median and interquartile range. Unpaired Student's t tests were used to compare continuous variables. The chi-square test or Fisher exact test was used to compare categorical data as appropriate. Receiver-operating characteristic (ROC) curve analysis was performed to define the diagnostic accuracy of CMR parameters and biomarkers. To assess the agreement of the presence/absence of intracardiac thrombi by two different observers, the intraclass correlation coefficient was calculated. Statistical significance was defined as $p < 0.05$.

Results

Study population

Three hundred and twenty-four patients with cardiac amyloidosis were enrolled (256 male, 79%; age 71 ± 11 years) (Table 8). One hundred and sixty-six patients had

cardiac ATTR amyloidosis (42 ATTRm, 124 ATTRwt), 155 had cardiac AL amyloidosis, 2 patients had Apolipoprotein A-I amyloidosis (AApoAI), and 1 had Apolipoprotein A-IV (AApoAIV) cardiac amyloidosis. The TTR mutations in cardiac amyloidosis were as follows: V122I (n = 19); T60A (n = 8); V30M (n = 3); A97S (n=3); and V20I, A120S, G47V, G89G, G89L, A90D, I107V, I68L, and S50R (1 case each).

Table 8: Biomarkers, echocardiographic and CMR findings in patients with cardiac amyloidosis.

	All cardiac amyloidosis (n=324)	**Cardiac AL (n=155)**	**Cardiac ATTR (n=166)**
Age, years	71 ± 11	66 ± 10	75 ± 9†
Biomarkers			
NT-proBNP, ng/L	3457 (1417-6571)	4032 (1315-8201)	2955 (1471-5386)
Troponin, ng/L	68 (40-108)	76 (40-154)	63 (41-89)†
Echocardiographic parameters			
E wave, m/s	0.84 ± 0.20	0.85 ± 0.22	0.82 ± 0.19
A wave, m/s	0.55 ± 0.28	0.63 ± 0.29	0.45 ± 0.23†
E/A	1.96 ± 1.13	1.74 ± 1.08	2.29 ± 1.14†
Average E', m/s	0.06 ± 0.04	0.06 ± 0.05	0.05 ± 0.01
E/E'	17 ± 7	17 ± 7	17 ± 6
E wave DT, ms	177.98 ± 58.18	174.76 ± 59.69	181.89 ± 56.29
2D GLS, %	-11.6 ± 4.1	-12.1 ± 4.5	-11.1 ± 3.7
CMR parameters			
LV mass, g	213 ± 67	190 ± 66	233 ± 61†
LV $mass_i$, g/m^2	114 ± 32	103 ± 31	123 ± 30†
LVEDV, mL	133 ± 38	127 ± 38	139 ± 38†
$LVEDV_i$, mL/m^2	71 ± 17	69 ± 17	73 ± 17†
SV, mL	75 ± 21	73 ± 21	76 ± 22
SV_i, mL/m^2	40 ± 10	40 ± 10	40 ± 10
LVEF, %	57 ± 12	59 ± 13	55 ± 11†
LA area, cm^2	30 ± 7	28 ± 6	33 ± 7†
RA area, cm^2	26 ± 8	24 ± 7	29 ± 8†

MAPSE, mm	7 ± 3	7 ± 3	8 ± 3
TAPSE, mm	13 ± 5	14 ± 6	12 ± 5†
Native T1, ms	1159 ± 85	1179 ± 100	1137 ± 57†
T2, ms	51 ± 4	53 ± 4	50 ± 3†
ECV	0.53 ± 0.9	0.52 ± 0.9	0.55 ± 0.8†

AL, light-chain amyloidosis; ATTR, transthyretin amyloidosis; NT-proBNP, N-terminal pro-brain natriuretic peptide; DT, deceleration time; GLS, global longitudinal strain; LV, left ventricle; LVEDV, left ventricular end diastolic volume; SV, stroke volume; LVEF, left ventricular ejection fraction; LA, left atrium; RA, right atrium; MAPSE, mitral annular plane systolic excursion; TAPSE, tricuspid annular plane systolic excursion; ECV, extracellular volume fraction. All continuous variables are presented as mean and standard deviation with non-transformed NT-proBNP and troponin presented as median and interquartile range. † P<0.05 cardiac AL vs ATTR patients

Two patterns of late gadolinium enhancement (LGE) were observed: subendocardial LGE and transmural LGE. Both patterns were present in AL and ATTR amyloidosis but to different extents, with subendocardial LGE being more prevalent in AL (45.8% in AL, 27.1% in ATTR, p<0.01) and transmural LGE more prevalent in ATTR (54.2% in AL and 72.9% in ATTR, p<0.01). Average ECV was 0.51 in AL and 0.55 in ATTR (p<0.01).

The prevalence of sinus rhythm in the overall population was 69.4% (225 patients), 94 patients had atrial fibrillation (29%) and 5 patients had atrial flutter (1.5%). The prevalence of atrial fibrillation was higher in ATTR than in AL (46.4% vs 14.2%, p<0.001).

Of the patients in atrial fibrillation, 7 were not on anticoagulation (7.1%), 32 were on vitamin K antagonists (32.7%), 58 were on DOACs (59.2%) and one patient was on heparin (1.0%).

In all patients, early gadolinium images were completed with no delay to the start of LGE acquisition, consequently avoiding increase in the overall acquisition time.

Intracardiac thrombi

The prevalence of intracardiac thrombi was 6.2% (95% CI 3.5, 8.8%) (20 patients) in the overall population, comprising 5.2% (95% CI 1.6, 8.8%) (8 patients) of those with AL and 7.2% (95% CI 3.3, 11.2%) (12 patients) with ATTR (p=0.45). No thrombi were observed in the AApoAI and AApoAIV patients. There was excellent interobserver agreement in the assignment of the presence/absence of intracardiac thrombi (intraclass correlation coefficient 1.0).

Of the patients with intracardiac thrombi (20 patients), 13 patients were in atrial fibrillation and 7 in sinus rhythm.

Overall the prevalence of thrombi in patients in atrial fibrillation/flutter was high (13.1%) (95% CI 6.4, 19.9%), 9.1% in AL (95% CI -4.0, 22.1%) (2 out of 22) versus 14.3% (6.3, 22.3%) in ATTR (11 out of 77) (p=0.52). All the patients with intracardiac thrombi in atrial fibrillation had received long term anticoagulation: 6 patients were on warfarin and 7 on DOACs (3 on apixaban, 3 on rivaroxaban and 1 on edoxaban).

The prevalence of intracardiac thrombi in patients in sinus rhythm and AL amyloidosis was 4.5% (95% CI 0.9, 8.1%) (6 out of 133) whilst in ATTR was 1.1% (-1.1, 3.4%) (1 out of 89) (p=0.11). Of the patients with intracardiac thrombi in sinus rhythm, 3 patients were not anticoagulated, 2 patients were on long term anticoagulation with DOACs (one on apixaban due to paroxysmal AF and one on rivaroxaban due to previous atrial flutter that underwent electrical cardioversion) and 2 patients were on long term warfarin (due to previous DVTs).

The prevalence of thrombi in anticoagulated patients was 12.2% (17 out of 139), 10.2% (95% CI 1.4, 19.0%) in AL, 5 out of 49, and 13.3% (95% CI 6.2, 20.5%) in ATTR, 12 out of 90 (p=0.59).

None of the patients with intracardiac thrombi had a known heritable thrombophilia or antiphospholipid syndrome. Two patients had a history of arterial emboli (one pulmonary and one renal) and 2 patients had nephrotic syndrome.

Most of the patients with intracardiac thrombi presented thrombi in the LAA (90%, 18 out of 20). However, thrombi in other locations were found in six patients (30%, 6 out of 20); 2 of them in isolation (without thrombi in the LAA) and 4 patients had thrombi in other locations as well as in the LAA (Figure 22).

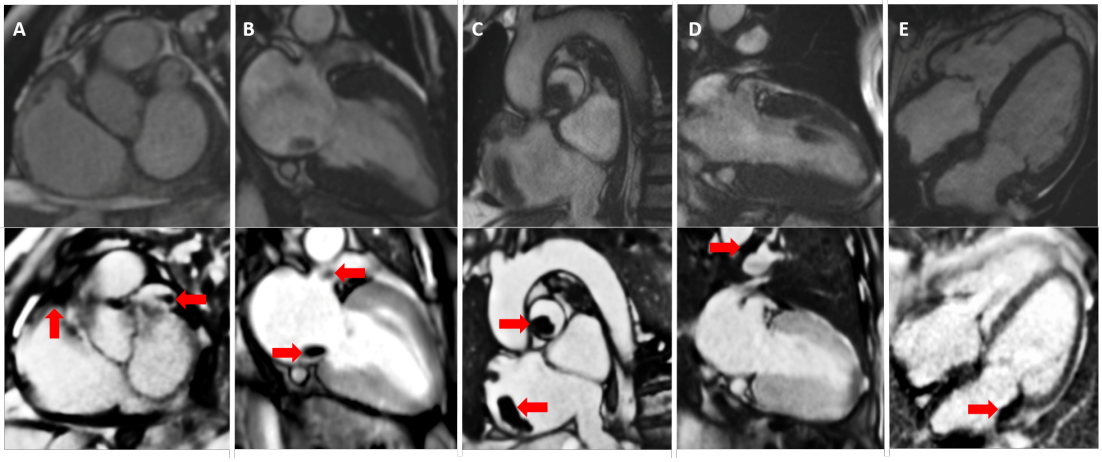

Figure 22. Location of intracardiac thrombi in cardiac amyloidosis.

Of the patients with thrombi in the LAA: a) 2 had also thrombi in the right atrial appendage (AL patients, one in sinus rhythm with no anticoagulation and one in AF on apixaban); b) one patient had multiple thrombi, including thrombus in the right atrial wall and in the proximal left and right pulmonary arteries (ATTR patient in AF on warfarin); c) and one patient was referred to our centre with the diagnosis of pedunculated mass in the left atrium, likely a benign myxoma, which was not present in an echocardiogram two years before. The findings on early gadolinium imaging, rest perfusion, T1 and T2 mapping confirmed the diagnosis of thrombus in the left atrium as well as in the LAA.

Two patients had thrombi in other locations without thrombi in the LAA: one patient had isolated thrombus in the right atrial appendage (ATTR patient in AF on warfarin) and one patient with AL amyloidosis had an isolated thrombus in the lateral wall of the left atrium.

Clinical variables, echo and CMR characteristics, and intracardiac thrombi

The presence of intracardiac thrombi was significantly higher in patients with more severe biventricular systolic dysfunction (stroke volume, $p<0.01$; ejection fraction, $p<0.05$; MAPSE, $p<0.01$, TAPSE, $p<0.01$, and global longitudinal strain, $p<0.01$), left and right atrial dilatation (LA $p<0.05$, RA $p<0.01$), and more severe degree of amyloid infiltration (ECV, $p< 0.01$). Finally, intracardiac thrombi was associated with higher levels of NT pro-BNP ($p<0.01$) (Table 9). Unsurprisingly, the presence of thrombi in the LAA was also higher in atrial fibrillation ($p<0.05$).

Table 9. Biomarkers, echocardiographic and CMR findings in patients with and without intracardiac thrombi.

	All (n=324)	**With (n=20)**	**Without (n=304)**	**P**
Age, years	71 ± 11	68 ± 13	71 ± 10	0.508
Biomarkers				
NT-proBNP, ng/L	3472 (1394-6692)	5537 (2999-15321)	3306 (1373-6362)	<0.01
Troponin, ng/L	68 (40-108)	85 (63-124)	67 (39-106)	0.058
Echocardiographic parameters				
E wave, m/s	0.84 ± 0.20	0.85 ± 0.18	0.83 ± 0.20	0.802
A wave, m/s	0.55 ± 0.28	0.42 ± 0.26	0.56 ± 0.28	0.144
E/A	1.96 ± 1.13	2.48 ± 1.09	1.93 ± 1.13	0.181
Average E', m/s	0.06 ± 0.04	0.05 ± 0.01	0.06 ± 0.04	0.216
E/E'	17 ± 7	20 ± 8	17 ± 6	0.067

E wave DT, ms	177.98 ± 58.18	157.69 ± 46.49	178.87 ± 58.28	0.199
2D GLS, %	-11.6 ± 4.1	-8.2 ± 3.3	-11.8 ± 4.0	<0.01
CMR parameters				
LV mass, g	213 ± 68	229 ± 66	212 ± 68	0.181
LV $mass_i$, g/m^2	114 ± 33	122 ± 27	113 ± 33	0.110
LVEDV, mL	134 ± 39	127 ± 34	134 ± 39	0.259
$LVEDV_i$, mL/m^2	71 ± 17	66 ± 16	71 ± 17	0.121
SV, mL	75 ± 22	62 ± 18	76 ± 21	<0.01
SV_i, mL/m^2	40 ± 11	33 ± 9	40 ± 10	<0.01
LVEF, %	57 ± 12	50 ± 12	57 ± 12	<0.05
LA area, cm^2	30 ± 7	34 ± 7	30 ± 7	<0.05
RA area, cm^2	26 ± 8	31 ± 9	26 ± 7	<0.01
MAPSE, mm	7 ± 3	6 ± 1	8 ± 3	<0.01
TAPSE, mm	13 ± 5	8 ± 3	14 ± 5	<0.01
Native T1, ms	1158 ± 84	1204 ± 244	1155 ± 58	0.386
T2, ms	51 ± 4	53 ± 7	51 ± 4	0.290
ECV	0.53 ± 0.9	0.59 ± 0.9	0.53 ± 0.9	<0.01

NT-proBNP, N-terminal pro-brain natriuretic peptide; DT, deceleration time; GLS, global longitudinal strain; LV, left ventricle; LVEDV, left ventricular end diastolic volume; SV, stroke volume; LVEF, left ventricular ejection fraction; LA, left atrium; RA, right atrium; MAPSE, mitral annular plane systolic excursion; TAPSE, tricuspid annular plane systolic excursion; ECV, extracellular volume fraction.

Receiver-operating characteristics analysis for all CMR parameters, echocardiographic parameters, and biomarkers to predict presence of intracardiac thrombus was performed (Table 10). Among all variables, tricuspid annular plane systolic excursion (TAPSE) was the parameter with the highest area under the curve (AUC) of 0.82, $p<0.001$ for presence of intracardiac thrombi. With ≤9mm as the cut-off, TAPSE had a sensitivity of 85% and a specificity of 72%.

Table 10. Area under the curve (AUC) of the receiver operative characteristic curve (ROC) for diagnosis of thrombosis in the left atrial appendage by biomarkers, echocardiographic and CMR parameters.

	AUC	**CI**	**P**
Biomarkers			
NT-proBNP, ng/L	0.68	0.55-0.81	<0.01
Troponin, ng/L	0.64	0.53-0.76	<0.05
Echocardiographic parameters			
E wave, m/s	0.54	0.40-0.68	0.57
A wave, m/s	0.68	0.48-0.88	0.08
E/A	0.34	0.18-0.50	0.13
Average E', m/s	0.66	0.53-0.78	<0.05
E/E'	0.64	0.52-0.76	0.08
E wave DT, ms	0.59	0.44-074	0.28
2D GLS, %	0.77	0.64-0.90	<0.001
CMR parameters			
LV mass, g	0.62	0.49-0.74	0.08
LV $mass_i$, g/m^2	0.62	0.50-0.73	0.08
LVEDV, mL	0.45	0.32-0.57	0.42
$LVEDV_i$, mL/m^2	0.42	0.29-0.55	0.24
SV, mL	0.67	0.56-0.78	<0.05
SV_i, mL/m^2	0.71	0.61-0.82	<0.01
LVEF, %	0.66	0.56-0.77	<0.05
LA area, cm^2	0.67	0.55-0.79	<0.05
RA area, cm^2	0.68	0.56-0.80	<0.01

MAPSE, mm	0.75	0.67-0.83	<0.001
TAPSE, mm	0.82	0.74-0.89	<0.001
Native T1, ms	0.48	0.33-0.63	0.78
T2, ms	0.57	0.41-0.72	0.31
ECV	0.66	0.53-0.78	<0.05

AUC, area under the curve; CI, confidence interval NT-proBNP, N-terminal pro-brain natriuretic peptide; DT, deceleration time; GLS, global longitudinal strain; LV, left ventricle; LVEDV, left ventricular end diastolic volume; SV, stroke volume; LVEF, left ventricular ejection fraction; LA, left atrium; RA, right atrium; MAPSE, mitral annular plane systolic excursion; TAPSE, tricuspid annular plane systolic excursion; ECV, extracellular volume fraction.

Discussion

We report here a large prospective study to determine the prevalence of intracardiac thrombi in a large unselected cohort of patients with cardiac amyloidosis. The principal findings were: 1) the prevalence of intracardiac thrombi in an unselected cohort of patients with cardiac amyloidosis was high; 2) in contrast with what is known in the general population, intracardiac thrombi were highly prevalent in patients with cardiac amyloidosis who had atrial fibrillation/flutter despite long term anticoagulation (13.1%); 3) intracardiac thrombi were present in a significant proportion of patients in sinus rhythm (4.5% in AL and 1.1% in ATTR); 4) the presence of intracardiac thrombi is associated with more severe systolic and diastolic dysfunction and myocardial amyloid infiltration, with TAPSE being the parameter with higher diagnostic power. 5) CMR is a useful non-invasive tool to assess the presence of intracardiac thrombi in patients with a new diagnosis of cardiac amyloidosis (Figure 23).

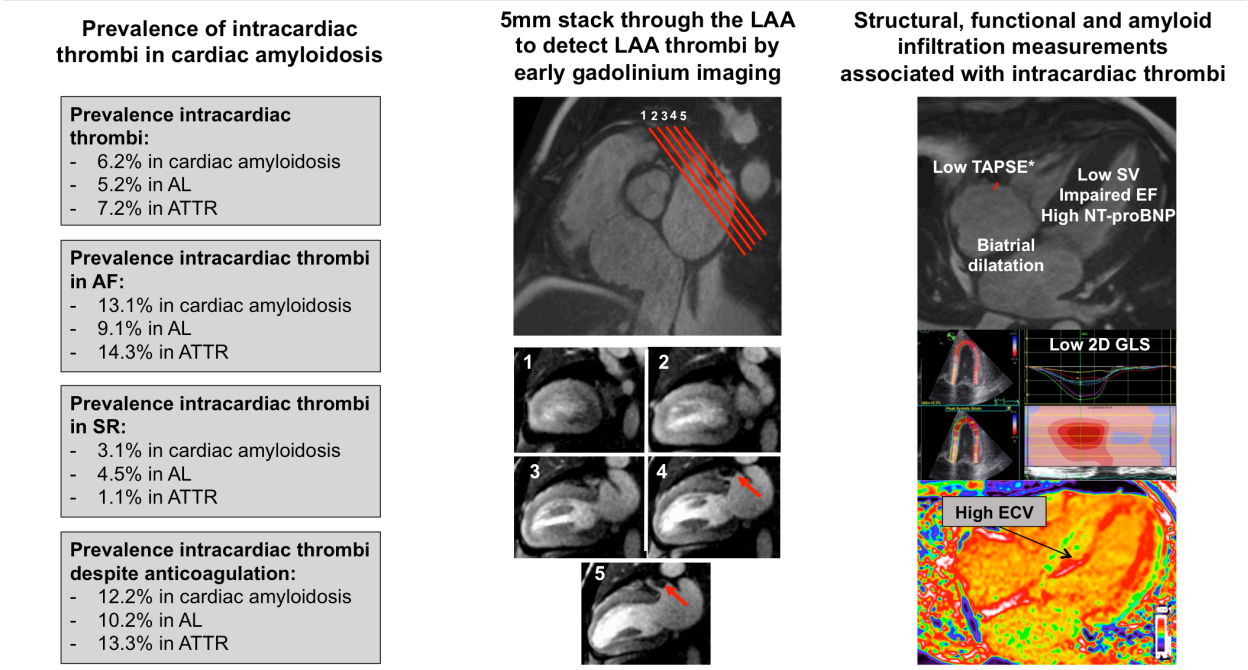

Figure 23. Summary of findings. Left panel describes the prevalence of intracardiac thrombi in cardiac amyloidosis. Central panel shows the acquisition of the stack through the left atrial appendage. Right panel shows the variables associated with intracardiac thrombi.

This is the first study to report the prevalence of intracardiac thrombi in an unselected cohort of patients with newly diagnosed cardiac amyloidosis. In contrast to the general anticoagulated atrial fibrillation population, in whom the prevalence of LAA thrombi is less than 3% (187-190), we report a high prevalence of intracardiac thrombi in atrial fibrillation associated with cardiac amyloidosis despite anticoagulation (13.1%). These findings suggest that current European and American recommendations for cardioversion for anticoagulated patients with AF should not be applied to those with cardiac amyloidosis (191,192). Current guidelines recommend that patients who have been in AF for longer than 48 hours should start oral

anticoagulation at least 3 weeks before cardioversion and continue it for 4 weeks afterwards. Guidelines do not consider routine exclusion of thrombus in the LAA necessary. Our results do not support the use of this recommendation in patients with amyloidosis and highlight the need for specific imaging to exclude intracardiac thrombi before undergoing cardioversion. Furthermore, our study shows that intracardiac thrombi can be found also in patients in sinus rhythm with no significant difference between the two main types (4.5% in AL and 1.1% in ATTR, p=0.11), suggesting that other mechanisms beyond AF play an important role in patients with cardiac amyloidosis.

There are three key mechanisms involved in thrombus formation according to Virchow's triad: circulation stasis, vascular wall injury and hypercoagulability. Cardiac AL and ATTR amyloidosis differentially compromise these three key processes within the cardiovascular system and each of these may be more or less prominent depending upon the individual, the disease type, treatment, clonal response and co-morbidities. Firstly, circulation stasis is a characteristic feature of cardiac amyloidosis: uncoordinated atrial contraction is undoubtedly pro-thrombotic but haemodynamic compromise is present also in patients in sinus rhythm where systolic and diastolic dysfunction along with atrial impairment, secondary to direct amyloid infiltration, contribute to blood stasis. Patients with ATTR amyloidosis traditionally present a more severe degree of structural and functional changes compared to patients with AL amyloidosis, making blood stasis a mechanism more likely to be predominant in ATTR compared to AL. Secondly, vascular wall injury caused by direct amyloid infiltration, myocardial ischaemia and light chain toxicity occurs throughout the body resulting in endothelial damage and dysfunction (193,194). The degree of amyloid infiltration and probably myocardial ischaemia is more prominent

in ATTR compared to AL amyloidosis, but light chain toxicity is a specific feature of AL amyloidosis during the phase of active amyloid production. Thirdly, hypercoagulability is commonly seen in cardiac amyloidosis, especially AL, where a wide spectrum of clotting factor abnormalities, impairment of the thrombin-antithrombin pathway and comorbidities such as nephrotic syndrome frequently occur (195-197). In line with these hypotheses, in our study population, the presence of intracardiac thrombi was associated with evidence of poorer LV and RV systolic function (LV stroke volume, LV ejection fraction, MAPSE, TAPSE and global longitudinal strain), increased left and right atrial area, and higher degree of amyloid infiltration estimated by extracellular volume measurements. In keeping with previous observations, we showed a more severe degree of functional and structural impairment, and amyloid infiltration in ATTR compared to AL. However, there was no difference in the prevalence of intracardiac thrombi between cardiac AL and ATTR in the overall population (5.2% vs 7.2% p=0.45), in the subset of patients with atrial fibrillation (9.1% vs 14.3 p=0.52) or in anticoagulated patients (10.2% vs 13.3% p=0.59). These results are in keeping with the hypothesis that other mechanisms beyond circulation stasis play an important role in thrombus formation, especially in AL amyloidosis, where hypercoagulability and vascular wall injury may be predominant. All patients with AL amyloidosis in our study were assessed before chemotherapy treatment, when light chain toxicity dominates the disease course, and two of the patients with intracardiac thrombi had nephrotic syndrome.

CMR is one of the non-invasive reference standards to assess cardiac amyloidosis with pathognomonic findings on late gadolinium imaging (67) and very elevated native T1 and ECV values (68). This study shows that CMR can also be used to assess the prevalence of intracardiac thrombi with no appreciable increase in overall

scan duration (184). We demonstrate that widely available CMR sequences can be used to detect thrombi in different intracardiac locations (the most common being the LAA, followed by the right atrial appendage and LA). This supports adoption of wider screening for intracardiac thrombi in routine clinical practice, which should not only include the left but also the right atrial appendage and atrial walls. Interestingly, TAPSE was the parameter most strongly associated with the presence of intracardiac thrombi. TAPSE has been previously described as the most statistically significant independent marker of prognosis in a previous study (42) and the simplicity of TAPSE measurement makes this parameter an attractive way to stratify the risk of intracardiac thrombi in patients with cardiac amyloidosis.

This study has a number of limitations. The assessment of thrombi in the LAA was performed by CMR, and TOE, the current gold standard, was not performed in any of our patients. However, CMR has been demonstrated to be superior to echocardiography and TOE for the detection of thrombus in the left ventricle and offers a comparable and equally specific alternative to TOE for the non- invasive evaluation of thrombus in the LAA (184). The right atrial appendage was not systematically studied performing a 5 mm contiguous stack; therefore, thrombi in that location could be underestimated.

These findings have a number of potential implications for the management of patients with cardiac amyloidosis, underpinning the importance of greater consideration of the possibility of intracardiac thrombus regardless of underlying rhythm or the presence of anticoagulation.

CHAPTER 7: MYOCARDIAL HYPOPERFUSION IN CARDIAC AMYLOIDOSIS: PREVALENCE, DETERMINANTS, AND CLINICAL SIGNIFICANCE

Introduction

Cardiac amyloidosis is characterised by widespread infiltration of amyloid deposits throughout the extracellular space in the heart (5). Two types commonly affect the heart leading to a restrictive cardiomyopathy: monoclonal immunoglobulin light-chain (AL or primary systemic) type and transthyretin (ATTR) type. Amyloid can involve all cardiac chambers (175,198).

The infiltrative process results in biventricular wall thickening with non-dilated ventricles, systolic and diastolic dysfunction, and low cardiac output. Within the ventricular myocardium, biopsy and autopsy studies have shown that amyloid deposits accumulate in the interstitial space and perivascular structures (179,199-201), resulting in narrowing of vessel lumens and capillary disruption and rarefaction. The effects of systolic and diastolic ventricular dysfunction along with direct amyloid infiltration of the vessel wall and capillaries thus have obvious potential to reduce myocardial perfusion.

Previous studies using PET imaging have indicated a reduction in perfusion and myocardial perfusion reserve in small cohorts of patients with cardiac amyloidosis (202,203). However, no information on disease severity, extent of myocardial amyloid infiltration or degree of systolic and diastolic dysfunction has been available in these studies, leaving a knowledge gap on the main determinants of myocardial hypoperfusion and its prevalence across a wide spectrum of disease severity.

Recently, a new CMR myocardial perfusion method with automated in-line perfusion mapping has been developed, allowing pixel-wise quantification of myocardial blood flow (MBF) (78) during patient evaluations that include structural and functional information as well as tissue composition studies with surrogate measurements of amyloid burden.

The aims of this study were 1) to determine the prevalence of myocardial hypoperfusion across a wide spectrum of cardiac amyloid infiltration in the two main types of cardiac amyloidosis; 2) to correlate abnormalities of perfusion with the extent of amyloid deposits and markers of disease severity.

Methods

Study population

A total of 200 consecutive patients undergoing CMR were prospectively recruited between January 2016 and June 2017. All patients underwent a comprehensive clinical assessment at the National Amyloidosis Centre, London, including clinical evaluation, echocardiography, CMR with gadolinium contrast, serum and urine biochemistry including N-terminal pro-B-type natriuretic peptide (NT-proBNP) and troponin T. The study population comprised the two groups described below and an additional twenty-three healthy volunteers who underwent evaluation by CMR. Ethical approval was granted by the University College London/University College London Hospitals Joint Committees on the Ethics of Human Research Committee, and all participants provided written informed consent.

ATTR amyloidosis patients. Cardiac ATTR amyloidosis was defined as the combination of symptoms with an echocardiogram consistent with or suggestive of cardiac amyloidosis, a grade 2 or 3 cardiac uptake on ^{99m}Tc-DPD scintigraphy in the

absence of a monoclonal gammopathy or, in the presence of monoclonal gammopathy, a cardiac biopsy confirming ATTR (21). All subjects underwent sequencing of exons 2, 3, and 4 of the *TTR* gene. One-hundred consecutive patients (93 male, 93%; age 76 ± 9 years) with cardiac ATTR amyloidosis were recruited.

AL amyloidosis patients. Cardiac AL amyloidosis was determined on the basis of international consensus criteria (185) as well as the combination of typical features on CMR and biopsy proven systemic AL amyloidosis on cardiac or non-cardiac biopsy. One-hundred consecutive patients with cardiac AL amyloidosis (63 male, 63%; age 64 ± 10 years) were recruited.

Healthy volunteers. Twenty-three healthy volunteers (18 male, 78%; age 45 ± 9 years) with no symptoms and no past history of cardiovascular disease, hypertension or diabetes were also recruited and underwent CMR only.

CMR image acquisition

All participants underwent CMR on a 1.5T scanner (Magnetom Aera, Siemens Healthcare, Erlangen, Germany). Scans were performed in accordance with local protocols and included localisers, cine imaging (with steady state free precession (SSFP) sequence), native T1 mapping, late gadolinium enhancement (LGE) imaging with phase sensitive inversion recovery (PSIR) and extracellular volume (ECV) mapping. Basal, mid-ventricular, and apical short-axis perfusion images were acquired at rest. Image acquisition was performed over 60 heart beats with a bolus of 0.1mmol/kg gadoterate meglumine (Dotarem, Guerbet SA, Paris, France) administered (4 ml/sec with 20 ml saline flush) during acquisition of the perfusion sequence. The arterial input function was calculated using the left ventricular (LV) blood pool which was automatically segmented from optimised low-resolution images acquired prior to higher spatial resolution images used for estimating myocardial

perfusion. In order to achieve a linear relationship between the input function and the gadolinium concentration, a number of steps were taken in the design of the sequence protocol and image reconstruction as previously described (78). Briefly, the sequence uses a low flip angle FLASH low resolution protocol with 2 echoes such that the echo times were short to minimize T2* losses at high concentration, and so that remaining T2* losses could be estimated and corrected. The non-linearity of saturation recovery was minimized by using a short saturation delay achieved using a small matrix and parallel imaging to reduce the number of phase encode lines. The remaining non-linear response was corrected by converting to gadolinium concentration units by means of a look-up-table calculated by a Bloch simulation of the specific protocol, which was recalculated for each scan as part of the image reconstruction. Myocardial perfusion was then calculated using a blood tissue exchange model (130) and pixel-wise perfusion maps were automatically generated in-line.

For native and post-contrast T1 mapping, 4-chamber long-axis images were acquired using the modified look-locker inversion recovery (MOLLI) sequence after regional shimming. After administration of contrast and standard LGE imaging, the T1 measurement was repeated with the MOLLI sequence and ECV maps where reconstructed inline on the scanner using the haematocrit as previously described (186).

CMR image analysis

All CMR images were analysed using offline using Osirix MD 9.0 (Bernex, Switzerland).

T1 and ECV measurements were performed by drawing a region of interest (ROI) in the basal to mid septum of the appropriate 4-chamber map.

The LGE pattern was classified into 3 groups reflecting the extent of amyloid deposition according to the degree of transmurality: group 1, no LGE; group 2, subendocardial LGE (i.e. when there was global subendocardial but no regions of transmural LGE); and group 3, transmural LGE (when the LGE was extending transmurally). Thus, a patient with basal transmural LGE but apical subendocardial LGE would be classified as transmural LGE (67).

MBF measurements were performed by drawing a ROI in the basal inferoseptum of the basal short axis perfusion map.

Statistical analysis

Statistical analysis was performed using IBM SPSS Statistics Version 25 (IBM, Somers, New York). All continuous variables were normally distributed (Shapiro-Wilk), other than NT-proBNP and Troponin T, which were natural log (ln) transformed for bivariate testing. All continuous variables are presented as mean ± standard deviation (SD) with non-ln transformed NT-proBNP and non-ln transformed Troponin T presented as median and interquartile range. For normally distributed variables, the unpaired Student t-test was used to compare the means between two groups and one-way analysis of variance (ANOVA) with post-hoc Bonferroni correction to compare the means of multiple groups. The chi-square test or Fisher exact test was used to compare categorical data as appropriate. Correlations between parameters were assessed using Pearson (r) or Spearman's rho. Statistical significance was defined as $p < 0.05$.

Results

The details of the 200 patients with cardiac amyloidosis subjects are shown in Table 11. A total of 100 patients with ATTR amyloidosis and 100 patients with AL amyloidosis were enrolled. These subjects were compared with 23 healthy volunteers. Of the patients with ATTR amyloidosis, 79 had wild-type ATTR and 21 hereditary ATTR (ATTRm); the TTR mutations were V122I (n = 9); T60A (n = 9); and F33V, H90D, V20I in one case each.

Table 11. Biomarkers, echocardiographic and CMR findings in all patients with cardiac amyloidosis, ATTR and AL amyloidosis.

	AL (n = 100)	**ATTR (n = 100)**	**P**
Age, years	64 ± 10	76 ± 9	**<0.001**
Biomarkers			
NT-proBNP, ng/L	3009 (935 - 6544)	2496 (1274 -4262)	0.525
Troponin T, ng/L	59 (36-102)	56 (33-73)	0.404
Echocardiographic Parameters			
IVS, cm	1.46 ± 0.25	1.73 ± 0.23	**<0.001**
LA area, cm^2	23.00 ± 6.84	26.78 ± 5.87	**<0.001**
E/A	1.74 ± 0.98	2.68 ± 1.24	**<0.001**
E/E’	15 ± 8	15 ± 8	0.935
E-wave deceleration time, ms	200 ± 63	200 ± 56	0.938
2D GLS	-13.6 ± 5.4	-11.7 ± 3.9	**0.001**
CMR parameters			
LV mass, g	195 ± 75	248 ± 66	**<0.001**
LV $mass_i$, g/m^2	101 ± 33	131 ± 33	**<0.001**
LVEDV, mL	119 ± 37	139 ± 35	**<0.001**
$LVEDV_i$, mL/m^2	62 ± 15	72 ± 17	**<0.001**
LVESV, mL	44 ± 26	63 ± 34	**<0.001**
$LVESV_i$, mL/m^2	39 ± 10	33 ± 18	**<0.001**
LVSV, mL	74 ± 25	76 ± 20	0.473
$LVSV_i$, mL/m^2	39 ± 10	43 ± 26	0.218
LVEF, %	64 ± 12	64 ± 73	0.918

MAPSE, mm	8 ± 3	7 ± 3	**0.025**
TAPSE, mm	15 ± 6	14 ± 6	0.073
ECV	0.49 ± 0.8	0.53 ± 0.8	**<0.001**
Native Myocardial T1, ms	1169 ± 66	1131 ± 52	**<0.001**
Myocardial T2, ms	52 ± 3	50 ± 3	**<0.001**
Myocardial blood flow, ml/min/g	0.73 ± 0.21	0.50 ± 0.13	**<0.001**
Myocyte mass, g	98 ± 36	114 ± 31	**<0.01**
MBF/myocyte mass, ml/min	0.009 ± 0.005	0.004 ± 0.002	**<0.001**

Values are mean ± SD, %, or median (interquartile range). ATTR = transthyretin amyloidosis; CMR = cardiac magnetic resonance; ECV = extracellular volume; GLS = global longitudinal strain; IVS = interventricular septum; LA = left atrium; LV = left ventricular; LVEDD = left ventricular end-diastolic diameter; LVEDV = left ventricular end-diastolic volume; LVEF = left ventricular ejection fraction; LVESV = left ventricular end systolic volume; LVSV = left ventricular stroke volume; MAPSE = mitral annular plane systolic excursion; MBF = myocardial blood flow; NT-proBNP = N-terminal pro-B-type natriuretic peptide; TAPSE = tricuspid annular plane systolic excursion.

Late gadolinium enhancement

Two patterns of late gadolinium enhancement (LGE) were observed: subendocardial LGE and transmural LGE. In line with previous publications (68), both patterns were present in AL and ATTR amyloidosis but to different extents, with subendocardial LGE being more prevalent in AL (60% in AL, 31% in ATTR, $p<0.01$) and transmural LGE more prevalent in ATTR (40% in AL and 69% in ATTR, $p<0.01$). All healthy volunteers had no late gadolinium enhancement. Consistent with previously reports (5,77), native T1 and T2 values were higher in AL than in ATTR (T1: 1169ms vs 1131 ms, $p<0.001$, T2: 52 vs 50ms, $p<0.001$). Average ECV was 0.49 in AL and 0.53 in ATTR ($p<0.01$). Average ECV in healthy volunteers was 0.27 (Figure 24).

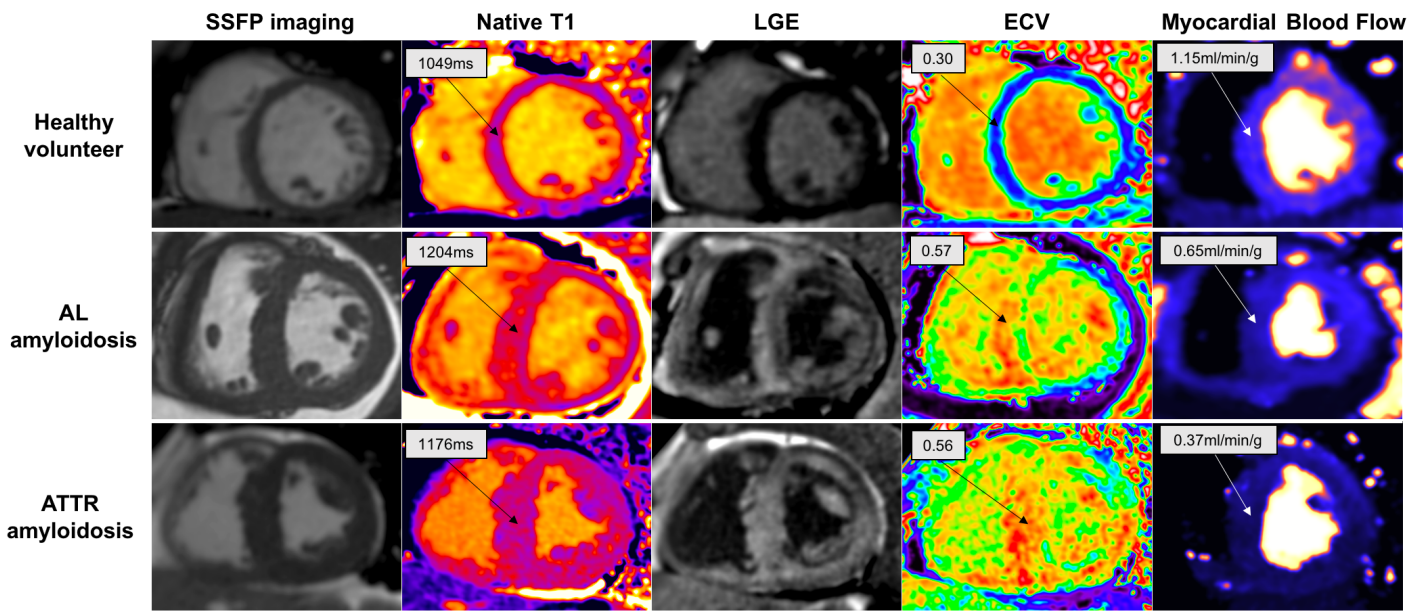

Figure 24. Native T1, LGE, ECV and myocardial blood flow in a healthy volunteer, a patient with AL and a patient with ATTR cardiac amyloidosis

Myocardial perfusion in cardiac amyloidosis

The pixel-wise MBF maps at rest were generated automatically within 2.5 minutes after image acquisition in all patients and healthy volunteers.

Myocardial perfusion was significantly reduced in cardiac amyloidosis compared to healthy volunteers (0.61±0.21ml/min/g vs 0.85±0.17ml/min/g, $p<0.001$) with the degree of reduction being greater in ATTR compared to AL (0.50ml/min/g in ATTR vs 0.73ml/min/g in AL ($p<0.001$)). The reduction in myocardial perfusion was also confirmed after adjusting for myocyte mass (MBF/myocyte mass: 0.011 ± 0.006 ml/min in healthy volunteers vs 0.007 ± 0.004 ml/min in cardiac amyloidosis, $p<0.001$), with the degree of reduction being greater in ATTR compared to AL (MBF/myocyte mass: 0.004 ± 0.002 ml/min in ATTR vs 0.009 ± 0.005 ml/min in AL, $p< 0.001$), in spite of a higher myocyte mass (myocyte mass: 114 ± 31 g in ATTR vs 98 ± 36 g in AL, $p<0.01$) (Figure 25).

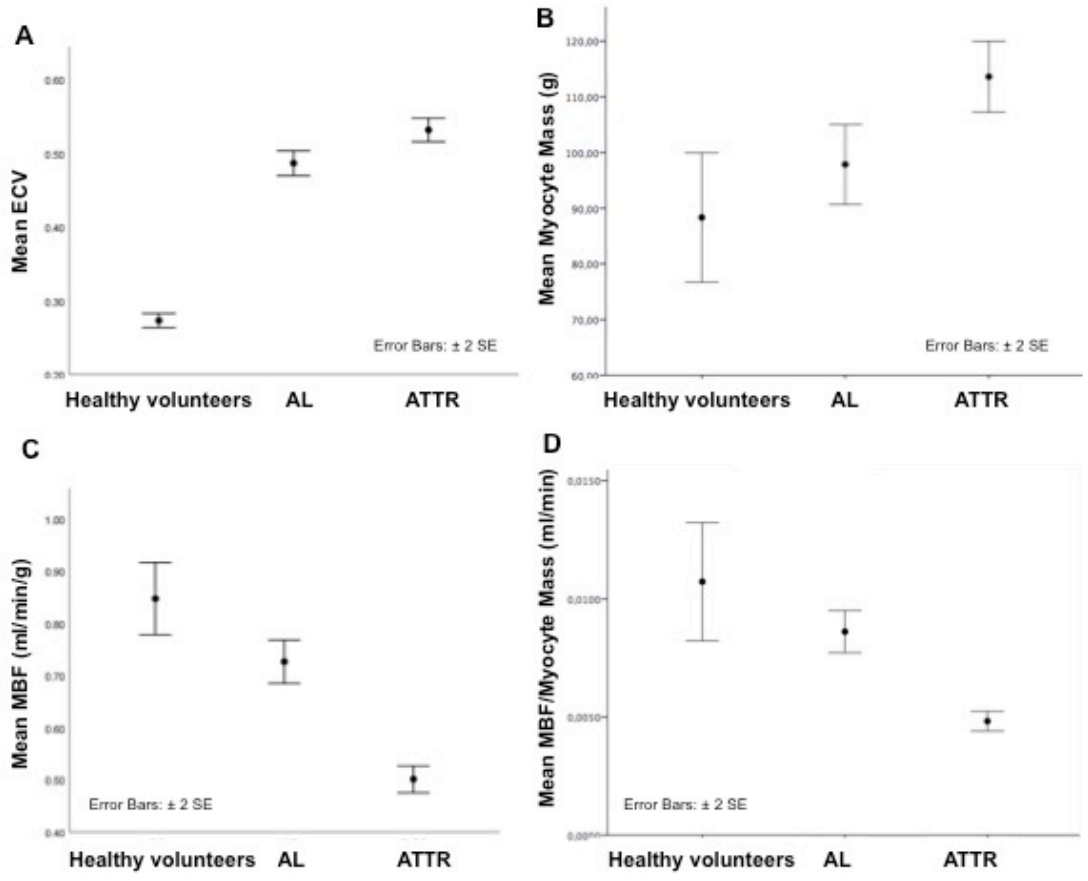

Figure 25. Mean ECV, mean myocyte mass, mean myocardial blood flow (MBF) and mean MBF/myocyte mass in healthy volunteers, AL and ATTR amyloidosis patients.

Myocardial perfusion inversely correlated with the transmurality of LGE (no LGE 0.86±0.17ml/min/g, subendocardial LGE 0.75±0.20ml/min/g and transmural LGE 0.50±0.13ml/min/g, $p<0.001$) (Figure 25) and showed a good inverse correlation with ECV fraction ($r = -0.637$, $p<0.001$) (Figure 25). There was also an inverse correlation between MBF and myocardial mass index ($r=-0.481$, $p<0.001$) and with the thickness of the interventricular septum (IVSd) by echocardiography ($r=-0.554$, $p<0.001$). There was correlation between MBF and markers of systolic function (stroke volume, $r = 0.156$, $p<0.01$; MAPSE, $r=0.392$, $p<0.001$; TAPSE, $r=0.372$, $p<0.001$; global longitudinal strain; $r=0.498$, $p<0.001$) as well as inverse correlation with markers of diastolic function (E/A, $r=-0.444$, $p<0.001$; E/E', $r=-0.197$, $p<0.01$) and blood

biomarkers (NT-proBNP, r = -0.262, p<0.001 and Troponin T, r = -0.242, p<0.01) (Table 12).

Table 12: Correlations between MBF and CMR findings in patients with cardiac amyloidosis.

	All cardiac amyloidosis (n = 200)	**AL (n = 100)**	**ATTR (n = 100)**
Biomarkers			
NT-proBNP, ng/L	**-0.262****	**-0.389****	**-0.272***
Troponin T, ng/L	**-0.242****	**-0.362****	**-0.268***
Echocardiographic Parameters			
IVS, cm	**-0.554****	**-0.438****	**-0.315****
LA area, cm^2	**-0.403****	**-0.358****	**-0.224***
E/A	**-0.444****	**-0.407****	-0.169
E/E'	**-0.197****	**-0.317****	-0.115
E-wave deceleration time, ms	0.29	0.065	-0.011
2D GLS, %	**0.498****	**0.478****	**0.383****
CMR parameters			
LVEDV, mL	**-0.233****	-0.073	-0.157
$LVEDV_i$, mL/m^2	**-0.205****	-0.042	-0.055
LVESV, mL	**-0.379****	**-0.288****	**-0.286****
$LVESV_i$, mL/m^2	**-0.378****	**-0.288****	**-0.266****
LVSV, mL	**0.156***	**0.226***	**0.211***
$LVSV_i$, mL/m^2	0.012	**0.289****	-0.035
LVEF, %	0.072	**0.418***	0.040
MAPSE, mm	**0.392****	**0.409****	**0.298****
TAPSE, mm	**0.372****	**0.401****	**0.324****
ECV, %	**-0.637****	**-0.632****	**-0.590****
Native Myocardial T1, ms	0.073	-0.161	-0.036
Myocardial T2, ms	**0.194****	-0.076	0.196
Myocyte mass, g	**-0.157***	-0.129	0.136

Values are Pearson's correlation coefficient. Bold indicates statistically significant values. **p<0.01, *p<0.05. Abbreviations as in Table 11.

In the multivariate analysis that included markers of systolic function (2D GLS, stroke volume and TAPSE), diastolic function (E/A, E/E'), and amyloid burden (ECV and T2), only 2D GLS, E/A and ECV remained independent predictors of myocardial hypoperfusion.

Discussion

The present study shows that this novel automated in-line myocardial perfusion mapping technique can be used routinely to quantify myocardial perfusion in cardiac amyloidosis. Our findings show that myocardial perfusion at rest is significantly reduced in the two most common types of cardiac amyloidosis, AL and ATTR, including when adjusting for myocyte mass, and that myocardial perfusion is influenced by various mechanisms including the extent of amyloid deposition and the degree of systolic and diastolic dysfunction.

A non-invasive method to measure myocardial perfusion in cardiac amyloidosis during a clinical study that evaluates structure and function as well as tissue composition with surrogate measures of amyloid burden, provides an accessible means to explore the contribution of myocardial perfusion to the pathophysiology of amyloid heart disease. This is the first study to demonstrate that this novel technique can be used to measure myocardial perfusion in patients with cardiac amyloidosis, expanding the role of CMR in assessing myocardial physiology in patients with cardiac amyloidosis. Our study demonstrates that the myocardium is significantly hypoperfused in both AL and ATTR types of cardiac amyloidosis, also adjusting for myocyte mass, with the degree of reduction being greater in ATTR amyloidosis. Cardiac amyloidosis is the exemplar interstitial disease of the myocardium, with amyloid deposits causing very substantial expansion of the extracellular space and increase in LV mass. Simple detection of reduced perfusion is therefore not enough, as correction for the degree of amyloid infiltration, with the measurement of myocyte mass, is an essential step to measure effective myocyte perfusion.

Myocardial hypoperfusion correlates with amyloid burden (inverse correlation with ECV, transmurality of LGE), markers of diastolic function (E/A, E/E') and systolic

function (SV, MAPSE, TAPSE and GLS) by CMR and echocardiography. In the multivariate analysis that included markers of systolic function (2D GLS, stroke volume and TAPSE), diastolic function (E/A, E/E') and amyloid burden (ECV and T2), only 2D GLS, E/A and ECV remained independent predictors of myocardial hypoperfusion. This confirms the complexity of the mechanisms underlying myocardial perfusion in amyloidosis, where myocardial perfusion is the final common pathway of different pathways, which not only include the existing amyloid deposits but also the consequences of amyloid infiltration on systolic and diastolic myocardial mechanics. Interestingly, 2D global longitudinal strain remains an independent predictor of myocardial perfusion, confirming the role of longitudinal strain as a better marker of systolic impairment compared to non-deformation parameters.

This study has some limitations. Cardiac biopsy was available in only a minority of patients. Patients with pacemakers or defibrillators were also excluded. Healthy volunteers were significantly younger than amyloid patients and this could have potential consequences for comparison of myocardial perfusion at rest between cohorts.

Recently, there have been great advances in potential therapies for cardiac amyloidosis. Many treatments aim to specifically inhibit production of amyloid fibril precursor proteins, but therapies that target existing amyloid deposits with the aim of promoting their clearance are also being developed. In order to be able to directly target amyloid deposits, a therapeutic agent must be delivered to the affected tissue, a requirement for which is preserved organ perfusion. Our study demonstrates that the myocardium is significantly hypoperfused in both types of cardiac amyloidosis with the degree of reduction being related to disease severity. This may have important implications for novel strategies that aim to directly target amyloid in the tissues,

notably for example delivery of large molecules such as monoclonal antibodies to amyloid deposits in patients with advanced cardiac amyloidosis in whom myocardial perfusion is substantially reduced. Consequently, myocardial perfusion has the potential to become an important biomarker to assess the differential responses to different treatment approaches in the disease subclasses.

CHAPTER 8: GENERAL CONCLUSIONS

The studies presented in this thesis address key areas of diagnosis, monitoring, and outcome of patients with cardiac amyloidosis.

Regarding diagnosis, in this thesis I describe that the morphological phenotype of patients with ATTR cardiac amyloidosis is different from the one traditionally described: asymmetrical LVH is the commonest pattern of ventricular hypertrophy in cardiac ATTR, with reverse septal contour, classically associated with hypertrophic cardiomyopathy, being present in one-quarter of patients with ATTR. LGE and ECV present typical features in patients with ATTR amyloidosis, with very elevated ECV values and subendocardial or transmural LGE pattern. CMR-determined native myocardial T1 and ECV provided excellent diagnostic accuracy for identification of cardiac ATTR, and both methodologies tracked cardiac uptake on DPD scintigraphy well.

I also describe in this thesis that there is a high prevalence of intracardiac thrombi in patients with cardiac amyloidosis (in AL and ATTR amyloidosis) despite anticoagulation, with significant thrombus prevalence even in sinus rhythm. Poor systolic function, atrial enlargement, and amyloid burden are associated with intracardiac thrombi, predominantly in the LAA. Therefore, early gadolinium images of the LAA should be included in the routine clinical scan protocol of patients with suspected or proven cardiac amyloidosis.

Regarding outcomes; native T1 and ECV predict survival in ATTR; however, ECV is a more robust predictor. ECV, a noninvasive quantification of the cardiac amyloid burden, remains an independent predictor of prognosis after adjustment for known prognostic factors and provided unique insight into tissue composition in cardiac amyloidosis.

In terms of monitoring; cardiac organ response to chemotherapy in AL amyloidosis has historically been sought using echocardiography, but improvements are seldom evident, engendering the belief that cardiac amyloid may only stabilize following successful chemotherapy. Tracking changes in the cardiac amyloid burden has the potential to redefine cardiac response to treatment, enabling the stratification of patients with lower risk of progression and better prognosis and in whom the need to intensify chemotherapy may not be required. Furthermore, the development of immunotherapies to promote regression of amyloid is well advanced as well as new treatments for ATTR cardiac amyloidosis and the ability to measure amyloid regression could be of great value as an endpoint.

Finally, I explored the role of myocardial hypoperfusion in cardiac amyloidosis, finding that myocardial perfusion can be measured in patients with cardiac amyloidosis during routine CMR scans with fully automated MBF mapping. Myocardial hypoperfusion is prevalent in patients with the two most frequently encountered types of cardiac amyloidosis, though to a greater degree in those with ATTR type than AL, and is likely the final common pathway of multiple mechanisms (including amyloid deposition, systolic and diastolic dysfunction). These are important findings as they might impact negatively on the delivery of new amyloid therapies that target amyloid deposits directly in the myocardium.

APPENDIX I – FUTURE WORK

The results of chapter 3, exploring the dynamic response of cardiac AL amyloidosis to chemotherapy, have demonstrated that cardiac AL amyloidosis can regress from the heart after successful chemotherapy. Following on from chapter 3, I am conducting a prospective study, in patients with cardiac AL amyloidosis and performing CMRs at baseline, 6 months, one year and two years after starting chemotherapy to investigate factors that can predict regression or progression of amyloid burden in the heart.

Following the use of cardiac MRI for monitoring amyloid burden in the heart, we are conducting a prospective study in patients with ATTR cardiac amyloidosis (wild-type and hereditary type), performing CMRs at one year and two years from diagnosis. The aim of this study is to explore the natural history of this disease and describe the different phenotypes across the different variants and also establish the rate of progression.

With several new drug therapies currently in development for ATTR cardiac amyloidosis, the potential of imaging in diagnosing and managing cardiac amyloidosis is greater than ever. The ATTR-ACT study (**REF 24 Nature review) demonstrated that tafamidis, a transthyretin stabilizer, improves survival, reduces cardiovascular hospitalizations and preserves quality of life and exercise tolerance in patients with ATTR-CM. Reductions in cardiovascular hospitalizations and mortality were observed only at 9 and 18 months after treatment, respectively. Additionally, patients with less severe disease derived the greatest benefits from tafamidis

treatment. Other agents that inhibit the production of transthyretin (via RNA interference) have subsequently been shown to be effective in patients with ATTRm and peripheral neuropathy (13,14) and are currently being tested in patients with ATTR cardiac amyloidosis. Currently, we are conducting a prospective study, performing CMRs in patients with ATTR cardiac amyloidosis undergoing modifying disease treatments (TTR stabilizers or RNA interference treatments) aiming to evaluate these novel therapies.

APPENDIX II – PUBLICATIONS ARISING FROM RESEARCH FELLOWSHIP

1. Diagnostic imaging of cardiac amyloidosis. **Martinez-Naharro A**, Baksi AJ, Hawkins PN, Fontana M. Nat Rev Cardiol. 2020 Feb 10. doi: 10.1038/s41569-020-0334-7. [Epub ahead of print] Review.

2. Amyloidosis Diagnosed in Solid Organ Transplant Recipients. Sharpley FA, Fontana M, Gilbertson JA, Gillmore JD, Hawkins PN, Mahmood S, Manwani R, **Martinez-Naharro A**, Quarta C, Rezk TM, Rowczenio D, Sachchithanantham S, Whelan CJ, Wechalekar AD, Lachmann HJ. Transplantation. 2020 Feb;104(2):415-420

3. Use of ixazomib, lenalidomide and dexamethasone in patients with relapsed amyloid light-chain amyloidosis. Cohen OC, Sharpley F, Gillmore JD, Lachmann HJ, Sachchithanantham S, Mahmood S, Fontana M, Whelan CJ, **Martinez-Naharro A**, Kyriakou C, Rabin N, Popat R, Yong K, Cheesman S, Shah R, Hawkins PN, Wechalekar AD. Br J Haematol. 2020 Jan 26. doi: 10.1111/bjh.16401. [Epub ahead of print]

4. Echocardiographic phenotype and prognosis in transthyretin cardiac amyloidosis. Chacko L, Martone R, Bandera F, Lane T, **Martinez-Naharro A**, Boldrini M, Rezk T, Whelan C, Quarta C, Rowczenio D, Gilbertson JA, Wongwarawipat T, Lachmann H, Wechalekar A, Sachchithanantham S, Mahmood S, Marcucci R,

Knight D, Hutt D, Moon J, Petrie A, Cappelli F, Guazzi M, Hawkins PN, Gillmore JD, Fontana M. Eur Heart J. 2020 Jan 17. pii: ehz905. doi: 10.1093/eurheartj/ehz905. [Epub ahead of print]

5. Multiparametric Echocardiography Scores for the Diagnosis of Cardiac Amyloidosis. Boldrini M, Cappelli F, Chacko L, Restrepo-Cordoba MA, Lopez-Sainz A, Giannoni A, Aimo A, Baggiano A, **Martinez-Naharro A**, Whelan C, Quarta C, Passino C, Castiglione V, Chubuchnyi V, Spini V, Taddei C, Vergaro G, Petrie A, Ruiz-Guerrero L, Moñivas V, Mingo-Santos S, Mirelis JG, Dominguez F, Gonzalez-Lopez E, Perlini S, Pontone G, Gillmore J, Hawkins PN, Garcia-Pavia P, Emdin M, Fontana M. JACC Cardiovasc Imaging. 2019 Dec 18. pii: S1936-878X(19)31007-1. doi: 10.1016/j.jcmg.2019.10.011. [Epub ahead of print]

6. Intracardiac melanoma metastases on $_{18}$F-FDG PET-CT-a case report and review of literature with imaging features. Sweni S, Fontana M, **Martinez-Naharro A**, Nathan M. BJR Case Rep. 2019 Mar 28;5(3):20180118. doi: 10.1259/bjrcr.20180118. eCollection 2019 Sep.

7. Noninvasive Mapping of the Electrophysiological Substrate in Cardiac Amyloidosis and Its Relationship to Structural Abnormalities. Orini M, Graham AJ, **Martinez-Naharro A**, Andrews CM, de Marvao A, Statton B, Cook SA, O'Regan DP, Hawkins PN, Rudy Y, Fontana M, Lambiase PD. J Am Heart Assoc. 2019 Sep 17;8(18):e012097. doi: 10.1161/JAHA.119.012097.

8. Cardiovascular magnetic resonance-guided right heart catheterization in a conventional CMR environment - predictors of procedure success and duration in pulmonary artery hypertension. Knight DS, Kotecha T, **Martinez-Naharro A**, Brown JT, Bertelli M, Fontana M, Muthurangu V, Coghlan JG. J Cardiovasc Magn Reson. 2019 Sep 9;21(1):57.

9. A 24-year experience of autologous stem cell transplantation for light chain amyloidosis patients in the United Kingdom. Sharpley FA, Petrie A, Mahmood S, Sachchithanantham S, Lachmann HJ, Gillmore JD, Whelan CJ, Fontana M, **Martinez-Naharro A**, Quarta C, Hawkins PN, Wechalekar AD. Br J Haematol. 2019 Dec;187(5):642-652.

10. Cardiac biomarkers are prognostic in systemic light chain amyloidosis with no cardiac involvement by standard criteria. Sharpley FA, Fontana M, **Martinez-Naharro A**, Manwani R, Mahmood S, Sachchithanantham S, Lachmann HJ, Gillmore JD, Whelan CJ, Hawkins PN, Wechalekar AD. Haematologica. 2019 Aug 8. pii: haematol.2019.217695. doi: 10.3324/haematol.2019.217695. [Epub ahead of print]

11. Noncontrast Magnetic Resonance for the Diagnosis of Cardiac Amyloidosis. Baggiano A, Boldrini M, **Martinez-Naharro A**, Kotecha T, Petrie A, Rezk T, Gritti M, Quarta C, Knight DS, Wechalekar AD, Lachmann HJ, Perlini S, Pontone G, Moon JC, Kellman P, Gillmore JD, Hawkins PN, Fontana M. JACC Cardiovasc Imaging. 2020 Jan;13(1 Pt 1):69-80.

12. Natural History, Quality of Life, and Outcome in Cardiac Transthyretin Amyloidosis. Lane T, Fontana M, **Martinez-Naharro A**, Quarta CC, Whelan CJ, Petrie A, Rowczenio DM, Gilbertson JA, Hutt DF, Rezk T, Strehina SG, Caringal-Galima J, Manwani R, Sharpley FA, Wechalekar AD, Lachmann HJ, Mahmood S, Sachchithanantham S, Drage EPS, Jenner HD, McDonald R, Bertolli O, Calleja A, Hawkins PN, Gillmore JD. Circulation. 2019 Jul 2;140(1):16-26.

13. High Prevalence of Intracardiac Thrombi in Cardiac Amyloidosis. **Martinez-Naharro A**, Gonzalez-Lopez E, Corovic A, Mirelis JG, Baksi AJ, Moon JC, Garcia-Pavia P, Gillmore JD, Hawkins PN, Fontana M. J Am Coll Cardiol. 2019 Apr 9;73(13):1733-1734.

14. Automated Pixel-Wise Quantitative Myocardial Perfusion Mapping by CMR to Detect Obstructive Coronary Artery Disease and Coronary Microvascular Dysfunction: Validation Against Invasive Coronary Physiology. **Martinez-Naharro A**, Kotecha T, Boldrini M, Knight D, Hawkins P, Kalra S, Patel D, Coghlan G, Moon J, Plein S, Lockie T, Rakhit R, Patel N, Xue H, Kellman P, Fontana M. JACC Cardiovasc Imaging. 2019 Oct;12(10):1958-1969.

15. Acute changes in cardiac structural and tissue characterisation parameters following haemodialysis measured using cardiovascular magnetic resonance. **Martinez-Naharro A**, Kotecha T, Yoowannakul S, Lambe T, Rezk T, Knight DS, Hawkins PN, Moon JC, Muthurangu V, Kellman P, Rakhit RD, Gillmore JD, Jeetley P, Davenport A, Fontana M. Sci Rep. 2019 Feb 4;9(1):1388.

16. Bioimpedance vector analysis for the detection of extracellular volume overload and sarcopenia in systemic AL amyloidosis. Rezk T, Davenport A, Gan JJ, Lachmann HJ, Fontana M, **Martinez-Naharro A**, Sachchithanantham S, Guillotte C, Mahmood S, Petrie A, Whelan CJ, Pinney JH, Foard D, Lane T, Youngstein T, Wechalekar AD, Hawkins PN, Gillmore JD. Br J Haematol. 2019 Jun;185(5):977-980.

17. Analysis of the TTR gene in the investigation of amyloidosis: A 25-year single UK center experience. Rowczenio D, Quarta CC, Fontana M, Whelan CJ, **Martinez-Naharro A**, Trojer H, Baginska A, Ferguson SM, Gilbertson J, Rezk T, Sachchithanantham S, Mahmood S, Manwani R, Sharpley F, Wechalekar AD, Hawkins PN, Gillmore JD, Lachmann HJ. Hum Mutat. 2019 Jan;40(1):90-96.

18. Myocardial Edema and Prognosis in Amyloidosis. **Martinez-Naharro A**, Kotecha T, Treibel TA, Francis R, Nordin S, Abdel-Gadir A, Knight DS, Zumbo G, Rosmini S, Maestrini V, Bulluck H, Rakhit RD, Wechalekar AD, Gilbertson J, Sheppard MN, Kellman P, Gillmore JD, Moon JC, Hawkins PN, Fontana M. J Am Coll Cardiol. 2018 Jun 26;71(25):2919-2931

19. Cardiac amyloidosis. **Martinez-Naharro A**, Hawkins PN, Fontana M. Clin Med (Lond). 2018 Apr 1;18 (Suppl 2):s30-s35.

20. Cardiac structural and functional consequences of amyloid deposition by CMR and echocardiography and their prognostic roles. Knight DS, Zumbo G, Barcella

W, Steeden JA, Muthurangu V, **Martinez-Naharro A**, Treibel TA, Abdel-Gadir A, Bulluck H, Kotecha T, Francis R, Rezk T, Quarta CC, Whelan CJ, Lachmann HJ, Wechalekar AD, Gillmore JD, Moon JC, Hawkins PN, Fontana M. JACC Cardiovasc Imaging. 2019 May;12(5):823-833.

21. Native T1 and Extracellular Volume in Transthyretin Amyloidosis. **Martinez-Naharro A**, Kotecha T, Norrington K, Boldrini M, Rezk T, Quarta C, Treibel TA, Whelan CJ, Knight DS, Kellman P, Ruberg FL, Gillmore JD, Moon JC, Hawkins PN, Fontana M. JACC Cardiovasc Imaging. 2019 May;12(5):810-819.

22. Prospective comparison of novel dark blood late gadolinium enhancement with conventional bright blood imaging for the detection of scar. Francis R, Kellman P, Kotecha T, Baggiano A, Norrington K, **Martinez-Naharro A**, Nordin S, Knight DS, Rakhit RD, Lockie T, Hawkins PN, Moon JC, Hausenloy DJ, Xue H, Hansen MS, Fontana M. J Cardiovasc Magn Reson. 2017 Nov 21;19(1):91.

23. Extracellular volume with bolus-only technique in amyloidosis patients: Diagnostic accuracy, correlation with other clinical cardiac measures, and ability to track changes in amyloid load over time. Zumbo G, Barton SV, Thompson D, Sun M, Abdel-Gadir A, Treibel TA, Knight D, **Martinez-Naharro A**, Thirusha L, Gillmore JD, Moon JC, Hawkins PN, Fontana M. J Magn Reson Imaging. 2018 Jun;47(6):1677-1684.

24. A new staging system for cardiac transthyretin amyloidosis. Gillmore JD, Damy T, Fontana M, Hutchinson M, Lachmann HJ, **Martinez-Naharro A**, Quarta CC,

Rezk T, Whelan CJ, Gonzalez-Lopez E, Lane T, Gilbertson JA, Rowczenio D, Petrie A, Hawkins PN. Eur Heart J. 2018 Aug 7;39(30):2799-2806.

25. Magnetic Resonance in Transthyretin Cardiac Amyloidosis. **Martinez-Naharro A**, Treibel TA, Abdel-Gadir A, Bulluck H, Zumbo G, Knight DS, Kotecha T, Francis R, Hutt DF, Rezk T, Rosmini S, Quarta CC, Whelan CJ, Kellman P, Gillmore JD, Moon JC, Hawkins PN, Fontana M. J Am Coll Cardiol. 2017 Jul 25;70(4):466-477.

26. CMR-verified regression of AL cardiac amyloid after chemotherapy. **Martinez-Naharro A**, Abdel-Gadir A, Treibel TA, Zumbo G, Knight DS, Rosmini S, Lane T, Mahmood S, Sachchithanantham S, Whelan CJ, Lachmann HJ, Wechalekar AD, Kellman P, Gillmore JD, Moon JC, Hawkins PN, Fontana M. JACC Cardiovasc Imaging. 2018 Jan;11(1):152-154.

27. Prognostic utility of the Perugini grading of 99mTc-DPD scintigraphy in trasthyretin (ATTR) amyloidosis and its relationship with skeletal muscle and soft tissue amyloid. Hutt DF, Fontana M, Burniston M, Quigley AM, Petrie A, Ross JC, Page J, **Martinez-Naharro A**, Wechalekar AD, Lachmann HJ, Quarta CC, Rezk T, Mahmood S, Sachchithanantham S, Youngstein T, Whelan CJ, Lane T, Gilbertson JA, Rowczenio D, Hawkins PN, Gillmore JD. Eur Heart J Cardiovasc Imaging. 2017 Dec 1;18(12):1344-1350.

28. A good clonal response to chemotherapy in AL amyloidosis is associated with improved quality of life and function at 1 year. Carter JP, Foard D, Rannigan L,

Aliaz K, Mahmood S, Sachchitanantham S, Fontana M, Quarta CC, **Martinez-Naharro A**, Youngstein T, Rezk T, Wechalekar AD, Whelan CJ, Lachmann HJ, Hawkins PN, Gillmore JD, Lane T. Amyloid. 2017 Mar;24(sup1):72-73.

29. A case report in cardiovascular magnetic resonance: the contrast agent matters in amyloid. Fontana M, Treibel TA, **Martinez-Naharro A**, Rosmini S, Kwong RY, Gillmore JD, Hawkins PN, Moon JC. BMC Med Imaging. 2017 Jan 7;17(1):3.

30. Staging cardiac amyloidosis with CMR: understand the different phenotypes. Editorial. Fontana M, **Martinez-Naharro A**, Hawkins PN. JACC Cardiovasc Imaging. 2016 Nov; 9(11):1278-1279.

APPENDIX III – PRIZES DURING RESEARCH FELLOWSHIP

1. Winner of the Best Oral Abstract, EuroCMR 2017 for the work: "Spectrum and significance of CMR findings in cardiac Transthyretin Amyloidosis".
2. Runner-up best ePoster, BSCMR Annual Meeting 2017 for the work: "Demonstration of cardiac AL amyloidosis regression after successful chemotherapy. A CMR study".
3. Finalist of the Early Career Award, SCMR 2017 for the work: "T1, extracellular volume and myocardial blood flow mapping: a multi-parametric mapping approach in cardiac amyloidosis".
4. Finalist of the Young Investigator Award, BCVI 2018 for the work: "Regression of cardiac AL amyloidosis demonstrated by CMR: a new era of understanding".
5. Best 3' Research oral presentation, Division of Medicine Research Retreat, 2018 for the work: "CMR to assess treatment response in cardiac AL amyloidosis. Updated findings from the ALchemy study".
6. Finalist of the 2018 CVRI Melvin Judkins Young Investigator Award. AHA 2018 for the work: "Treatment response in cardiac AL amyloidosis assessed by CMR: findings at 3 months, 6 months and 1 year post-chemotherapy".
7. Young Author Achievement Award 2019. In recognition of an Outstanding Manuscript by a Young Investigator in JACC: Cardiovascular Medicine.
8. Nominated for the Dean's UCL Research Prize, 2019.

APPENDIX IV – ORAL PRESENTATIONS

1. High prevalence of intracardiac thrombi in cardiac amyloidosis. Martinez-Naharro A, Kotecha T, Gonzalez-Lopez E, Corovic A, Anderson S, Chacko L, Brown J, Knight D, Baksi A. J, Moon J, Kellman P, Garcia-Pavia P, Gillmore J, Hawkins P, Fontana M. *EuroCMR 2019, Venice, Italy.*
2. Treatment response in cardiac AL amyloidosis assessed by CMR: findings at 3 months, 6 months and 1 year post-chemotherapy. Martinez-Naharro A, Kotecha T, Baggiano A, Boldrini M, Rezk T, Francis R, Fayed H, Knight D, Moon J, Kellman P, Gillmore J, Hawkins P, Fontana M. *AHA Scientific Sessions 2019. Chicago, USA.*
3. CMR to assess treatment response in cardiac AL amyloidosis. Updated findings from the ALchemy study. Martinez-Naharro A, Kotecha T, Rezk T, Manwani R, Sharpley F, Quarta C, Whelan C, Lachmann H, Wechalekar A, Gillmore J, Hawkins P, Fontana M. *UCL Division of Medicine Research Retreat 2018. London, UK.*
4. Regression of cardiac AL amyloidosis demonstrated by CMR: a new era of understanding. Martinez-Naharro A, Kotecha T, Baggiano A, Boldrini M, Rezk T, Francis R, Fayed H, Knight D, Moon J, Kellman P, Gillmore J, Hawkins P, Fontana M. *BCVI 2018. Edinburgh, UK.*
5. CMR to assess treatment response in cardiac AL amyloidosis. Findings from the ALchemy study. Martinez-Naharro A, Kotecha T, Baggiano A, Boldrini M, Rezk T, Francis R, Fayed H, Knight D, Moon J, Kellman P, Gillmore J, Hawkins P, Fontana M. *CMR 2018. Barcelona, Spain.*

6. Improving recognition of intra-myocardial fat by CMR. Martinez-Naharro A, Kotecha T, Francis R, Fayed H, Knight D, Hawkins P, Kellman P, Fontana M. *CMR 2018. Barcelona, Spain.*
7. T1, extracellular volume and myocardial blood flow mapping in cardiac ATTR amyloidosis. Martinez-Naharro A, Kotecha T, Knight D, Francis R, Rezk T, Quarta C, Gonzalez E, Manwani R, Whelan C, Lachmann H, Wechalekar A, Gillmore J, Hawkins P, Fontana M. *1st European ATTR Amyloidosis Meeting for Patients and Doctors. Paris, France.*
8. Spectrum and significance of CMR findings in cardiac Transthyretin Amyloidosis. Martinez-Naharro A, Treibel T, Abdel-Gadir A, Bulluck H, Zumbo G, Knight D, Kotecha T, Francis R, Hutt D, Rezk T, Rosmini S, Quarta C, Whelan C, Kellman P, Gillmore J, Moon J, Hawkins P, Fontana M. *EuroCMR 2017. Prague, Czech Republic.*
9. T1, extracellular volume and myocardial blood flow mapping: a multi-parametric mapping approach in cardiac amyloidosis. Martinez-Naharro A, Knight D, Kotecha T, Francis R, Zumbo G, Treibel T, Nickander J, Themudo R, Gillmore J, Ugander M, Moon J, Xue H, Kellman P, Hawkins P, Fontana M. *SCMR 2017. Washington, USA.*
10. Regression of cardiac AL amyloidosis after successful chemotherapy. A CMR study. Martinez-Naharro A, Abdel-Gadir A, Treibel T, Zumbo G, Knight D, Rosmini S, Lane T, Mahmood S, Sachchithanantham S**,** Whelan C, Lachmann H, Wechalekar A, Kellman P, Gillmore J, Moon J, Hawkins P, Fontana M. *SCMR 2017. Washington, USA*.

11. Pseudo cardiac amyloidosis; where an ECV map makes the difference. Martinez-Naharro A, Knight D, Kotecha T, Zumbo G, Coghlan G, Moon J, Kellman P, Fontana M. *SCMR 2017. Washington, USA.*
12. Regression of cardiac AL amyloidosis demonstrated by cardiovascular magnetic resonance. Martinez-Naharro A, Knight D, Treibel T, Abdel-Gadir A, Zumbo G, Rosmini S, Lane T, Mahmood S, Sachchithanantham S, Whelan C, Quarta C, Lachmann H, Wechalekar A, Gillmore J, Moon J, Hawkins P, Fontana M. *XV International Symposium on Amyloidosis. Uppsala, Sweden.*

BIBLIOGRAPHY

1. Lachmann HJ, Hawkins PN. Systemic amyloidosis. Curr Opin Pharmacol 2006;6:214-20.
2. Sipe JD, Benson MD, Buxbaum JN et al. Nomenclature 2014: Amyloid fibril proteins and clinical classification of the amyloidosis. Amyloid 2014;21:221-4.
3. Maurer MS, Elliott P, Comenzo R, Semigran M, Rapezzi C. Addressing Common Questions Encountered in the Diagnosis and Management of Cardiac Amyloidosis. Circulation 2017;135:1357-1377.
4. Wechalekar AD, Gillmore JD, Hawkins PN. Systemic amyloidosis. Lancet 2016;387:2641-2654.
5. Fontana M, Banypersad SM, Treibel TA et al. Differential Myocyte Responses in Patients with Cardiac Transthyretin Amyloidosis and Light-Chain Amyloidosis: A Cardiac MR Imaging Study. Radiology 2015;277:388-97.
6. Falk RH. Diagnosis and management of the cardiac amyloidoses. Circulation 2005;112:2047-60.
7. Pinney JH, Smith CJ, Taube JB et al. Systemic amyloidosis in England: an epidemiological study. Br J Haematol 2013;161:525-32.
8. Gertz MA, Lacy MQ, Dispenzieri A, Hayman SR. Amyloidosis. Best Pract Res Clin Haematol 2005;18:709-27.
9. Merlini G. CyBorD: stellar response rates in AL amyloidosis. Blood 2012;119:4343-5.
10. Falk RH, Alexander KM, Liao R, Dorbala S. AL (Light-Chain) Cardiac Amyloidosis: A Review of Diagnosis and Therapy. J Am Coll Cardiol 2016;68:1323-41.
11. Rapezzi C, Merlini G, Quarta CC et al. Systemic cardiac amyloidoses: disease profiles and clinical courses of the 3 main types. Circulation 2009;120:1203-12.
12. Gillmore JD, Damy T, Fontana M et al. A new staging system for cardiac transthyretin amyloidosis. Eur Heart J 2018;39:2799-2806.
13. Adams D, Gonzalez-Duarte A, O'Riordan WD et al. Patisiran, an RNAi Therapeutic, for Hereditary Transthyretin Amyloidosis. N Engl J Med 2018;379:11-21.
14. Benson MD, Waddington-Cruz M, Berk JL et al. Inotersen Treatment for Patients with Hereditary Transthyretin Amyloidosis. N Engl J Med 2018;379:22-31.
15. Berk JL, Suhr OB, Obici L et al. Repurposing diflunisal for familial amyloid polyneuropathy: a randomized clinical trial. JAMA 2013;310:2658-67.

16. Maurer MS, Schwartz JH, Gundapaneni B et al. Tafamidis Treatment for Patients with Transthyretin Amyloid Cardiomyopathy. N Engl J Med 2018;379:1007-1016.

17. Ruberg FL, Berk JL. Transthyretin (TTR) Cardiac Amyloidosis. Circulation 2012;126:1286-1300.

18. Cornwell GG, 3rd, Murdoch WL, Kyle RA, Westermark P, Pitkanen P. Frequency and distribution of senile cardiovascular amyloid. A clinicopathologic correlation. Am J Med 1983;75:618-23.

19. Tanskanen M, Peuralinna T, Polvikoski T et al. Senile systemic amyloidosis affects 25% of the very aged and associates with genetic variation in alpha2-macroglobulin and tau: a population-based autopsy study. Ann Med 2008;40:232-9.

20. Fontana M, Banypersad SM, Treibel TA et al. Native T1 mapping in transthyretin amyloidosis. JACC Cardiovasc Imaging 2014;7:157-165.

21. Gillmore JD, Maurer MS, Falk RH et al. Nonbiopsy Diagnosis of Cardiac Transthyretin Amyloidosis. Circulation 2016;133:2404-12.

22. Pinney JH, Whelan CJ, Petrie A et al. Senile systemic amyloidosis: clinical features at presentation and outcome. Journal of the American Heart Association 2013;2:e000098.

23. Connors LH, Lim A, Prokaeva T, Roskens VA, Costello CE. Tabulation of human transthyretin (TTR) variants, 2003. Amyloid 2003;10:160-84.

24. Merlini G, Westermark P. The systemic amyloidoses: clearer understanding of the molecular mechanisms offers hope for more effective therapies. J Intern Med 2004;255:159-78.

25. Sattianayagam PT, Hahn AF, Whelan CJ et al. Cardiac phenotype and clinical outcome of familial amyloid polyneuropathy associated with transthyretin alanine 60 variant. Eur Heart J 2012;33:1120-1127.

26. Andrade C. A peculiar form of peripheral neuropathy; familiar atypical generalized amyloidosis with special involvement of the peripheral nerves. Brain 1952;75:408-27.

27. Connors LH, Prokaeva T, Lim A et al. Cardiac amyloidosis in African Americans: comparison of clinical and laboratory features of transthyretin V122I amyloidosis and immunoglobulin light chain amyloidosis. Am Heart J 2009;158:607-14.

28. Guy CD, Jones CK. Abdominal fat pad aspiration biopsy for tissue confirmation of systemic amyloidosis: specificity, positive predictive value, and diagnostic pitfalls. Diagn Cytopathol 2001;24:181-5.

29. Grogan M, Scott CG, Kyle RA et al. Natural History of Wild-Type Transthyretin Cardiac Amyloidosis and Risk Stratification Using a Novel Staging System. J Am Coll Cardiol 2016;68:1014-20.

30. Comenzo RL, Reece D, Palladini G et al. Consensus guidelines for the conduct and reporting of clinical trials in systemic light-chain amyloidosis. Leukemia 2012;26:2317-25.

31. Sperry BW, Vranian MN, Hachamovitch R et al. Are classic predictors of voltage valid in cardiac amyloidosis? A contemporary analysis of electrocardiographic findings. Int J Cardiol 2016;214:477-81.

32. Dubrey SW, Cha K, Anderson J et al. The clinical features of immunoglobulin light-chain (AL) amyloidosis with heart involvement. QJM 1998;91:141-57.

33. Murtagh B, Hammill SC, Gertz MA, Kyle RA, Tajik AJ, Grogan M. Electrocardiographic findings in primary systemic amyloidosis and biopsy-proven cardiac involvement. Am J Cardiol 2005;95:535-7.

34. Habib G, Bucciarelli-Ducci C, Caforio ALP et al. Multimodality Imaging in Restrictive Cardiomyopathies: An EACVI expert consensus document In collaboration with the "Working Group on myocardial and pericardial diseases" of the European Society of Cardiology Endorsed by The Indian Academy of Echocardiography. Eur Heart J Cardiovasc Imaging 2017;18:1090-1121.

35. Ruberg FL, Grogan M, Hanna M, Kelly JW, Maurer MS. Transthyretin Amyloid Cardiomyopathy: JACC State-of-the-Art Review. J Am Coll Cardiol 2019;73:2872-2891.

36. Cyrille NB, Goldsmith J, Alvarez J, Maurer MS. Prevalence and prognostic significance of low QRS voltage among the three main types of cardiac amyloidosis. Am J Cardiol 2014;114:1089-93.

37. Hongo M, Yamamoto H, Kohda T et al. Comparison of electrocardiographic findings in patients with AL (primary) amyloidosis and in familial amyloid polyneuropathy and anginal pain and their relation to histopathologic findings. Am J Cardiol 2000;85:849-53.

38. Dungu J, Sattianayagam PT, Whelan CJ et al. The electrocardiographic features associated with cardiac amyloidosis of variant transthyretin isoleucine 122 type in Afro-Caribbean patients. Am Heart J 2012;164:72-9.

39. Mints YY, Doros G, Berk JL, Connors LH, Ruberg FL. Features of atrial fibrillation in wild-type transthyretin cardiac amyloidosis: a systematic review and clinical experience. ESC Heart Fail 2018;5:772-779.

40. Gertz MA, Comenzo R, Falk RH et al. Definition of organ involvement and treatment response in immunoglobulin light chain amyloidosis (AL): a consensus opinion from the 10th International Symposium on Amyloid and Amyloidosis, Tours, France, 18-22 April 2004. Am J Hematol 2005;79:319-28.

41. Austin BA, Duffy B, Tan C, Rodriguez ER, Starling RC, Desai MY. Comparison of functional status, electrocardiographic, and echocardiographic parameters to mortality in endomyocardial-biopsy proven cardiac amyloidosis. Am J Cardiol 2009;103:1429-33.

42. Knight DS, Zumbo G, Barcella W et al. Cardiac Structural and Functional Consequences of Amyloid Deposition by Cardiac Magnetic Resonance and Echocardiography and Their Prognostic Roles. JACC Cardiovasc Imaging 2019;12:823-833.

43. Tsang W, Lang RM. Echocardiographic evaluation of cardiac amyloid. Current cardiology reports 2010;12:272-6.

44. Klein AL, Hatle LK, Burstow DJ et al. Doppler characterization of left ventricular diastolic function in cardiac amyloidosis. J Am Coll Cardiol 1989;13:1017-26.

45. King DL, El-Khoury Coffin L, Maurer MS. Myocardial contraction fraction: a volumetric index of myocardial shortening by freehand three-dimensional echocardiography. J Am Coll Cardiol 2002;40:325-9.

46. Pozo E, Kanwar A, Deochand R et al. Cardiac magnetic resonance evaluation of left ventricular remodelling distribution in cardiac amyloidosis. Heart 2014;100:1688-95.

47. Pagourelias ED, Mirea O, Duchenne J et al. Echo Parameters for Differential Diagnosis in Cardiac Amyloidosis: A Head-to-Head Comparison of Deformation and Nondeformation Parameters. Circulation Cardiovascular imaging 2017;10:e005588.

48. Pewsner D, Battaglia M, Minder C, Marx A, Bucher HC, Egger M. Ruling a diagnosis in or out with "SpPIn" and "SnNOut": a note of caution. BMJ 2004;329:209-13.

49. Phelan D, Collier P, Thavendiranathan P et al. Relative apical sparing of longitudinal strain using two-dimensional speckle-tracking echocardiography is both sensitive and specific for the diagnosis of cardiac amyloidosis. Heart 2012;98:1442-8.

50. Senapati A, Sperry BW, Grodin JL et al. Prognostic implication of relative regional strain ratio in cardiac amyloidosis. Heart 2016;102:748-54.

51. Rapezzi C, Fontana M. Relative Left Ventricular Apical Sparing of Longitudinal Strain in Cardiac Amyloidosis: Is it Just Amyloid Infiltration? JACC Cardiovasc Imaging 2019;12:1174-1176.

52. Banypersad SM. The Evolving Role of Cardiovascular Magnetic Resonance Imaging in the Evaluation of Systemic Amyloidosis. Magn Reson Insights 2019;12:1178623X19843519.

53. Pennell DJ. Cardiovascular magnetic resonance: twenty-first century solutions in cardiology. Clin Med 2003;3:273-278.

54. White SK, Sado DM, Fontana M et al. T1 mapping for myocardial extracellular volume measurement by CMR: bolus only versus primed infusion technique. JACC Cardiovasc Imaging 2013;6:955-62.

55. Fontana M, Martinez-Naharro A, Hawkins PN. Staging Cardiac Amyloidosis With CMR: Understanding the Different Phenotypes. JACC Cardiovasc Imaging 2016;9:1278-1279.

56. Reiter T, Ritter O, Prince MR et al. Minimizing risk of nephrogenic systemic fibrosis in cardiovascular magnetic resonance. J Cardiovasc Magn Reson 2012;14:31.

57. Koenig SH, Spiller M, Brown RD, 3rd, Wolf GL. Relaxation of water protons in the intra- and extracellular regions of blood containing Gd(DTPA). Magn Reson Med 1986;3:791-5.

58. Kim RJ, Judd RM, Chen EL, Fieno DS, Parrish TB, Lima JA. Relationship of elevated 23Na magnetic resonance image intensity to infarct size after acute reperfused myocardial infarction. Circulation 1999;100:185-92.

59. Rehwald WG, Fieno DS, Chen EL, Kim RJ, Judd RM. Myocardial magnetic resonance imaging contrast agent concentrations after reversible and irreversible ischemic injury. Circulation 2002;105:224-9.

60. Fontana M, Chung R, Hawkins PN, Moon JC. Cardiovascular magnetic resonance for amyloidosis. Heart failure reviews 2015;20:133-144.

61. Maceira AM, Joshi J, Prasad SK et al. Cardiovascular magnetic resonance in cardiac amyloidosis. Circulation 2005;111:186-93.

62. Fontana M, Chung R, Hawkins PN, Moon JC. Cardiovascular magnetic resonance for amyloidosis. Heart failure reviews 2015;20:133-44.

63. Kwong RY, Falk RH. Cardiovascular magnetic resonance in cardiac amyloidosis. Circulation 2005;111:122-4.

64. Fontana M, Treibel TA, Martinez-Naharro A et al. A case report in cardiovascular magnetic resonance: the contrast agent matters in amyloid. BMC Med Imaging 2017;17:3.

65. Moon JC, Messroghli DR, Kellman P et al. Myocardial T1 mapping and extracellular volume quantification: a Society for Cardiovascular Magnetic Resonance (SCMR) and CMR Working Group of the European Society of Cardiology consensus statement. J Cardiovasc Magn Reson 2013;15:92.

66. Kellman P, Arai AE, McVeigh ER, Aletras AH. Phase-sensitive inversion recovery for detecting myocardial infarction using gadolinium-delayed hyperenhancement. Magn Reson Med 2002;47:372-83.

67. Fontana M, Pica S, Reant P et al. Prognostic Value of Late Gadolinium Enhancement Cardiovascular Magnetic Resonance in Cardiac Amyloidosis. Circulation 2015;132:1570-9.

68. Martinez-Naharro A, Treibel TA, Abdel-Gadir A et al. Magnetic Resonance in Transthyretin Cardiac Amyloidosis. J Am Coll Cardiol 2017;70:466-477.

69. Bollee G, Guery B, Joly D et al. Presentation and outcome of patients with systemic amyloidosis undergoing dialysis. Clin J Am Soc Nephrol 2008;3:375-81.

70. Lachmann HJ, Gillmore JD. Renal amyloidosis. Brit J Hosp Med 2010;71:83-86.

71. Fontana M, Banypersad SM, Treibel TA et al. Native T1 mapping in transthyretin amyloidosis. JACC Cardiovasc Imaging 2014;7:157-65.

72. Karamitsos TD, Piechnik SK, Banypersad SM et al. Noncontrast T1 mapping for the diagnosis of cardiac amyloidosis. JACC Cardiovasc Imaging 2013;6:488-97.

73. Sado DM, White SK, Piechnik SK et al. Identification and assessment of Anderson-Fabry disease by cardiovascular magnetic resonance noncontrast myocardial T1 mapping. Circulation Cardiovascular imaging 2013;6:392-8.

74. Baggiano A, Boldrini M, Martinez-Naharro A et al. Noncontrast Magnetic Resonance for the Diagnosis of Cardiac Amyloidosis. JACC Cardiovasc Imaging 2020;13:69-80.

75. Banypersad SM, Sado DM, Flett AS et al. Quantification of myocardial extracellular volume fraction in systemic AL amyloidosis: an equilibrium contrast cardiovascular magnetic resonance study. Circulation Cardiovascular imaging 2013;6:34-9.

76. Banypersad SM, Fontana M, Maestrini V et al. T1 mapping and survival in systemic light-chain amyloidosis. Eur Heart J 2015;36:244-51.

77. Kotecha T, Martinez-Naharro A, Treibel TA et al. Myocardial Edema and Prognosis in Amyloidosis. J Am Coll Cardiol 2018;71:2919-2931.

78. Kellman P, Hansen MS, Nielles-Vallespin S et al. Myocardial perfusion cardiovascular magnetic resonance: optimized dual sequence and reconstruction for quantification. J Cardiovasc Magn Reson 2017;19:43.

79. Shirahama T, Cohen AS. High-resolution electron microscopic analysis of the amyloid fibril. J Cell Biol 1967;33:679-708.

80. Nordlinger M, Magnani B, Skinner M, Falk RH. Is elevated plasma B-natriuretic peptide in amyloidosis simply a function of the presence of heart failure? Am J Cardiol 2005;96:982-4.

81. Wizenberg TA, Muz J, Sohn YH, Samlowski W, Weissler AM. Value of positive myocardial technetium-99m-pyrophosphate scintigraphy in the noninvasive diagnosis of cardiac amyloidosis. Am Heart J 1982;103:468-73.

82. Puille M, Altland K, Linke RP et al. 99mTc-DPD scintigraphy in transthyretin-related familial amyloidotic polyneuropathy. Eur J Nucl Med Mol Imaging 2002;29:376-9.

83. Bokhari S, Shahzad R, Castano A, Maurer MS. Nuclear imaging modalities for cardiac amyloidosis. Journal of nuclear cardiology : official publication of the American Society of Nuclear Cardiology 2014;21:175-84.

84. Bokhari S, Castano A, Pozniakoff T, Deslisle S, Latif F, Maurer MS. (99m)Tc-pyrophosphate scintigraphy for differentiating light-chain cardiac amyloidosis from the transthyretin-related familial and senile cardiac amyloidoses. Circulation Cardiovascular imaging 2013;6:195-201.

85. Castano A, Haq M, Narotsky DL et al. Multicenter Study of Planar Technetium 99m Pyrophosphate Cardiac Imaging: Predicting Survival for Patients With ATTR Cardiac Amyloidosis. JAMA cardiology 2016;1:880-889.

86. Perugini E, Guidalotti PL, Salvi F et al. Noninvasive etiologic diagnosis of cardiac amyloidosis using 99mTc-3,3-diphosphono-1,2-propanodicarboxylic acid scintigraphy. J Am Coll Cardiol 2005;46:1076-84.

87. Rapezzi C, Quarta CC, Guidalotti PL et al. Role of (99m)Tc-DPD scintigraphy in diagnosis and prognosis of hereditary transthyretin-related cardiac amyloidosis. JACC Cardiovasc Imaging 2011;4:659-70.

88. Papantoniou V, Valsamaki P, Kastritis S et al. Imaging of cardiac amyloidosis by (99m)Tc-PYP scintigraphy. Hell J Nucl Med 2015;18 Suppl 1:42-50.

89. Galat A, Rosso J, Guellich A et al. Usefulness of (99m)Tc-HMDP scintigraphy for the etiologic diagnosis and prognosis of cardiac amyloidosis. Amyloid 2015;22:210-20.

90. Glaudemans AW, van Rheenen RW, van den Berg MP et al. Bone scintigraphy with (99m)technetium-hydroxymethylene diphosphonate allows early diagnosis of cardiac involvement in patients with transthyretin-derived systemic amyloidosis. Amyloid 2014;21:35-44.

91. Rapezzi C, Gagliardi C, Milandri A. Analogies and disparities among scintigraphic bone tracers in the diagnosis of cardiac and non-cardiac ATTR amyloidosis. Journal of nuclear cardiology : official publication of the American Society of Nuclear Cardiology 2019;26:1638-1641.

92. Pilebro B, Suhr OB, Naslund U, Westermark P, Lindqvist P, Sundstrom T. (99m)Tc-DPD uptake reflects amyloid fibril composition in hereditary transthyretin amyloidosis. Ups J Med Sci 2016;121:17-24.

93. Stats MA, Stone JR. Varying levels of small microcalcifications and macrophages in ATTR and AL cardiac amyloidosis: implications for utilizing nuclear medicine studies to subtype amyloidosis. Cardiovasc Pathol 2016;25:413-7.

94. Falk RH, Lee VW, Rubinow A, Hood WB, Jr., Cohen AS. Sensitivity of technetium-99m-pyrophosphate scintigraphy in diagnosing cardiac amyloidosis. Am J Cardiol 1983;51:826-30.

95. Hutt DF, Quigley AM, Page J et al. Utility and limitations of 3,3-diphosphono-1,2-propanodicarboxylic acid scintigraphy in systemic amyloidosis. Eur Heart J Cardiovasc Imaging 2014;15:1289-98.

96. Paulus WJ, Tschope C, Sanderson JE et al. How to diagnose diastolic heart failure: a consensus statement on the diagnosis of heart failure with normal left ventricular ejection fraction by the Heart Failure and Echocardiography Associations of the European Society of Cardiology. Eur Heart J 2007;28:2539-50.

97. Komajda M, Lam CS. Heart failure with preserved ejection fraction: a clinical dilemma. Eur Heart J 2014;35:1022-32.

98. Gonzalez-Lopez E, Gallego-Delgado M, Guzzo-Merello G et al. Wild-type transthyretin amyloidosis as a cause of heart failure with preserved ejection fraction. Eur Heart J 2015;36:2585-94.

99. Treibel TA, Fontana M, Gilbertson JA et al. Occult Transthyretin Cardiac Amyloid in Severe Calcific Aortic Stenosis: Prevalence and Prognosis in Patients Undergoing Surgical Aortic Valve Replacement. Circulation Cardiovascular imaging 2016;9.

100. Longhi S, Guidalotti PL, Quarta CC et al. Identification of TTR-related subclinical amyloidosis with 99mTc-DPD scintigraphy. JACC Cardiovasc Imaging 2014;7:531-2.

101. Cavalcante JL, Rijal S, Abdelkarim I et al. Cardiac amyloidosis is prevalent in older patients with aortic stenosis and carries worse prognosis. J Cardiovasc Magn Reson 2017;19:98.

102. Castano A, Narotsky DL, Hamid N et al. Unveiling transthyretin cardiac amyloidosis and its predictors among elderly patients with severe aortic stenosis undergoing transcatheter aortic valve replacement. Eur Heart J 2017;38:2879-2887.

103. Moon JC, Sachdev B, Elkington AG et al. Gadolinium enhanced cardiovascular magnetic resonance in Anderson-Fabry disease. Evidence for a disease specific abnormality of the myocardial interstitium. Eur Heart J 2003;24:2151-5.

104. Shah KB, Mankad AK, Castano A et al. Transthyretin Cardiac Amyloidosis in Black Americans. Circulation Heart failure 2016;9:e002558.

105. Vogelsberg H, Mahrholdt H, Deluigi CC et al. Cardiovascular magnetic resonance in clinically suspected cardiac amyloidosis: noninvasive imaging compared to endomyocardial biopsy. J Am Coll Cardiol 2008;51:1022-30.

106. Syed IS, Glockner JF, Feng D et al. Role of cardiac magnetic resonance imaging in the detection of cardiac amyloidosis. JACC Cardiovasc Imaging 2010;3:155-64.

107. Damy T, Costes B, Hagege AA et al. Prevalence and clinical phenotype of hereditary transthyretin amyloid cardiomyopathy in patients with increased left ventricular wall thickness. Eur Heart J 2016;37:1826-34.

108. Sperry BW, Reyes BA, Ikram A et al. Tenosynovial and Cardiac Amyloidosis in Patients Undergoing Carpal Tunnel Release. J Am Coll Cardiol 2018;72:2040-2050.

109. Fosbol EL, Rorth R, Leicht BP et al. Association of Carpal Tunnel Syndrome With Amyloidosis, Heart Failure, and Adverse Cardiovascular Outcomes. J Am Coll Cardiol 2019;74:15-23.

110. Venner CP, Lane T, Foard D et al. Cyclophosphamide, bortezomib, and dexamethasone therapy in AL amyloidosis is associated with high clonal response rates and prolonged progression-free survival. Blood 2012;119:4387-4390.

111. Wechalekar AD, Schonland SO, Kastritis E et al. A European collaborative study of treatment outcomes in 346 patients with cardiac stage III AL amyloidosis. Blood 2013;121:3420-3427.

112. Venner CP, Gillmore JD, Sachchithanantham S et al. A matched comparison of cyclophosphamide, bortezomib and dexamethasone (CVD) versus risk-adapted cyclophosphamide, thalidomide and dexamethasone (CTD) in AL amyloidosis. Leukemia 2014;28:2304-10.

113. Gertz MA, Lacy MQ, Dispenzieri A et al. Refinement in patient selection to reduce treatment-related mortality from autologous stem cell transplantation in amyloidosis. Bone Marrow Transplant 2013;48:557-561.

114. Sekijima Y, Tojo K, Morita H, Koyama J, Ikeda S. Safety and efficacy of long-term diflunisal administration in hereditary transthyretin (ATTR) amyloidosis. Amyloid 2015;22:79-83.

115. Ikram A, Donnelly JP, Sperry BW, Samaras C, Valent J, Hanna M. Diflunisal tolerability in transthyretin cardiac amyloidosis: a single center's experience. Amyloid 2018;25:197-202.

116. Rosenblum H, Castano A, Alvarez J, Goldsmith J, Helmke S, Maurer MS. TTR (Transthyretin) Stabilizers Are Associated With Improved Survival in Patients With TTR Cardiac Amyloidosis. Circulation Heart failure 2018;11:e004769.

117. Coelho T, Maia LF, Martins da Silva A et al. Tafamidis for transthyretin familial amyloid polyneuropathy: a randomized, controlled trial. Neurology 2012;79:785-92.

118. Maurer MS, Elliott P, Merlini G et al. Design and Rationale of the Phase 3 ATTR-ACT Clinical Trial (Tafamidis in Transthyretin Cardiomyopathy Clinical Trial). Circulation Heart failure 2017;10.

119. Suhr OB, Coelho T, Buades J et al. Efficacy and safety of patisiran for familial amyloidotic polyneuropathy: a phase II multi-dose study. Orphanet J Rare Dis 2015;10:109.

120. Solomon SD, Adams D, Kristen A et al. Effects of Patisiran, an RNA Interference Therapeutic, on Cardiac Parameters in Patients With Hereditary Transthyretin-Mediated Amyloidosis. Circulation 2019;139:431-443.

121. Benson MD, Dasgupta NR, Rissing SM, Smith J, Feigenbaum H. Safety and efficacy of a TTR specific antisense oligonucleotide in patients with transthyretin amyloid cardiomyopathy. Amyloid 2017;24:219-225.

122. O'Nuallain B, Hrncic R, Wall JS, Weiss DT, Solomon A. Diagnostic and therapeutic potential of amyloid-reactive IgG antibodies contained in human sera. J Immunol 2006;176:7071-8.

123. Richards DB, Cookson LM, Berges AC et al. Therapeutic Clearance of Amyloid by Antibodies to Serum Amyloid P Component. N Engl J Med 2015;373:1106-1114.

124. Elliott P, Andersson B, Arbustini E et al. Classification of the cardiomyopathies: a position statement from the European Society Of Cardiology Working Group on Myocardial and Pericardial Diseases. Eur Heart J 2008;29:270-6.

125. Crapo RO, Casaburi R, Coates AL et al. ATS statement: Guidelines for the six-minute walk test. American journal of respiratory and critical care medicine 2002;166:111-117.

126. Decker I, Goodman SA, Phillips SE, Lenihan DJ, Cornell RF. The six-minute walk test is a valuable measure of functional change following chemotherapy for AL (light-chain) cardiac amyloidosis. Br J Haematol 2017;177:481-483.

127. Kellman P, Wilson JR, Xue H, Ugander M, Arai AE. Extracellular volume fraction mapping in the myocardium, part 1: evaluation of an automated method. J Cardiovasc Magn Reson 2012;14:63.

128. Piechnik SK, Ferreira VM, Dall'Armellina E et al. Shortened Modified Look-Locker Inversion recovery (ShMOLLI) for clinical myocardial T1-mapping at

1.5 and 3 T within a 9 heartbeat breathhold. J Cardiovasc Magn Reson 2010;12:69.

129. Fontana M, White SK, Banypersad SM et al. Comparison of T1 mapping techniques for ECV quantification. Histological validation and reproducibility of ShMOLLI versus multibreath-hold T1 quantification equilibrium contrast CMR. J Cardiovasc Magn Reson 2012;14:88.

130. Bassingthwaighte JB, Wang CY, Chan IS. Blood-tissue exchange via transport and transformation by capillary endothelial cells. Circ Res 1989;65:997-1020.

131. Grogan M, Dispenzieri A. Natural history and therapy of AL cardiac amyloidosis. Heart Fail Rev 2015;20:155-62.

132. Wechalekar AD, Gillmore JD, Bird J et al. Guidelines on the management of AL amyloidosis. Br J Haematol 2015;168:186-206.

133. Dispenzieri A, Gertz MA, Kyle RA et al. Serum cardiac troponins and N-terminal pro-brain natriuretic peptide: a staging system for primary systemic amyloidosis. J Clin Oncol 2004;22:3751-7.

134. Banypersad SM, Sado DM, Flett AS et al. Quantification of myocardial extracellular volume fraction in systemic AL amyloidosis: an equilibrium contrast cardiovascular magnetic resonance study. Circulation Cardiovascular imaging 2013;6:34-39.

135. Emdin M, Passino C, Prontera C et al. Cardiac natriuretic hormones, neuro-hormones, thyroid hormones and cytokines in normal subjects and patients with heart failure. Clin Chem Lab Med 2004;42:627-36.

136. Schelbert EB, Messroghli DR. State of the Art: Clinical Applications of Cardiac T1 Mapping. Radiology 2016;278:658-76.

137. Barison A, Aquaro GD, Pugliese NR et al. Measurement of myocardial amyloid deposition in systemic amyloidosis: insights from cardiovascular magnetic resonance imaging. J Intern Med 2015;277:605-14.

138. Brooks J, Kramer CM, Salerno M. Markedly increased volume of distribution of gadolinium in cardiac amyloidosis demonstrated by T1 mapping. J Magn Reson Imaging 2013;38:1591-5.

139. Robbers LF, Baars EN, Brouwer WP et al. T1 mapping shows increased extracellular matrix size in the myocardium due to amyloid depositions. Circ Cardiovasc Imaging 2012;5:423-6.

140. Hawkins PN, Lavender JP, Pepys MB. Evaluation of systemic amyloidosis by scintigraphy with 123I-labeled serum amyloid P component. N Engl J Med 1990;323:508-13.

141. Rydh A, Suhr O, Hietala SO, Ahlstrom KR, Pepys MB, Hawkins PN. Serum amyloid P component scintigraphy in familial amyloid polyneuropathy: regression of visceral amyloid following liver transplantation. Eur J Nucl Med 1998;25:709-13.

142. Gillmore JD, Lovat LB, Persey MR, Pepys MB, Hawkins PN. Amyloid load and clinical outcome in AA amyloidosis in relation to circulating concentration of serum amyloid A protein. Lancet 2001;358:24-9.

143. Hawkins PN. Studies with radiolabelled serum amyloid P component provide evidence for turnover and regression of amyloid deposits in vivo. Clinical science (London, England : 1979) 1994;87:289-95.

144. Hawkins PN. Diagnosis and monitoring of amyloidosis. Baillieres Clin Rheumatol 1994;8:635-59.

145. Gillmore JD, Hawkins PN, Pepys MB. Amyloidosis: a review of recent diagnostic and therapeutic developments. Br J Haematol 1997;99:245-56.

146. Hu K, Liu D, Nordbeck P et al. Impact of monitoring longitudinal systolic strain changes during serial echocardiography on outcome in patients with AL amyloidosis. Int J Cardiovasc Imaging 2015;31:1401-12.

147. Lang RM, Bierig M, Devereux RB et al. Recommendations for chamber quantification. Eur J Echocardiogr 2006;7:79-108.

148. Gottdiener JS, Bednarz J, Devereux R et al. American Society of Echocardiography recommendations for use of echocardiography in clinical trials. J Am Soc Echocardiogr 2004;17:1086-119.

149. Nagueh SF, Appleton CP, Gillebert TC et al. Recommendations for the evaluation of left ventricular diastolic function by echocardiography. J Am Soc Echocardiogr 2009;22:107-33.

150. Hawkins PN, Aprile C, Capri G et al. Scintigraphic imaging and turnover studies with iodine-131 labelled serum amyloid P component in systemic amyloidosis. Eur J Nucl Med 1998;25:701-8.

151. Gertz MA, Dispenzieri A. Immunoglobulin light-chain amyloidosis: growing recognition, new approaches to therapy, active clinical trials. Oncology (Williston Park) 2012;26:152-61.

152. Ishiguro K, Hayashi T, Igarashi T et al. Decrease of B-type natriuretic peptide to less than 200 pg/mL predicts longer survival in cardiac immunoglobulin light chain amyloidosis. Int J Hematol 2015;102:200-4.

153. Gillmore JD, Hawkins PN. Pathophysiology and treatment of systemic amyloidosis. Nat Rev Nephrol 2013;9:574-86.

154. Palladini G, Dispenzieri A, Gertz MA et al. New criteria for response to treatment in immunoglobulin light chain amyloidosis based on free light chain measurement and cardiac biomarkers: impact on survival outcomes. J Clin Oncol 2012;30:4541-9.

155. Palladini G, Lavatelli F, Russo P et al. Circulating amyloidogenic free light chains and serum N-terminal natriuretic peptide type B decrease simultaneously in association with improvement of survival in AL. Blood 2006;107:3854-8.

156. Gertz MA, Landau H, Comenzo RL et al. First-in-Human Phase I/II Study of NEOD001 in Patients With Light Chain Amyloidosis and Persistent Organ Dysfunction. J Clin Oncol 2016;34:1097-103.

157. Rapezzi C, Quarta CC, Riva L et al. Transthyretin-related amyloidoses and the heart: a clinical overview. Nat Rev Cardiol 2010;7:398-408.

158. Jacobson DR, Pastore RD, Yaghoubian R et al. Variant-sequence transthyretin (isoleucine 122) in late-onset cardiac amyloidosis in black Americans. N Engl J Med 1997;336:466-73.

159. Pinney JH, Smith CJ, Taube JB et al. Systemic amyloidosis in England: an epidemiological study. Br J Haematol 2013;161:525-532.

160. Castano A, DeLuca A, Weinberg R et al. Serial scanning with technetium pyrophosphate (99mTc-PYP) in advanced ATTR cardiac amyloidosis. Journal of nuclear cardiology : official publication of the American Society of Nuclear Cardiology 2016;23:1355-1363.

161. Hutt DF, Fontana M, Burniston M et al. Prognostic utility of the Perugini grading of 99mTc-DPD scintigraphy in transthyretin (ATTR) amyloidosis and its relationship with skeletal muscle and soft tissue amyloid. Eur Heart J Cardiovasc Imaging 2017.

162. Gillmore JD, Wechalekar A, Bird J et al. Guidelines on the diagnosis and investigation of AL amyloidosis. Br J Haematol 2015;168:207-218.

163. Lever HM, Karam RF, Currie PJ, Healy BP. Hypertrophic cardiomyopathy in the elderly. Distinctions from the young based on cardiac shape. Circulation 1989;79:580-9.

164. Solomon SD, Wolff S, Watkins H et al. Left ventricular hypertrophy and morphology in familial hypertrophic cardiomyopathy associated with mutations of the beta-myosin heavy chain gene. J Am Coll Cardiol 1993;22:498-505.

165. Florian A, Masci PG, De Buck S et al. Geometric assessment of asymmetric septal hypertrophic cardiomyopathy by CMR. JACC Cardiovasc Imaging 2012;5:702-11.

166. Dungu JN, Valencia O, Pinney JH et al. CMR-based differentiation of AL and ATTR cardiac amyloidosis. JACC Cardiovasc Imaging 2014;7:133-42.

167. Bandula S, Banypersad SM, Sado D et al. Measurement of Tissue interstitial volume in healthy patients and those with amyloidosis with equilibrium contrast-enhanced MR imaging. Radiology 2013;268:858-64.

168. Pepys MB. Amyloidosis. Annu Rev Med 2006;57:223-41.

169. Rapezzi C, Quarta CC, Guidalotti PL et al. Usefulness and limitations of 99mTc-3,3-diphosphono-1,2-propanodicarboxylic acid scintigraphy in the aetiological diagnosis of amyloidotic cardiomyopathy. Eur J Nucl Med Mol Imaging 2011;38:470-8.

170. Maurer MS. Noninvasive Identification of ATTRwt Cardiac Amyloid: The Re-emergence of Nuclear Cardiology. Am J Med 2015;128:1275-1280.

171. Gillmore JD, Damy T, Fontana M et al. A new staging system for cardiac transthyretin amyloidosis. Eur Heart J 2017.

172. Kotecha T, Martinez-Naharro A, Treibel TA et al. Multiparametric Mapping to Understand Pathophysiology in Cardiac Amyloidosis. Heart 2017;103:A1-A2.

173. Messroghli DR, Moon JC, Ferreira VM et al. Clinical recommendations for cardiovascular magnetic resonance mapping of T1, T2, T2* and extracellular

volume: A consensus statement by the Society for Cardiovascular Magnetic Resonance (SCMR) endorsed by the European Association for Cardiovascular Imaging (EACVI). J Cardiovasc Magn Reson 2017;19:75.

174. Kanda T, Ishii K, Kawaguchi H, Kitajima K, Takenaka D. High signal intensity in the dentate nucleus and globus pallidus on unenhanced T1-weighted MR images: relationship with increasing cumulative dose of a gadolinium-based contrast material. Radiology 2014;270:834-41.

175. Martinez-Naharro A, Hawkins PN, Fontana M. Cardiac amyloidosis. Clin Med 2018;18:S30-S35.

176. Gonzalez-Lopez E, Lopez-Sainz A, Garcia-Pavia P. Diagnosis and Treatment of Transthyretin Cardiac Amyloidosis. Progress and Hope. Rev Esp Cardiol (Engl Ed) 2017;70:991-1004.

177. Nochioka K, Quarta CC, Claggett B et al. Left atrial structure and function in cardiac amyloidosis. Eur Heart J Cardiovasc Imaging 2017;18:1128-1137.

178. Feng D, Edwards WD, Oh JK et al. Intracardiac thrombosis and embolism in patients with cardiac amyloidosis. Circulation 2007;116:2420-6.

179. Roberts WC, Waller BF. Cardiac amyloidosis causing cardiac dysfunction: analysis of 54 necropsy patients. Am J Cardiol 1983;52:137-46.

180. Feng D, Syed IS, Martinez M et al. Intracardiac thrombosis and anticoagulation therapy in cardiac amyloidosis. Circulation 2009;119:2490-7.

181. Martinez-Naharro A, Abdel-Gadir A, Treibel TA et al. CMR-Verified Regression of Cardiac AL Amyloid After Chemotherapy. JACC Cardiovasc Imaging 2018;11:152-154.

182. Mollet NR, Dymarkowski S, Volders W et al. Visualization of ventricular thrombi with contrast-enhanced magnetic resonance imaging in patients with ischemic heart disease. Circulation 2002;106:2873-6.

183. Srichai MB, Junor C, Rodriguez LL et al. Clinical, imaging, and pathological characteristics of left ventricular thrombus: a comparison of contrast-enhanced magnetic resonance imaging, transthoracic echocardiography, and transesophageal echocardiography with surgical or pathological validation. Am Heart J 2006;152:75-84.

184. Rathi VK, Reddy ST, Anreddy S et al. Contrast-enhanced CMR is equally effective as TEE in the evaluation of left atrial appendage thrombus in patients with atrial fibrillation undergoing pulmonary vein isolation procedure. Heart Rhythm 2013;10:1021-7.

185. Gillmore JD, Wechalekar A, Bird J et al. Guidelines on the diagnosis and investigation of AL amyloidosis. Br J Haematol 2015;168:207-18.

186. Martinez-Naharro A, Kotecha T, Norrington K et al. Native T1 and Extracellular Volume in Transthyretin Amyloidosis. JACC Cardiovasc Imaging 2019;12:810-819.

187. Manning WJ, Silverman DI, Keighley CS, Oettgen P, Douglas PS. Transesophageal echocardiographically facilitated early cardioversion from atrial fibrillation using short-term anticoagulation: final results of a prospective 4.5-year study. J Am Coll Cardiol 1995;25:1354-61.

188. Black IW, Hopkins AP, Lee LC, Jacobson BM, Walsh WF. Role of transoesophageal echocardiography in evaluation of cardiogenic embolism. Br Heart J 1991;66:302-7.

189. Klein AL, Grimm RA, Murray RD et al. Use of transesophageal echocardiography to guide cardioversion in patients with atrial fibrillation. N Engl J Med 2001;344:1411-20.

190. Weigner MJ, Thomas LR, Patel U et al. Early cardioversion of atrial fibrillation facilitated by transesophageal echocardiography: short-term safety and impact on maintenance of sinus rhythm at 1 year. Am J Med 2001;110:694-702.

191. Kirchhof P, Benussi S, Kotecha D et al. 2016 ESC Guidelines for the management of atrial fibrillation developed in collaboration with EACTS. Eur Heart J 2016;37:2893-2962.

192. January CT, Wann LS, Alpert JS et al. 2014 AHA/ACC/HRS guideline for the management of patients with atrial fibrillation: executive summary: a report of the American College of Cardiology/American Heart Association Task Force on practice guidelines and the Heart Rhythm Society. Circulation 2014;130:2071-104.

193. Berghoff M, Kathpal M, Khan F, Skinner M, Falk R, Freeman R. Endothelial dysfunction precedes C-fiber abnormalities in primary (AL) amyloidosis. Ann Neurol 2003;53:725-30.

194. Castano A, Drachman BM, Judge D, Maurer MS. Natural history and therapy of TTR-cardiac amyloidosis: emerging disease-modifying therapies from organ transplantation to stabilizer and silencer drugs. Heart failure reviews 2015;20:163-78.

195. Glaspy JA. Hemostatic abnormalities in multiple myeloma and related disorders. Hematol Oncol Clin North Am 1992;6:1301-14.

196. Greipp PR, Kyle RA, Bowie EJ. Factor-X deficiency in amyloidosis: a critical review. Am J Hematol 1981;11:443-50.

197. Gamba G, Montani N, Anesi E et al. Abnormalities in thrombin-antithrombin pathway in AL amyloidosis. Amyloid 1999;6:273-7.

198. Fontana M, Corovic A, Scully P, Moon JC. Myocardial Amyloidosis: The Exemplar Interstitial Disease. JACC Cardiovasc Imaging 2019;12:2345-2356.

199. Seward JB, Casaclang-Verzosa G. Infiltrative cardiovascular diseases: cardiomyopathies that look alike. J Am Coll Cardiol 2010;55:1769-79.

200. Merlini G, Bellotti V. Molecular mechanisms of amyloidosis. N Engl J Med 2003;349:583-96.

201. Falk RH, Dubrey SW. Amyloid heart disease. Progress in cardiovascular diseases 2010;52:347-61.

202. Bravo PE, Di Carli MF, Dorbala S. Role of PET to evaluate coronary microvascular dysfunction in non-ischemic cardiomyopathies. Heart failure reviews 2017;22:455-464.

203. Dorbala S, Bruyere J, Hanley M et al. Coronary microvascular function in cardiac amyloidosis. Journal of Nuclear Medicine 2012;53.